

INFORMATION TO USERS

This manuscript has been reproduced from the microfilm master. UMI films the text directly from the original or copy submitted. Thus, some thesis and dissertation copies are in typewriter face, while others may be from any type of computer printer.

The quality of this reproduction is dependent upon the quality of the copy submitted. Broken or indistinct print, colored or poor quality illustrations and photographs, print bleedthrough, substandard margins, and improper alignment can adversely affect reproduction.

In the unlikely event that the author did not send UMI a complete manuscript and there are missing pages, these will be noted. Also, if unauthorized copyright material had to be removed, a note will indicate the deletion.

Oversize materials (e.g., maps, drawings, charts) are reproduced by sectioning the original, beginning at the upper left-hand corner and continuing from left to right in equal sections with small overlaps. Each original is also photographed in one exposure and is included in reduced form at the back of the book.

Photographs included in the original manuscript have been reproduced xerographically in this copy. Higher quality 6" x 9" black and white photographic prints are available for any photographs or illustrations appearing in this copy for an additional charge. Contact UMI directly to order.

U·M·I

University Microfilms International
A Bell & Howell Information Company
300 North Zeeb Road, Ann Arbor, MI 48106-1500, USA
419.763.4700 • FAX 419.763.4210

Order Number 1345021

Viscosity modeling and glass formation studies in oxy-fluoride
melts

Hebbar, Kavitha N., M.S.
University of Nevada, Reno, 1991

U·M·I
300 N. Zeeb Rd.
Ann Arbor, MI 48106

University of Nevada, Reno

VISCOSITY MODELING AND GLASS FORMATION STUDIES
IN OXY-FLUORIDE MELTS.

A thesis submitted in partial fulfillment
of the requirements for the degree of

Master of Science
in
Metallurgical Engineering

by

Kavitha N. Hebbar

May 1991

The thesis of Kavitha N. Hebbar is approved:

Ramana Reddy

Thesis Advisor

[Signature]

Department Chairman

[Signature]

Dean, Graduate School

University of Nevada, Reno

Reno

May 1991

ACKNOWLEDGEMENTS

I am extremely grateful to Dr. R.G. Reddy, for his helpful guidance during the course of my study at UNR. I gratefully acknowledge Dr. D. Chandra and Dr. D. C. Noble for their advise and criticism of the work. Many thanks to the analytical staff at the US Bureau of Mines, Reno, NV for their help with analysis.

I express my sincere thanks to my parents and family for their encouragement and blessings. I am also grateful to my fiance, Harish for lending me moral support.

I am also indebted to Dr. R. Lee Byers and Dr. H.J. Hittner, ALCOA, Pittsburgh, PA, for supporting this research and the ALCOA foundation, Pittsburgh, PA for providing me with financial assistantship. Finally, I wish to thank the Department of Chemical and Metallurgical Engineering, University of Nevada, Reno for the financial support.

ABSTRACT

A structure based model that was developed was used to predict viscosities of MO-SiO₂ (where MO is CaO, MgO, MnO, BaO, SrO and FeO) and M₂O-SiO₂ (where M₂O is Na₂O, K₂O and Li₂O) and ternary MO-NO-SiO₂ (where MO and NO are CaO, FeO, MgO and MnO) type of melts in the composition range of $0.1 < X_{SiO_2} < 1$. Both composition and temperature effects are considered in coming up with the viscosity expression. In comparison to several existing empirical models, the present model seems to predict the viscosities more consistently over extended ranges of temperatures and composition. The effect of solids on viscosity has also been considered. The ternary model needs some modifications in order to predict the experimental isoviscosity contours.

The initial studies on the safe disposal of spent potliner (SPL) obtained from an aluminum electrolytic cell by fixing it in a glassy matrix have been done. The glassy nature of the melts of the as received SPL, the fused and the fused SPL with additions of varying percentages of silica and calcium oxide were determined using X-ray diffraction and SEM analysis. A comparison of the analysis on SPL melts with those containing various amounts of silica and calcium oxide indicates that more than 20 wt pct. silica is required to make a completely glassy matrix.

TABLE OF CONTENTS

| | |
|-----------------------|-----|
| ACKNOWLEDGEMENTS..... | i |
| ABSTRACT..... | ii |
| LIST OF FIGURES..... | iv |
| LIST OF TABLES..... | vii |

PART A

| | | |
|-----------|---|----|
| Chapter 1 | | |
| 1.1 | Introduction | 1 |
| 1.2 | Literature Review | 3 |
| 1.3 | Present Work | 11 |
| Chapter 2 | Theoretical Considerations | 12 |
| 2.1 | Calculation of NO° | 13 |
| 2.2 | Calculation of E | 19 |
| Chapter 3 | Results and Discussions | 24 |
| 3.1 | Pure liquid Silica | 24 |
| 3.2 | MO-SiO ₂ type of systems | 25 |
| 3.3 | M ₂ O-SiO ₂ type of systems | 62 |
| 3.4 | Ternary Systems | 96 |

PART B

| | | |
|-----------|--|-----|
| Chapter 4 | Spent Potliner | 111 |
| 4.1 | Literature Review | 111 |
| 4.2 | Glass formation characteristics | 113 |
| 4.3 | Experimental procedure | 128 |
| 4.4 | Results and Discussions | 130 |
| Chapter 5 | | |
| 5.1 | Conclusions | 145 |
| Chapter 6 | References | 149 |
| Chapter 7 | Appendix | |
| 1. | Free energy data for binary silicate melts | 155 |
| 2. | Calculations for binary systems | 156 |
| 3. | Calculations for ternary systems | 159 |
| 4. | Approximate analysis of SPL | 161 |

List of figures

| | | |
|-----|--|----|
| 1. | Effect of solids on viscosity..... | 10 |
| 2. | Plot of calculated and measured NO° in a PbO-SiO_2 binary system..... | 15 |
| 3. | Oxygen anions distribution in PbO-SiO_2 system..... | 18 |
| 4. | Schematic of a SiO_2 chain breaking and jumping to an adjacent hole | 20 |
| 5. | Energy changes in binary systems | 21 |
| 6. | Experimental and predicted viscosities of CaO-SiO_2 melts at 1823K..... | 26 |
| 7. | Experimental and predicted viscosities of CaO-SiO_2 melts at 1873K..... | 27 |
| 8. | Experimental and predicted viscosities of CaO-SiO_2 melts at 1973K..... | 28 |
| 9. | Experimental and predicted viscosities of MgO-SiO_2 melts at 1873K..... | 31 |
| 10. | Experimental and predicted viscosities of MgO-SiO_2 melts at 1923K..... | 32 |
| 11. | Experimental and predicted viscosities of MgO-SiO_2 melts at 1973K..... | 33 |
| 12. | Experimental and predicted viscosities of MgO-SiO_2 melts at 2023K..... | 34 |
| 13. | Experimental and predicted viscosities of MgO-SiO_2 melts at 2073K..... | 35 |
| 14. | Experimental and predicted viscosities of MnO-SiO_2 melts at 1673K..... | 36 |
| 15. | Experimental and predicted viscosities of MnO-SiO_2 melts at 1773K..... | 37 |
| 16. | Experimental and predicted viscosities of BaO-SiO_2 melts at 1773K..... | 39 |
| 17. | Experimental and predicted viscosities of BaO-SiO_2 melts at 1823K..... | 40 |
| 18. | Experimental and predicted viscosities of BaO-SiO_2 melts at 1873K..... | 41 |
| 19. | Experimental and predicted viscosities of BaO-SiO_2 melts at 1923K..... | 42 |
| 20. | Experimental and predicted viscosities of BaO-SiO_2 melts at 1973K..... | 43 |
| 21. | Experimental and predicted viscosities of BaO-SiO_2 melts at 2023K..... | 44 |
| 22. | Experimental and predicted viscosities of BaO-SiO_2 melts at 2073K..... | 45 |
| 23. | Experimental and predicted viscosities of SrO-SiO_2 melts at 1773K..... | 47 |
| 24. | Experimental and predicted viscosities of SrO-SiO_2 melts at 1823K..... | 48 |
| 25. | Experimental and predicted viscosities of SrO-SiO_2 melts at 1873K..... | 49 |

| | | |
|-----|--|----|
| 26. | Experimental and predicted viscosities of SrO-SiO ₂ melts at 1923K..... | 50 |
| 27. | Experimental and predicted viscosities of SrO-SiO ₂ melts at 1973K..... | 51 |
| 28. | Experimental and predicted viscosities of SrO-SiO ₂ melts at 2073K..... | 52 |
| 29. | Effect of Fe ₂ O ₃ /FeO on viscosities of FeO-SiO ₂ melts at 1573K..... | 55 |
| 30. | Experimental and predicted viscosities of FeO-SiO ₂ melts at 1523K..... | 57 |
| 31. | Experimental and predicted viscosities of FeO-SiO ₂ melts at 1573K..... | 58 |
| 32. | Experimental and predicted viscosities of FeO-SiO ₂ melts at 1623K..... | 59 |
| 33. | Experimental and predicted viscosities of FeO-SiO ₂ melts at 1673K..... | 60 |
| 34. | Experimental and predicted viscosities of Na ₂ O-SiO ₂ melts at 1373K..... | 64 |
| 35. | Experimental and predicted viscosities of Na ₂ O-SiO ₂ melts at 1423K..... | 65 |
| 36. | Experimental and predicted viscosities of Na ₂ O-SiO ₂ melts at 1473K..... | 66 |
| 37. | Experimental and predicted viscosities of Na ₂ O-SiO ₂ melts at 1523K..... | 67 |
| 38. | Experimental and predicted viscosities of Na ₂ O-SiO ₂ melts at 1573K..... | 68 |
| 39. | Experimental and predicted viscosities of Na ₂ O-SiO ₂ melts at 1623K..... | 69 |
| 40. | Experimental and predicted viscosities of Na ₂ O-SiO ₂ melts at 1673K..... | 70 |
| 41. | Experimental and predicted viscosities of Na ₂ O-SiO ₂ melts at 1723K..... | 71 |
| 42. | Experimental and predicted viscosities of Na ₂ O-SiO ₂ melts at 1773K..... | 72 |
| 43. | Experimental and predicted viscosities of Na ₂ O-SiO ₂ melts at 1823K..... | 73 |
| 44. | Experimental and predicted viscosities of K ₂ O-SiO ₂ melts at 1373K..... | 74 |
| 45. | Experimental and predicted viscosities of K ₂ O-SiO ₂ melts at 1423K..... | 75 |
| 46. | Experimental and predicted viscosities of K ₂ O-SiO ₂ melts at 1473K..... | 76 |
| 47. | Experimental and predicted viscosities of K ₂ O-SiO ₂ melts at 1523K..... | 77 |
| 48. | Experimental and predicted viscosities of K ₂ O-SiO ₂ melts at 1573K..... | 78 |
| 49. | Experimental and predicted viscosities of K ₂ O-SiO ₂ melts at 1623K..... | 79 |
| 50. | Experimental and predicted viscosities of K ₂ O-SiO ₂ | |

| | | |
|-----|---|-----|
| | melts at 1673K..... | 80 |
| 51. | Experimental and predicted viscosities of $\text{Li}_2\text{O-SiO}_2$ melts at 1473K..... | 82 |
| 52. | Experimental and predicted viscosities of $\text{Li}_2\text{O-SiO}_2$ melts at 1523K..... | 83 |
| 53. | Experimental and predicted viscosities of $\text{Li}_2\text{O-SiO}_2$ melts at 1573K..... | 84 |
| 54. | Experimental and predicted viscosities of $\text{Li}_2\text{O-SiO}_2$ melts at 1623K..... | 85 |
| 55. | Experimental and predicted viscosities of $\text{Li}_2\text{O-SiO}_2$ melts at 1673K..... | 86 |
| 56. | Experimental and predicted viscosities of $\text{Li}_2\text{O-SiO}_2$ melts at 1773K..... | 87 |
| 57. | Predicted viscosities at 1423K and 1823K for the system $\text{Na}_2\text{O-SiO}_2$ | 89 |
| 58. | Predicted viscosities at 1523K and 1673K for the system FeO-SiO_2 | 90 |
| 59. | Effect on temperature on viscosity of $\text{Na}_2\text{O-SiO}_2$ melts..... | 91 |
| 60. | Effect of temperature on viscosity of FeO-SiO_2 melts..... | 92 |
| 61. | Predicted and experimental viscosities of FeO-SiO_2 and $\text{Na}_2\text{O-SiO}_2$ melts..... | 94 |
| 62. | Viscosities of CaO-MnO-SiO_2 melts at 1673K..... | 101 |
| 63. | Viscosities of CaO-MnO-SiO_2 melts at 1723K..... | 102 |
| 64. | Viscosities of CaO-MnO-SiO_2 melts at 1823K..... | 103 |
| 65. | Viscosities of CaO-MgO-SiO_2 melts at 1773K..... | 105 |
| 66. | Viscosities of FeO-MnO-SiO_2 melts at 1673K..... | 107 |
| 67. | Structural schematic of cryatalline, glassy and sodium silicate glasses..... | 114 |
| 68. | Effect of temperature on glass formation..... | 117 |
| 69. | Free energy vs composition curve..... | 122 |
| 70. | Metastable and unstable regions of silicate glass..... | 127 |
| 71. | Block diagram of experimental procedure..... | 131 |
| 72. | X-ray diffraction pattern of SPL..... | 132 |
| 73. | SEM micrographs of Spent Potliner..... | 133 |
| 74. | SEM micrograph of fused Spent Potliner..... | 133 |
| 75. | X-ray diffraction pattern of fused SPL..... | 135 |
| 76. | X-ray diffraction pattern of $\text{SPL} + 14\% \text{SiO}_2$ | 137 |
| 77. | X-ray diffraction pattern of $\text{SPL} + 20\% \text{SiO}_2$ | 138 |
| 78. | SEM micrographs of Spent Potliner with silica additions..... | 139 |
| 79. | X-ray diffraction pattern of $\text{SPL} + 14\% \text{CaO}$ | 141 |
| 80. | X-ray diffraction pattern of $\text{SPL} + 20\% \text{CaO}$ | 142 |
| 81. | SEM micrographs of Spent Potliner with calcium oxide additions..... | 143 |

LIST OF TABLES

| | |
|---|-----|
| 1. Calculated and measured NO° in binary systems at 1623K..... | 16 |
| 2. Mean chain lengths for binary silicate systems..... | 61 |
| 3. Average percentage deviations for binary systems... | 95 |
| 4. Calculated and experimental viscosities of CaO-MnO-SiO ₂ at 1673K..... | 100 |
| 5. Calculated and experimental viscosities of CaO-MnO-SiO ₂ at 1773K..... | 100 |
| 6. Calculated and experimental viscosities of CaO-MgO-SiO ₂ at 1773K..... | 106 |
| 7. Calculated and experimental viscosities of FeO-MnO-SiO ₂ at 1673K..... | 106 |
| 8. Calculated and experimental viscosities of CaO-FeO-SiO ₂ at 1673K..... | 109 |
| 9. Intensities of various phases in SPL studies..... | 144 |

1. CHAPTER

1.1 INTRODUCTION

Knowledge of the physico-chemical properties of slags would contribute to a general understanding of the slag. Amongst these properties, the role of viscosities is indisputable. In many of the metallurgical processes like steelmaking, it is of prime importance. The viscosities of silicate melts are important in this case, as is in the case of glass making and in the study of magmas.

Even though viscosities are very important, several limitations exist, as the experimental measurements of viscosities are very difficult to make. The only resort in such cases is to come up with a reliable model that will predict viscosities in a self-consistent manner over the entire composition range. A structure based viscosity model has been proposed that predicts viscosities of $MO-SiO_2$, M_2O-SiO_2 and ternary melts as a function of temperature and composition. The results of this work has been presented in Part A.

Spent potliner (SPL) from an aluminum electrolytic cell mainly contains carbon in the form of graphite, fluoride, aluminum, sodium, silicon and calcium in various compounds, other than minor quantities of cyanide, elemental iron etc. Recently, Spent Potliner has been placed in the

environmentally hazardous materials list by the EPA. Thus to prevent its' leachability it is required to fix the cyanides, fluorides and alkaline metals so that the SPL is safe for disposal. One of the methods being considered for the safe disposal is to fix them in a glassy matrix. Preliminary studies were undertaken to understand the glass formation characteristics of SPL with glass formers like silica and glass modifiers like calcium oxide. The experimental results are presented in Part B.

PART A**1.2. LITERATURE REVIEW**EXISTING MODELS:

Several models exist for the estimation of viscosities of slags on the basis of chemical composition (Ochotin (1), Lyon (2), McCauley and Apelian (3), Mairy (4), Bottinga and Weill (5), Shaw (6), Watt and Fereday (7), Bokamp (8)). Most of these use an Arrhenius type of equation to express the temperature dependence of viscosity:

$$\eta = A \exp (E/RT) \quad (1-1)$$

where A is a constant, E is the activation energy, R is the gas constant, and T is the temperature in degrees kelvin.

This expression implies that a plot of $\ln \eta$ as a function of $1/T$ should yield a straight line making the intercept the value of the constant and the slope can be related to the energy term which should also be a constant. However, experimental observations made by several investigators do not confirm this. McCauley and Apelian (9) have measured the viscosities of continuous casting mold fluxes that contained SiO_2 , Al_2O_3 , CaO , Na_2O and CaF_2 . Plots of $\ln \eta$ as a function of $1/T$ (K^{-1}) showed non-linearity with the energy values varying from 27kcal/mol to 42kcal/mol. No correlation between the energy values and the composition were made. However, Shaw (6) who has made predictions for the viscosities of multicomponent

anhydrous silicate liquids based on the compilations and calculations of Bottinga and Weill (5) , suggest a simple pattern in the plot of $\ln \eta$ as a function of $1/T$. They report a strong dependence of slope with composition. Bottinga and Weill (5), showed that the Arrhenius equation adequately describes the behavior of magmatic silicate liquids within certain ranges of compositions, and Hofmaier and Urbain (10) report similar observations. But this is in conspicuous contradiction to the observations of Euler and Winkler (11), who found that the Arrhenius equation did not predict the experimental data in a consistent manner.

The absolute reaction rate theory was proposed by Glasstone et al. (12). This is an extension of the Arrhenius equation but includes terms like the molar volume and enthalpy of vaporization. The limitations arise, in the use of this equation because of non-availability of enthalpy of vaporization for most of the materials. Brostow equation (13), which has also been generated empirically, uses the Clausius-Clapeyron equation as the basis and can be applied to all types of Newtonian liquids with reasonable accuracy. But the question of whether silicate melts are Newtonian or non-Newtonian is still a matter of debate. The issue may have arisen as a result of the effect of fine solid particles that may be present in these slags, or as a result of the time

required for the internal structure of the slag to reach an equilibrium state.

The models proposed by Riboud et al. (14) and Urbain et al. (15) which was later modified by Urbain (16), in particular, use the Weymann equation

$$\eta = AT \exp(B/T) \quad (1-2)$$

Riboud model:

In this model, the slag constituents are classified in five different categories and the mole fractions (X) of these categories are given by:

1. $X_{SiO_2} = X_{SiO_2} + X_{PO_{2.5}} + X_{TiO_2} + X_{ZrO_2}$
2. $X_{CaO} = X_{CaO} + X_{MgO} + X_{FeO} + X_{FeO_{1.5}} + X_{MnO} + X_{BO_{1.5}}$
3. $X_{Al_2O_3}$
4. X_{CaF_2}
5. $X_{Na_2O} = X_{Na_2O} + X_{K_2O}$

The viscosity was calculated using the expression (1-2)

where the constants A and B are calculated using the following equations:

6. $A = \exp(-19.81 + 1.73X_{CaO} + 5.82X_{CaF_2} + 7.02X_{Na_2O} - 33.76X_{Al_2O_3})$
7. $B = +31140 - 23896X_{CaO} - 46356X_{CaF_2} - 39159X_{Na_2O} + 68833X_{Al_2O_3}$

Urbain et al. model:

In this model the viscosity was calculated using the

following equation:

$$\eta = AT \exp(10^3B/T). \quad (1-3)$$

and the parameters A and B are calculated by dividing the slag constituents into 3 categories:

1. "glass formers", $X_O = X(\text{SiO}_2) + X(\text{P}_2\text{O}_5)$
2. "modifiers", $X_M = X(\text{CaO}) + X(\text{MgO}) + X(\text{Na}_2\text{O}) + X(\text{K}_2\text{O}) + 3X(\text{CaF}_2) + X(\text{FeO}) + X(\text{MnO}) + 2X(\text{ZrO}_2)$
3. "amphoterics", $X_A = X(\text{Al}_2\text{O}_3) + X(\text{Fe}_2\text{O}_3) + X(\text{B}_2\text{O}_3)$.

However, normalized values X_O^* and X_M^* and X_A^* are obtained by dividing the mole fractions X_O , X_M and X_A by the term $(1+2X(\text{CaF}_2) + 0.5X(\text{FeO}_{1.5}) + X(\text{TiO}_2) + X(\text{ZrO}_2))$.

Urbain et al. have proposed that the parameter B was influenced both by the ratio $\beta = X_M^*/(X_M^* + X_A^*)$ and by X_O^* . The parameter B can be expressed in the form of the following two equations:

$$4. \quad B = B_0 + B_1 X_O^* + B_2 (X_O^*)^2 + B_3 (X_O^*)^3$$

$$5. \quad B_i = a_i + b_i \beta + c_i \beta^2$$

B_0, B_1, B_2, B_3 can be calculated from

$$6. \quad B_0 = 13.8 + 39.9355\beta - 44.049\beta^2$$

$$7. \quad B_1 = 30.481 - 117.1505\beta + 129.9978\beta^2$$

$$8. \quad B_2 = -40.9429 + 234.0486\beta - 300.04\beta^2$$

$$9. \quad B_3 = 60.7619 - 153.9276\beta + 211.1616\beta^2.$$

Parameter A is calculated from:

$$10. \quad -\ln A = 0.2693B + 11.6725$$

Later the modifications made to the model by Urbain led to the calculation of B values for different modifiers CaO, MgO and MnO as:

$$B_{\text{global}} = \frac{(X(\text{CaO})B(\text{CaO}) + X(\text{MgO})B(\text{MgO}) + X(\text{MnO})B(\text{MnO}))}{(X(\text{CaO}) + X(\text{MgO}) + X(\text{MnO}))}$$

Amongst the models investigated, the models of Riboud et al (14) and Urbain (16) gave closer agreement with the experimental data and wherever applicable, the present model has been compared with these two models.

But the models of Riboud et al. and Urbain et al. have a major drawback in that they predict the same viscosity value for all MO-SiO₂ systems and all M₂O-SiO₂ of the same composition, even though it is a known fact that the viscosities of say, CaO-SiO₂ and MgO-SiO₂ cannot be the same at a particular composition. This is because of the different extents of depolymerization brought about by the different cationic species. For example, at 1823K, for a mole fraction of 0.5 silica, in the case of CaO-SiO₂ a viscosity value of 1.95 poise has been reported while in the system MgO-SiO₂ a value of 3.16 has been reported. The Riboud et al. model gives a value of 3.13 for both these systems while Urbain et al. gives a value of 2.68. The models also cannot predict

viscosities of pure silica or of any compositions beyond the available experimental data. In fact, none of the existing models can predict viscosities at these silica compositions. One of the possible reasons for this is that most models are empirical in nature and do not take the effect of melt structure into account.

However, recently, Hu and Reddy (17), have proposed a model that takes the structure of the silicate melt into consideration. The proposed expression was:

$$\eta = 4.9 \times 10^9 \text{ NO}^\circ T^{1/2} \exp (E/RT) \text{ poise} \quad (1-4)$$

where, NO° incorporates the extent of depolymerization of the melt upon addition of metal oxide, E is the energy required to break the silicate bond and move it to an adjacent hole, R is the gas constant in J/mole K and T the temperature in K.

This model also has the drawback in that it does not predict viscosities in the entire composition range. The energy term has been fitted as a function of NO° only and has not been expressed as a function of temperature.

It is easy to see from the above discussions that the viscosity is a strong function of composition and temperature. Another factor that can affect experimental measurements of viscosities is the presence of solids in the melt.

EFFECT OF SOLIDS ON VISCOSITY:

Elliott (18) has discussed this aspect in great detail. The viscosity of a liquid slag could be increased greatly by

the presence of small solid particles or even by highly viscous liquid droplets. The presence of these particles and droplets could increase the viscosity to such an extent that the slag would not flow out of the furnace at all. This again could occur mainly due to error in feed preparation as has been discussed in the report by the Technical division of Savannah River Laboratory (19). Roscoe (20) has shown that the following relation can be used to calculate the effective viscosity η_c of a two-phase system consisting of monodispersed spherical particles suspended within a liquid:

$$\eta_c = \eta (1 - 1.35 \theta)^{-5/2}. \quad (1-5)$$

where η is the viscosity of the pure liquid that does not contain solids and θ is the volume fraction of the solid phase. From this expression, the apparent viscosity is seen to increase rapidly as the volume fraction increases. The influence of solid content of slag on the ratio of effective viscosity, η_c , to that of the pure liquid η has been illustrated in the figure 1 (18). However, the effect is still higher if the particles are of complex shapes or are rod-like. In general, gas bubbles on the other hand will decrease the apparent viscosity of the slag.

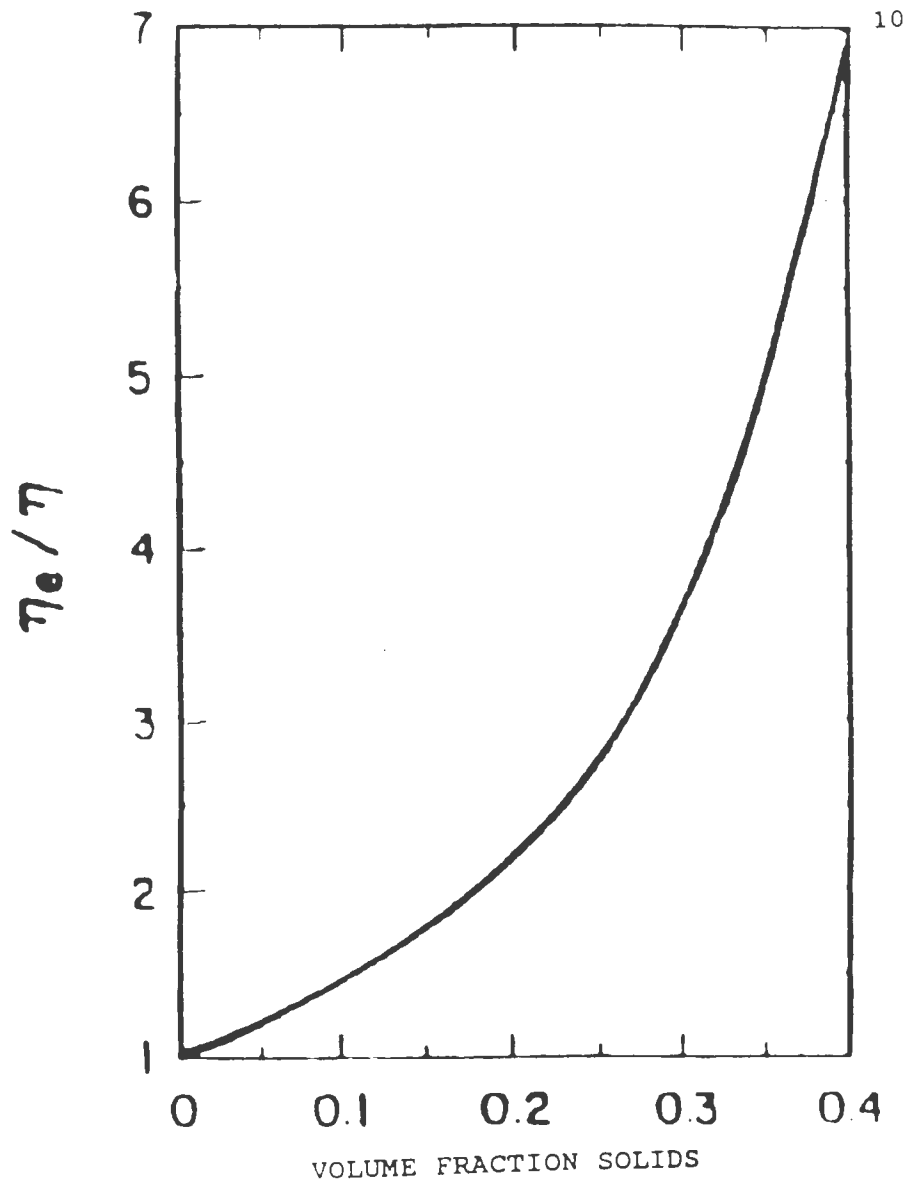


Fig.1-INFLUENCE OF SOLIDS CONTENT OF MELT ON THE RATIO OF APPARANT VISCOSITY, η_0 , TO THAT OF THE PURE LIQUID

1.3 PRESENT WORK

The present work addresses the applicability of the proposed structure based viscosity model to $MO-SiO_2$, M_2O-SiO_2 type of melts. The model has been developed to predict viscosities as a function of both composition and temperature. The effect of solids on viscosity has been shown for the $FeO-SiO_2$ system. The variation of viscosities with mean chain lengths of the melts has also been dealt with. The model has been further extended to ternary silicate systems. The agreement with experimental data is excellent in most cases.

Another aspect of this thesis is the safe disposal of Spent Potliner. The preliminary studies on fixing SPL in a glassy matrix has been completed. The appearance of the glassy state with additions of varying percentages of CaO and SiO_2 to the Spent Potliner are discussed.

CHAPTER 2

THEORETICAL CONSIDERATIONS

The addition of metal oxide to silica results in a breakdown of the silicate network. This in turn results in a bond rupture between the SiO_4^{4-} tetrahedrons. With an increase in the number of ruptures in the network there is an increase in the number of "free" or "dangling" ends of the ruptured network (SiO_4^{4-}). The network therefore, becomes increasingly distorted with increase in addition of metallic oxides. The extent of structure breakdown and change in properties depend on the concentration of the metal oxide (modifier).

These concepts have been taken into consideration in the proposed structure based viscosity model.

The viscosity expression was developed (17) using two aspects of the silicate melts- the structural and the kinetic. The expression is :

$$\eta = 4.9 \times 10^{-9} \text{ NO}^0 \text{ T}^{1/2} \exp(E/RT) \text{ poise} \quad (1-4)$$

where NO^0 is the number of bridging oxygen bonded to two silicate atoms, T is the absolute temperature and E is the energy needed to break the silicate bond into tetrahedral SiO_4^{4-} units and overcome the barrier to move it into an adjacent hole. A detailed discussion of the above expression is given elsewhere (17). Only a brief description of each of the parameters of equation (1-4) is given here.

For the ionic liquids containing holes, Bockris and Reddy (21) developed the following expression:

$$\eta = 2/3 N_h R_h (6.28 mKT)^{1/2} \exp(E/RT) \quad (2-1)$$

where N_h is the number of holes per unit volume, R_h is the average radius of the hole, m is the mass of an ionic unit, K is the Boltzmann constant and R is the gas constant.

The following deductions were made by Hu and Reddy (22). The value of R_h is $3.4A^0$. The term $(6.28mKT)^{1/2}$ is equal to $0.3637 \times 10^{-23} T^{1/2}$. The term N_h is expressed as $N_h = 6.023 \times 10^{23} NO^0$. Plugging these parameters into equation (2-1) the expression (1-4) for viscosity was obtained.

2.1 CALCULATION OF NO^0 :

The structural considerations of the silicate melt gives a means of calculating the term NO^0 in the viscosity expression that was developed in the previous section. The structure of these silicate melts is quite complex. Several models have been proposed amongst which the models of Masson et al. (23), Gaskell (24), Fincham and Richardson (25), Toop and Samis (26), Froberg et al. (27), Yokakawa and Niwa (28), Lin and Pelton (29) and Flood and Knapp (30) are noteworthy. Gaskell (31) has made a complete list and comparison of these various models. Most of the more recent models consider the following equilibrium:



which adequately describes the depolymerization of the melt on the addition of the metal oxide. In terms of simple electrochemical reaction this reaction can be written as:



where, O^0 , $O^{2\cdot}$ and O^{\cdot} are the free divalent oxygen anion, the oxygen bound to two silicon atoms and the oxygen ion bound to Si by one covalent bond respectively. Thus no specific anion has been assumed and O^{\cdot} and O^0 behave independent of the cationic species that they were bound to in the melt.

The NO^0 values for $PbO-SiO_2$, Na_2O-SiO_2 and $CaO-SiO_2$ systems at 1673K were calculated by Hu and Reddy (17) using the models of Toop et al. (26), Masson (23) and Yokokawa (28). The calculated NO^0 values were compared with the experimental data reported by Kaneko (32). The plot of the NO^0 values as a function of $XSiO_2$ for $PbO-SiO_2$ systems is shown in figure 2 and the calculated NO^0 values for all three systems are tabulated in Table 1.

As can be seen from this, the NO^0 values calculated using Yokokawa (28) model gave good agreement with the experimental data and hence further calculations were made using this model, which is a quasilattice treatment of the random network model on the silicate structure. According to this model, if N moles of SiO_2 and M moles of basic oxide, MO are reacted to form a binary silicate melt, the liquid melt is considered to be a mixture of cation (M^{2+}) and anions (O^0, O^{\cdot} and $O^{2\cdot}$).

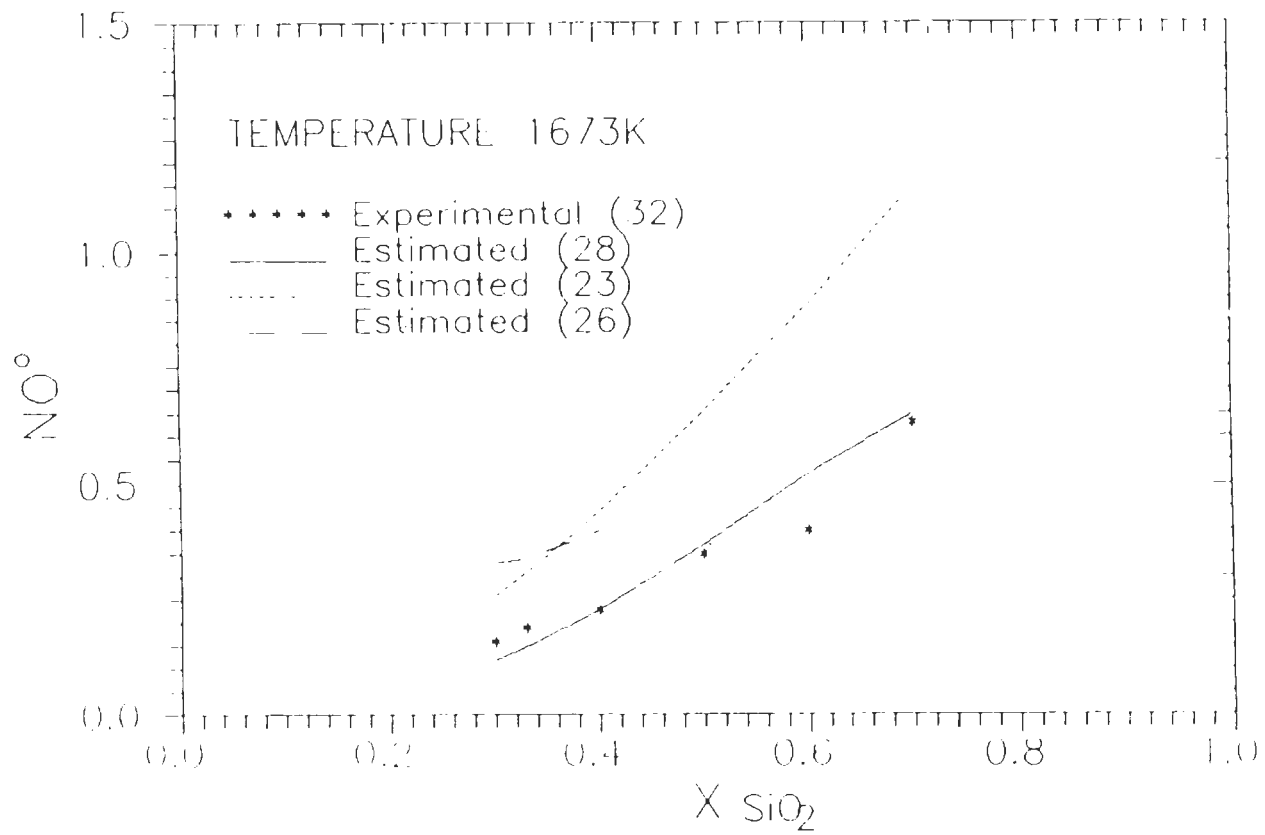


Fig.2—EXPERIMENTAL AND CALCULATED NO⁰ IN
PbO-SiO₂ MELTS

Table 1: The calculated and measured NO° in binary systems at 1623K (17)

| XSiO_2 | $\text{NO}^\circ(\text{Expt. } 32)$ | $\text{NO}^\circ(28)$ | $\text{NO}^\circ(23)$ | $\text{NO}^\circ(26)$ |
|---|-------------------------------------|-----------------------|-----------------------|-----------------------|
| PbO-SiO ₂ System | | | | |
| 0.3 | 0.16 | 0.12 | 0.26 | 0.33 |
| 0.33 | 0.19 | 0.15 | 0.31 | 0.34 |
| 0.4 | 0.23 | 0.23 | 0.44 | 0.40 |
| 0.5 | 0.35 | 0.37 | 0.65 | |
| 0.6 | 0.40 | 0.52 | 0.88 | |
| 0.7 | 0.63 | 0.65 | 1.14 | |
| Na ₂ O-SiO ₂ System | | | | |
| 0.67 | 0.62 | 0.62 | 1.03 | |
| CaO-SiO ₂ System | | | | |
| 0.6 | 0.48 | 0.50 | 0.80 | |
| 0.5 | 0.35 | 0.34 | 0.50 | |

The charge and mass balance considerations, respectively, give (28):

$$\text{NO}^0 = 2N - 1/2 \text{NO}^\cdot \quad (2-4)$$

$$\text{NO}^{2-} = M - 1/2 \text{NO}^\cdot \quad (2-5)$$

The total number of anions:

$$\text{NO}^0 + \text{NO}^{2-} + \text{NO}^\cdot = 2N + M \quad (2-6)$$

The complete ionic distribution thus consists of a

depolymerized region i.e. NO^2 decreases with increasing SiO_2 content in the melt and a polymerized region i.e. NO^0 increases with increasing SiO_2 content of the melt. This is illustrated in the plot of the charge as a function of mole fraction silica in figure 3. This plot applies specifically to the $PbO-SiO_2$ melts at 1673K and the anion distribution varies in value in different silicate systems. In systems like the iron silicate melts, NO^0 gives a finite value at infinitely low mole fractions of silica. This is because as can be seen from equation 2-8, NO^0 is a function of ΔG^0 , the free energy, which varies with temperature and melt.

The NO^0 was calculated using the following expression (22):

$$NO^0 = \frac{(4 - 4X_{MO} - NO^0)}{2(2 - X_{MO})} \quad (2-7)$$

where X_{MO} is the mole fraction of the metal oxide. NO^0 is calculated using equation (2-8):

$$(1 - \exp(\Delta G^0/RT)) (NO^0)^2 + (2X_{MO} - 4) (NO^0) + 8X_{MO} (1 - X_{MO}) = 0 \quad (2-8)$$

where, ΔG^0 is the standard free energy for the depolymerization reaction of the form given in equation (2-9 or 2-10):

For $MO-SiO_2$ type of melts:



For M_2O-SiO_2 type of melts:



The free energy data for several silicate systems that

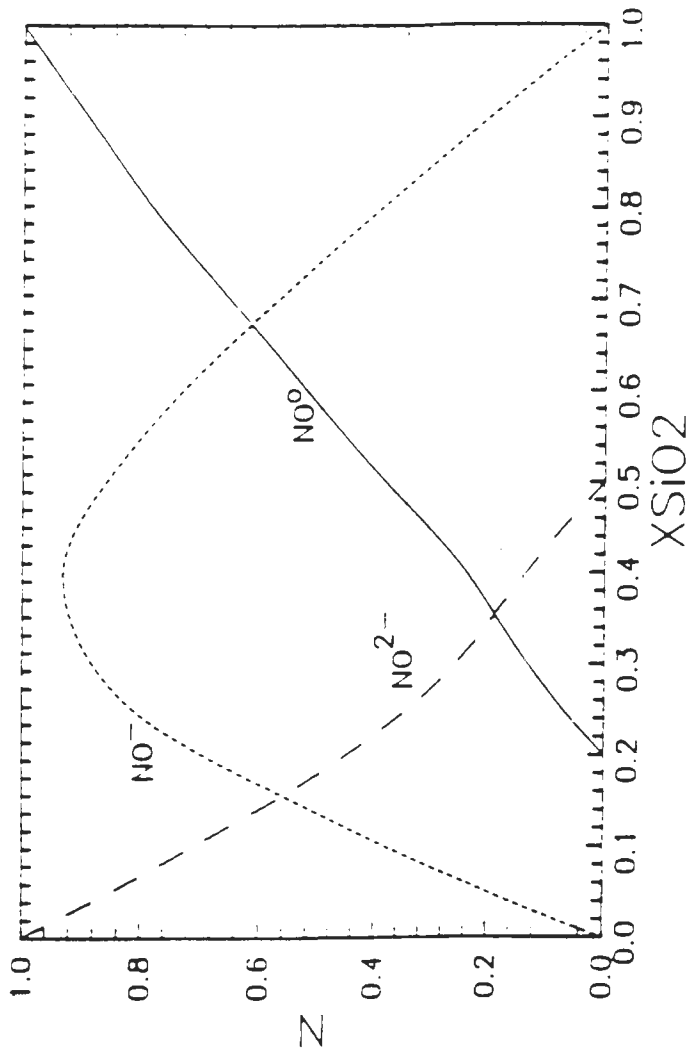


Fig. 3-THE THREE TYPE OXYGEN ANIONS DISTRIBUTION
IN PbO-SiO₂ SYSTEM AT 1673K

have been considered here are given in Appendix 1 (33,34).

2.2 CALCULATION OF E:

The hole theory (21) shows that the energy for particle motion includes two steps. One is the energy required to form a hole and another is the energy required to make a particle jump into the hole. In the case of silicate melts the energy term is considered to be composed of energy required to break the silicate bonds into SiO_4^{4-} tetrahedral units and move the tetrahedral unit into the adjacent hole. The silica network, bond rupture upon metal oxide addition, and the jump of a segment into an empty hole is illustrated in Figure 4 (21). Energy required for the jump is considerably small. This has been determined to be equal to $3.3RT_m$, where R is the gas constant and T_m is the melting temperature of the slag system. Hence, E is largely dependent on the number of Si-O-Si bonds to be broken. Based on experiments (35) it was concluded that the term E can be divided into three regions. The energy of activation for viscous flow of the pure nonmetallic oxide is very high. Then there is a rapid fall with the addition of the metallic oxide, whereupon there is a leveling off, which remains relatively unchanged till about 50 mole percent of metal oxide. There is a small reduction upon further addition (36). This is shown in figure 5. From this we also see that the energy change in the case of MO-SiO₂ type of systems is

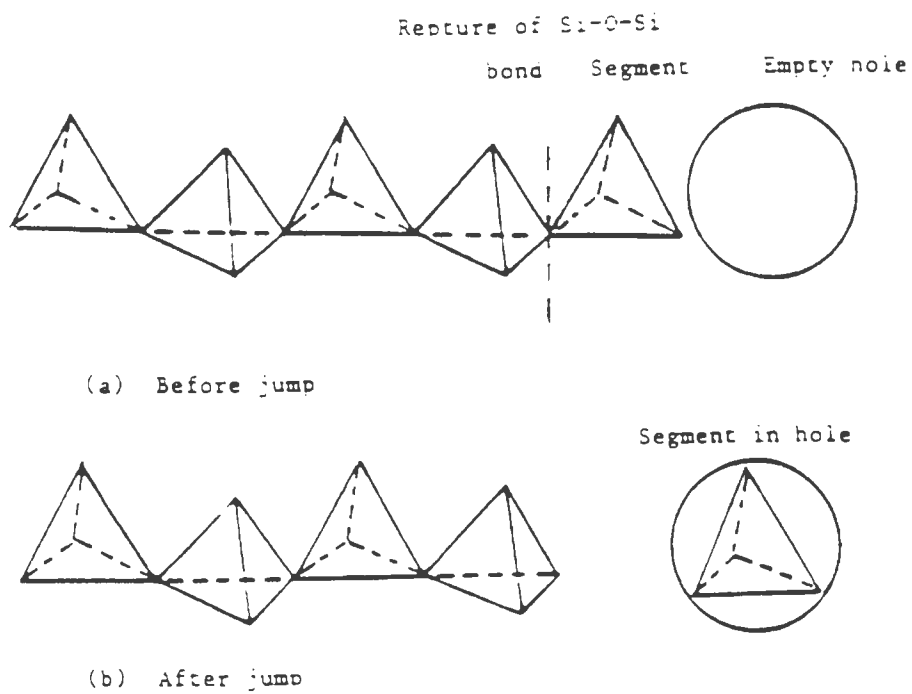


Fig.4-SCHEMATIC OF A SiO₂ CHAIN BREAKING AND JUMPING TO AN ADJACENT HOLE

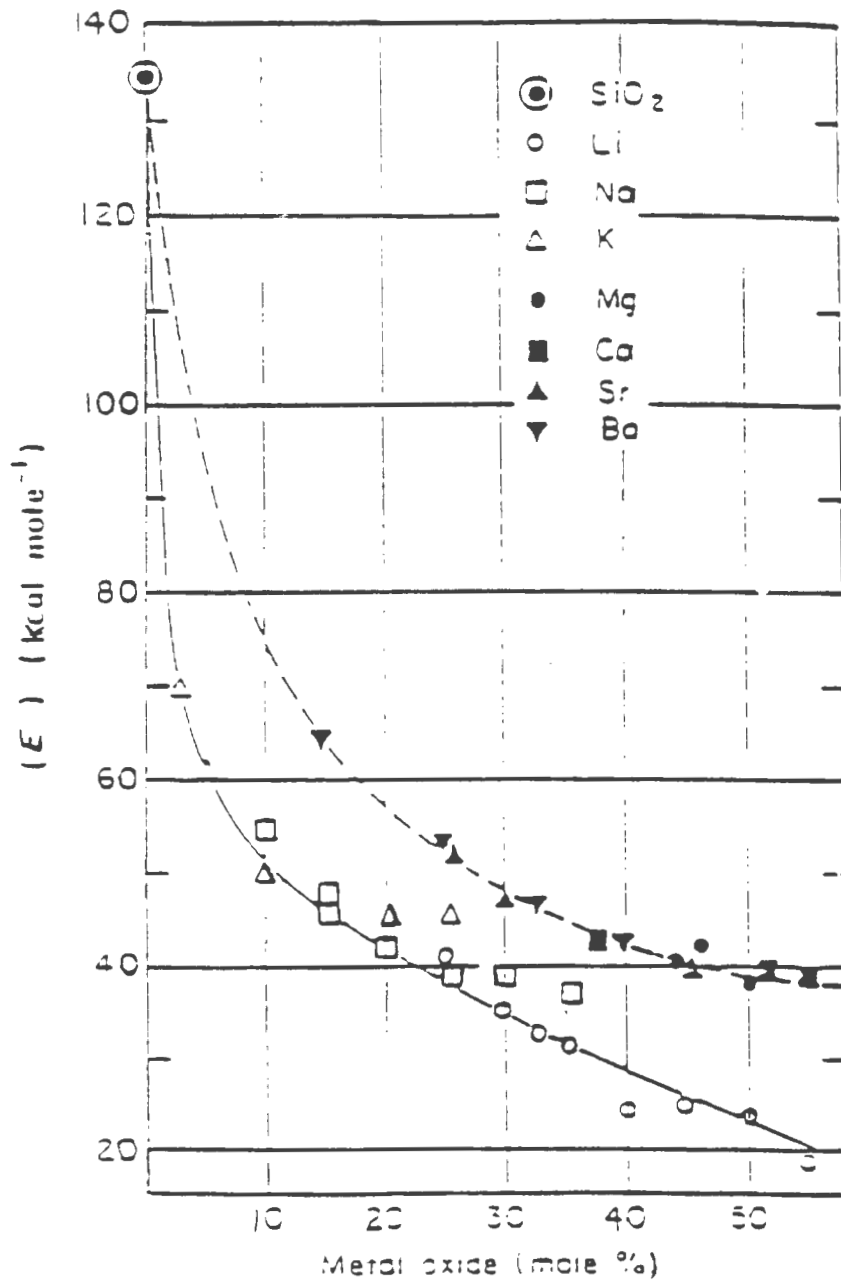


Fig.5-ENERGY CHANGES IN BINARY SYSTEMS

less as compared to that of M_2O-SiO_2 type of systems.

The value of E was calculated based on the available experimental viscosities using equation (1-4). All available experimental viscosity data has been used in obtaining a correlation between E and NO^0 . Available experimental viscosity data of all the $MO-SiO_2$ type of systems were clubbed together and similarly all the M_2O-SiO_2 were used together in reducing the polynomial expressions that is given below in equations (2-11 and 2-17). In cases where there was a lot of discrepancy in the published data, the more recent data have been used for the correlation as they are considered to be more accurate.

A correlation of these E values as a function of calculated NO^0 values was made. A fourth order polynomial expression gave better predictions in the case of $MO-SiO_2$ type of melts:

$$E = \alpha + \beta NO^0 + \gamma (NO^0)^2 + \delta (NO^0)^3 + \epsilon (NO^0)^4 \quad (2-11)$$

where $\alpha, \beta, \gamma, \delta,$ and ϵ are constants. These were further expressed as a function of temperature and the expressions obtained are given below (equations 2-12 to 2-16):

$$\alpha = 703820.4981 - 1.22206 \times 10^9 / T + 78.58757 \times 10^{+10} / T^2 \quad (2-12)$$

$$\beta = 1 / (-1.10344 \times 10^{-12} (-839.0098 + T)^2 - 1.87026 \times 10^{-6}) \quad (2-13)$$

$$\gamma = 954182.1129 + 1921.9294 T - 0.7953 T^2 \quad (2-14)$$

$$\delta = 1077387.128 + (-5732.0204) T + 1.8542 T^2 \quad (2-15)$$

$$\epsilon = (-809470.4077) + 3459.2634 T - 1.0581 T^2 \quad (2-16)$$

The constants $\alpha, \beta, \gamma, \delta$ and ϵ predicted using the above expressions were plugged into the polynomial expression (2-11) and the E values were thus calculated.

In the case of M_2O-SiO_2 , the constants were obtained using the following expressions (2-18 to 2-24), which was again plugged into equation (2-17) to give E.

$$E = \alpha + \beta(NO^0) + \gamma(NO^0)^2 + \delta(NO^0)^3 + \epsilon(NO^0)^4 + \zeta(NO^0)^5 + \kappa(NO^0)^6 \quad (2-17)$$

where,

$$\alpha = 150414 + 12.28T \quad (2-18)$$

$$\beta = 823802 + 171.88T \quad (2-19)$$

$$\gamma = -7074030 + 3097.8T \quad (2-20)$$

$$\delta = 2.73018E+7 - 14997.2T \quad (2-21)$$

$$\epsilon = -4.93182E+7 + 31569.2T \quad (2-22)$$

$$\zeta = 3.99832E+7 - 29460.8T \quad (2-23)$$

$$\kappa = -1.13349E+7 + 9942.6T \quad (2-24)$$

The E value that was calculated in this manner was substituted into equation (1-4) along with the NO^0 value to give the viscosity at a particular temperature and composition of the melt. The results obtained using these steps is applied to calculate viscosities in various binary silicate systems and the results obtained are discussed in the following chapter.

CHAPTER 3

RESULTS AND DISCUSSIONS

The viscosities of several silicate systems, CaO-SiO₂, MgO-SiO₂, MnO-SiO₂, BaO-SiO₂, SrO-SiO₂ and FeO-SiO₂ amongst MO-SiO₂ type of systems and Na₂O-SiO₂, K₂O-SiO₂ and Li₂O-SiO₂ amongst M₂O-SiO₂ systems were calculated at different temperatures by substituting the calculated values of E and NO⁰ into equation (1-4). The predicted viscosities were compared with the experimental viscosities and also with the data calculated values using the Riboud et al. (14) and Urbain et al. (15,16) models. The average percentage deviation, i.e. the average percentage of $(\log \eta_{cal} - \log \eta_{exp.})$ is calculated and the deviations in the individual systems are discussed below and also listed in Table 3.

3.1 PURE LIQUID SILICA:

The viscosity of pure liquid silica was calculated from equation (1-4) at 2223K using E equal to 519Kjoules/mol (37). The calculated value is 3.7×10^5 poise which is in good agreement with the experimental value of 1.72×10^5 poise that was reported by Rossin et al. (38). Similarly, viscosities of pure silica at other temperatures were calculated and are shown in the figures of the individual systems.

3.2 MO-SiO₂ TYPE OF SYSTEMS:

THE CaO-SiO₂ SYSTEM:

The data was available in the range of 0.42 to 0.6 XSiO₂ and in the temperature range of 1773 to 2073K. Data has been collected from various sources (5,39-41). Mills and Keene (39) have reported the data of various investigators (41-46) at 1873K. Bottinga et al. (5) have compiled data at various temperatures from several publications (41,47,48). The entire composition range that has been investigated lies well within the liquid portion of the phase diagram (49) and no error could have risen as a result of the presence of solids. However, most of the investigators have used the rotating cylinder method for measuring viscosities using graphite crucibles and bobs. But Endell et al. (42) have used platinum crucibles and bobs while Bockris and Lowe (41) have used molybdenum accessories. The use of graphite crucibles and bobs could lead to the formation of carbides in the melt and affect the viscosity values. Figures 6 to 8 show the variation of viscosity with mole fraction silica for several temperatures. As seen from the figures there is very good agreement between the calculated and experimental data. The average percentage deviation in the case of our model is 3.5% and the corresponding values in the case of Riboud et al. model and Urbain et al. models are 15.4% and 7.6% respectively. The variations within the experimental viscosities are reported to

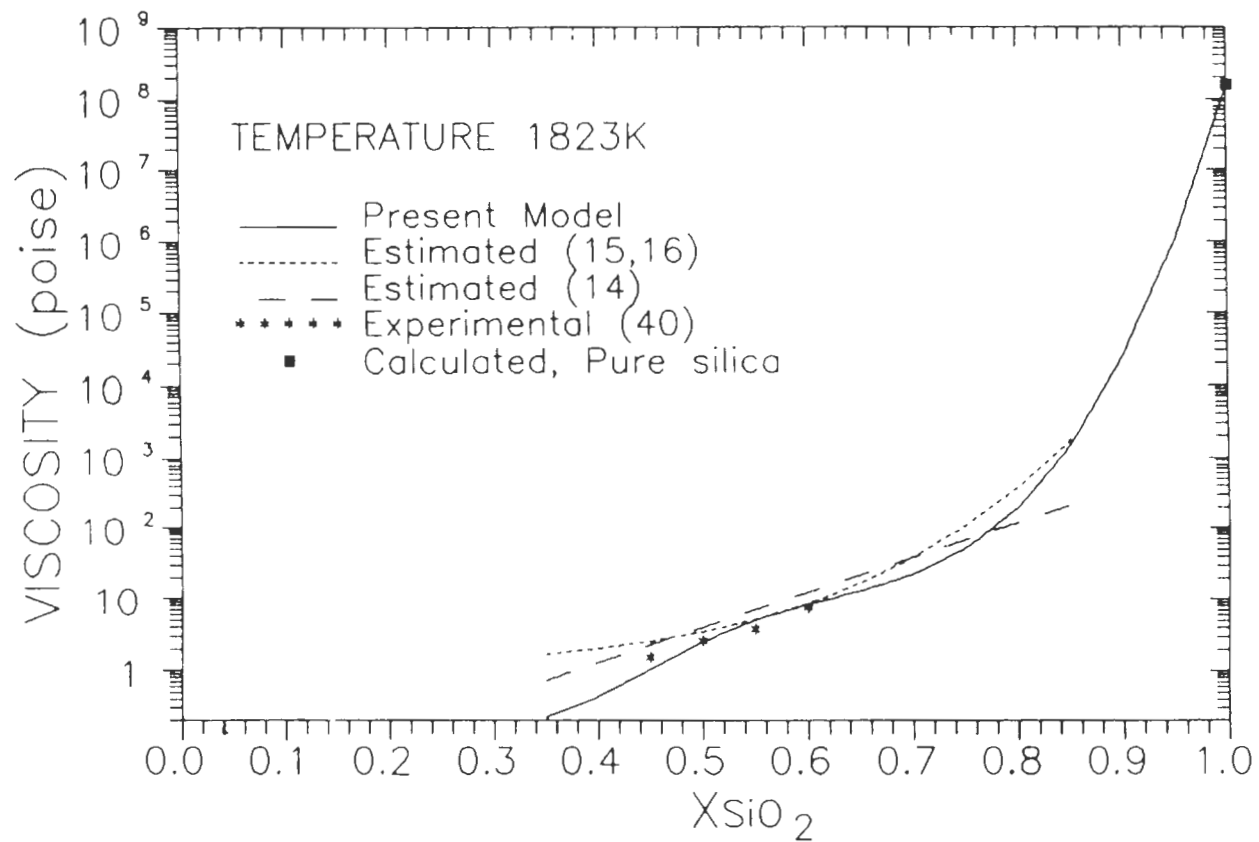


Fig.6—EXPERIMENTAL AND PREDICTED VISCOSITIES OF CaO-SiO₂ MELTS

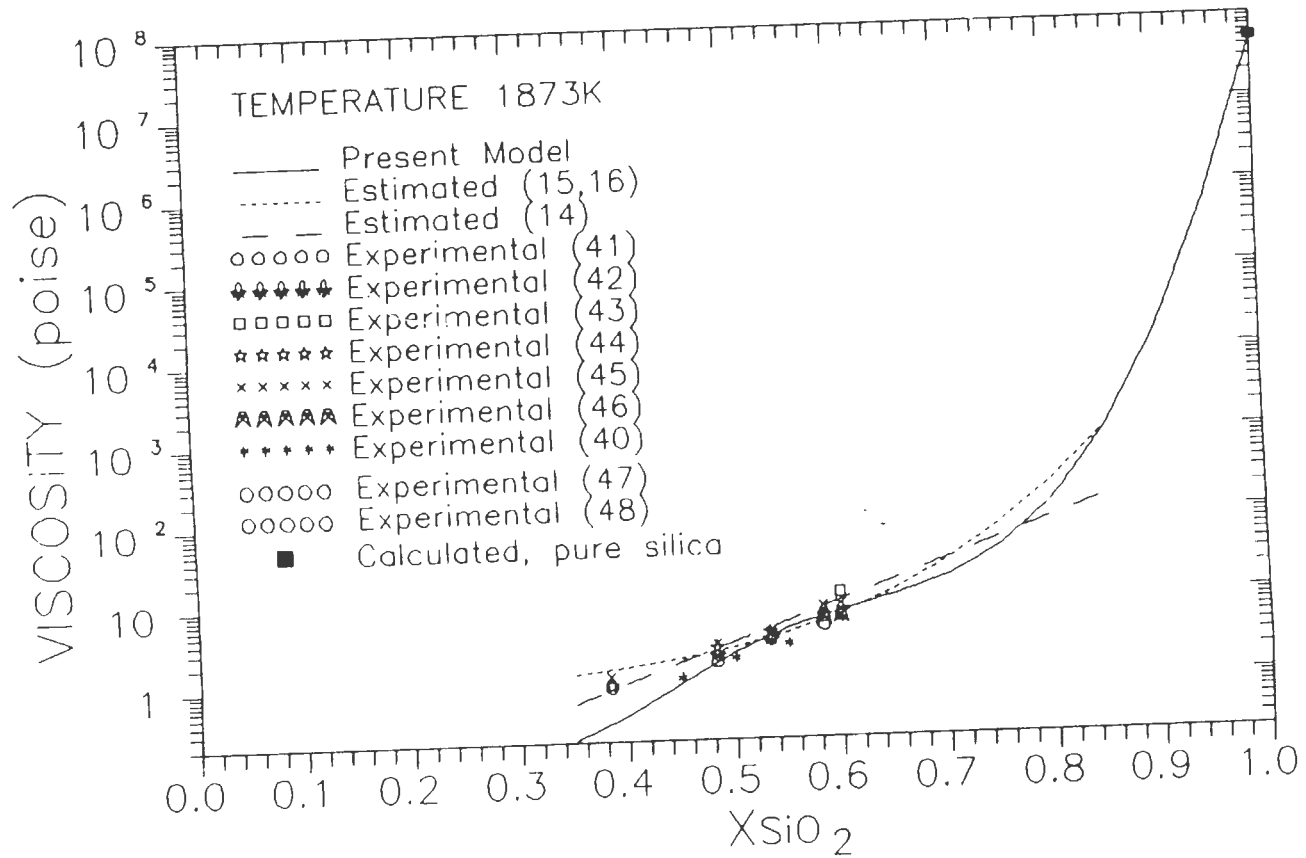


Fig.7—EXPERIMENTAL AND PREDICTED VISCOSITIES OF CaO—SiO₂ MELTS.

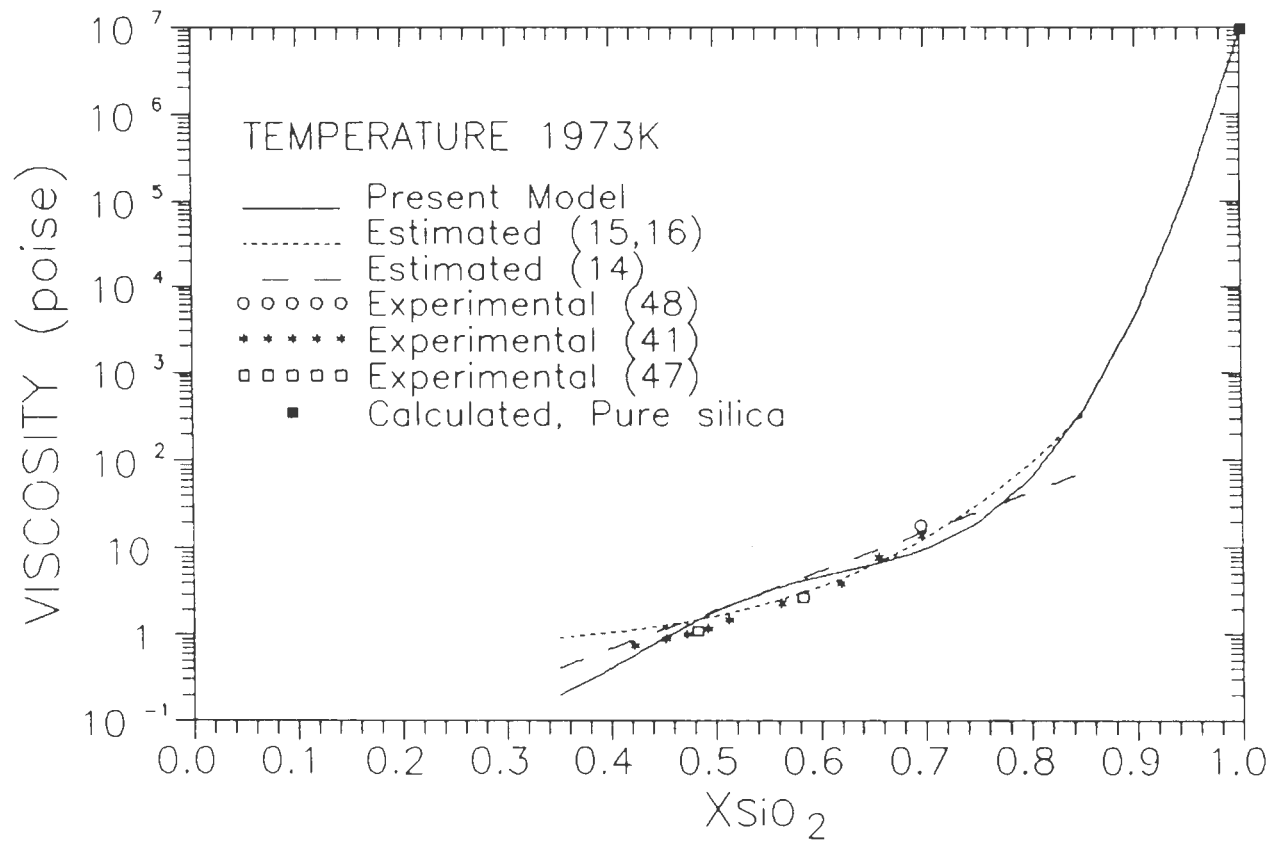


Fig.8—EXPERIMENTAL AND PREDICTED VISCOSITIES OF CaO—SiO₂ MELTS.

be 25-30% (39). Considering this, the deviations of the predicted viscosity values from the experimental viscosity data is rather small. The standard free energy for solid Ca_2SiO_4 has been used here and slightly lower values are expected when the liquid data is used. The upper limit of the Riboud et al. (14) and Urbain et al. (15,16) model have been set at 0.85 XSiO_2 , as there is, in general, no experimental data available above this. The lower limit is set at 0.34 XSiO_2 for all the three models. In the present model, a sharp decrease in viscosity is observed below this limit.

THE MgO-SiO₂ SYSTEM:

The data was available in the range of 0.49 to 0.56 XSiO_2 and in the temperature range of 1823 to 2073K. Mills and Keene (39) compiled experimental viscosity data of several investigators at 1873K (46,50,51). Experimental viscosity data for other temperatures were obtained from Bockris et al. (50). The data at lower temperatures maybe erroneous as almost the entire region that has been investigated at this temperature lies in the two phase region (49) and the presence of solids could affect the viscosity values as discussed in the section (1.2.2), on effect of solids. Bockris et al. (50) have used the rotating crucible method to determine viscosities using molybdenum crucibles and bobs, while Hofmann (51) have used the rotating cylinder method with graphite crucibles and bobs.

The variation of viscosities as a function of X_{SiO_2} for several temperatures are shown in figures 9 to 13. As seen from the figures the agreement between the calculated and experimental viscosities is excellent. The average percentage deviation in the case of the present model is -3.13%. The corresponding values in the Riboud et al. (14) and Urbain et al. (15,16) models are -1.12% and -11.12% respectively. The upper and lower limits for the Riboud et al. (14) and Urbain et al. (15,16) models are set at almost the same values as in the case of CaO-SiO₂ system.

THE MnO-SiO₂ SYSTEM:

Viscosity data has been collected mainly from Mills and Keene (39) who have used the viscosity data of Towers et al. (52) at temperatures 1673K, 1773K and 1873K in the range of 0.34 to 0.53 X_{SiO_2} and Bell (53) at 1673K. At higher temperatures in the range investigated the melt lies in the two phase region of cristobalite + liquid (above 1743K) and tridymite between 1564K and 1743K, especially at higher mole fractions of silica (49). Mills and Keene (39) have reported that according to Bell (53) the slags of this system appeared to be non-Newtonian in behavior. The oscillational method of determining viscosities have been used with platinum crucibles and bobs. The viscosity as a function of X_{SiO_2} at 1673K and 1773K are shown in figures 14 and 15. Excellent agreement is

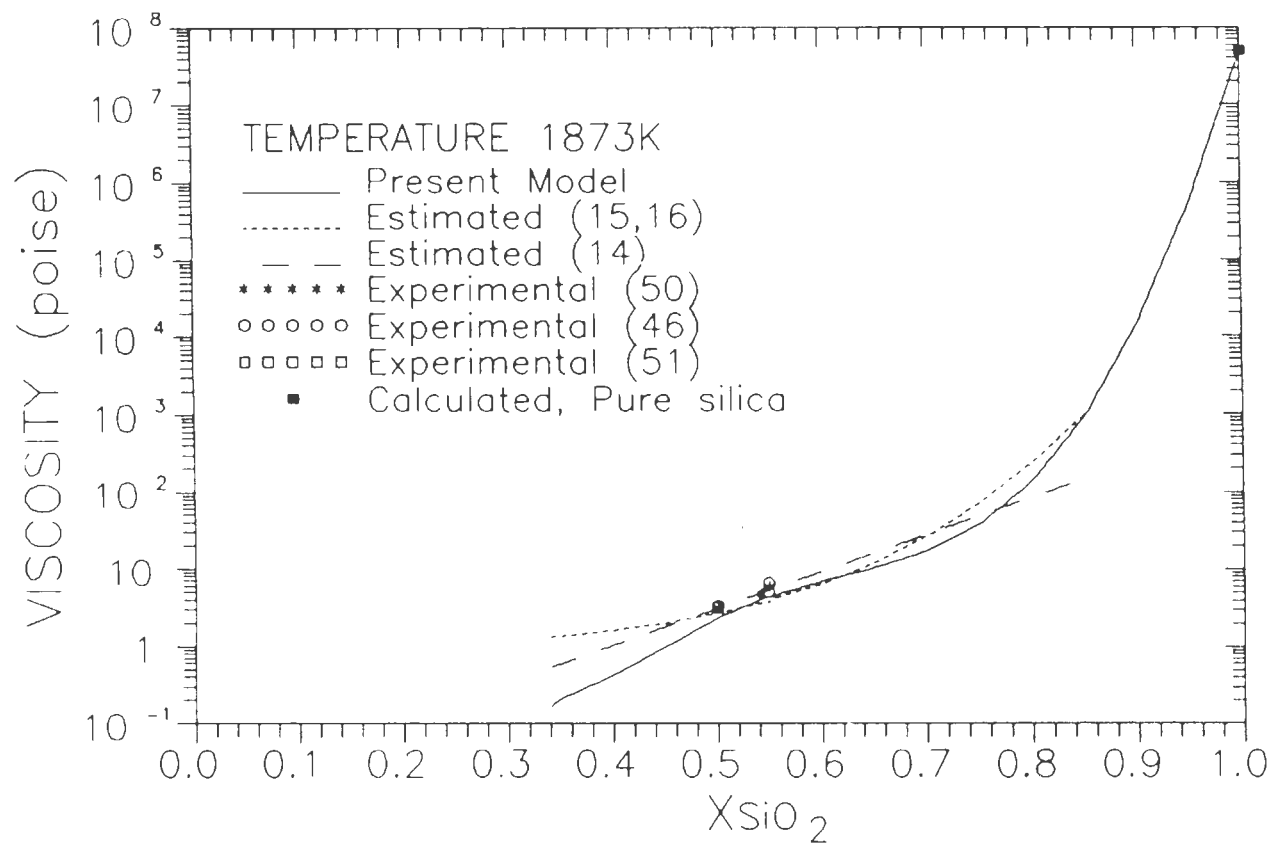


Fig.9—EXPERIMENTAL AND PREDICTED VISCOSITIES OF MgO—SiO₂ MELTS.

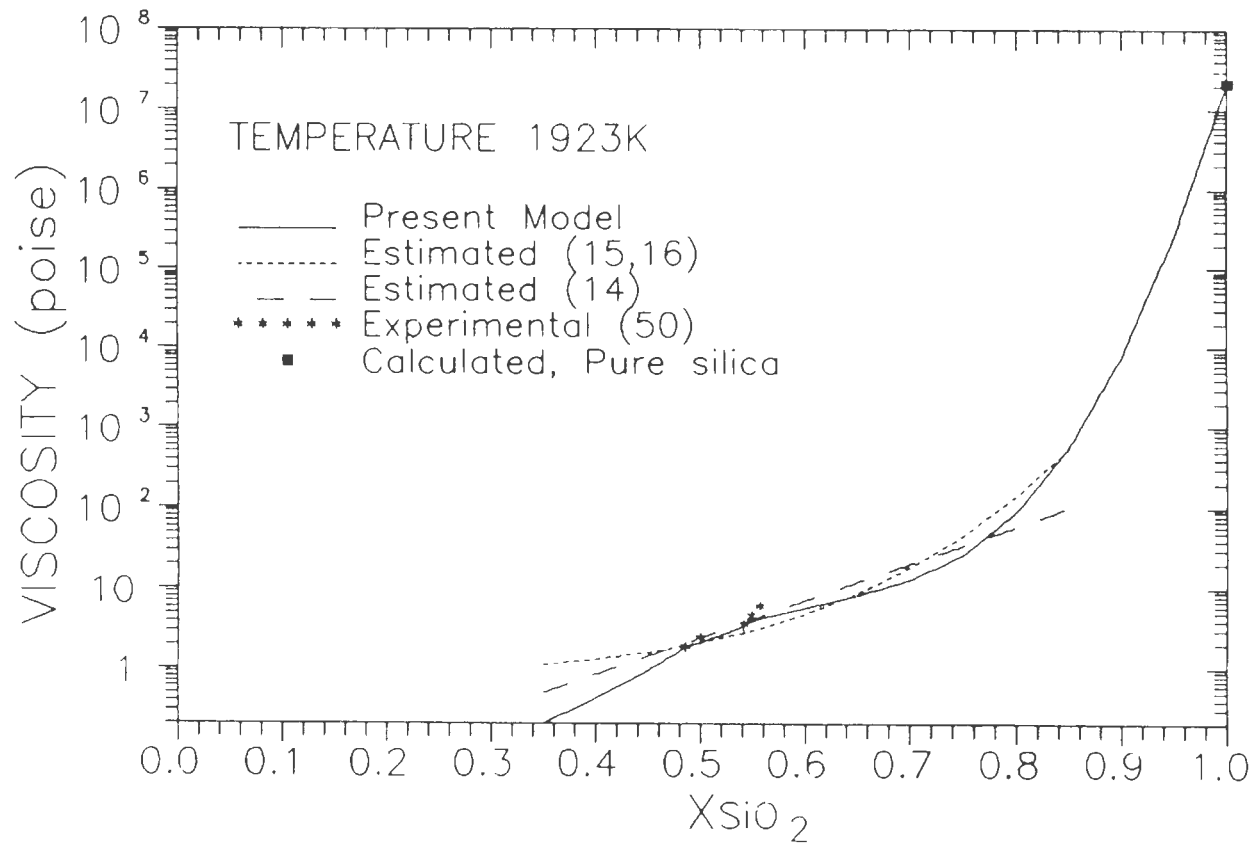


Fig.10—EXPERIMENTAL AND PREDICTED VISCOSITIES OF MgO-SiO₂ MELTS.

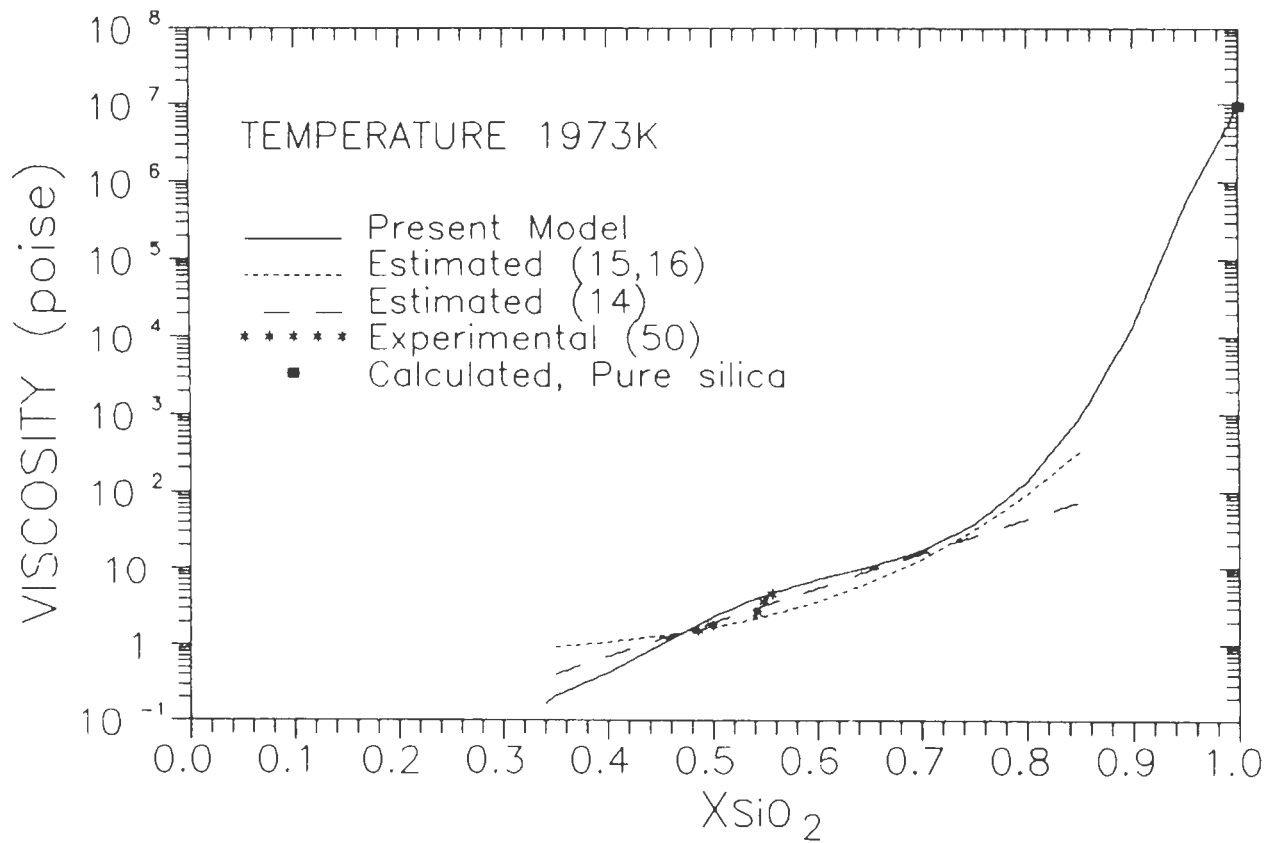


Fig.11—EXPERIMENTAL AND PREDICTED VISCOSITIES OF MgO-SiO₂ MELTS.

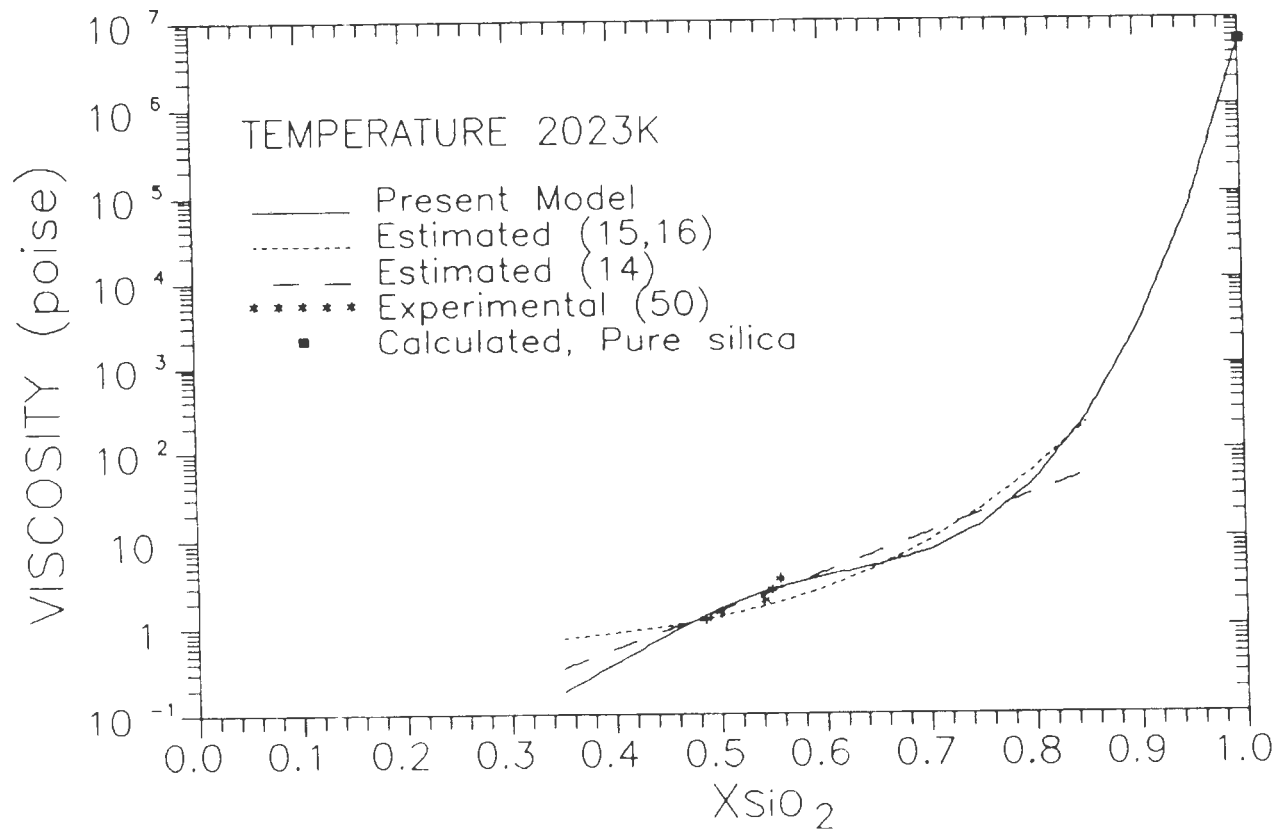


Fig.12—EXPERIMENTAL AND PREDICTED VISCOSITIES OF MgO—SiO₂ MELTS.

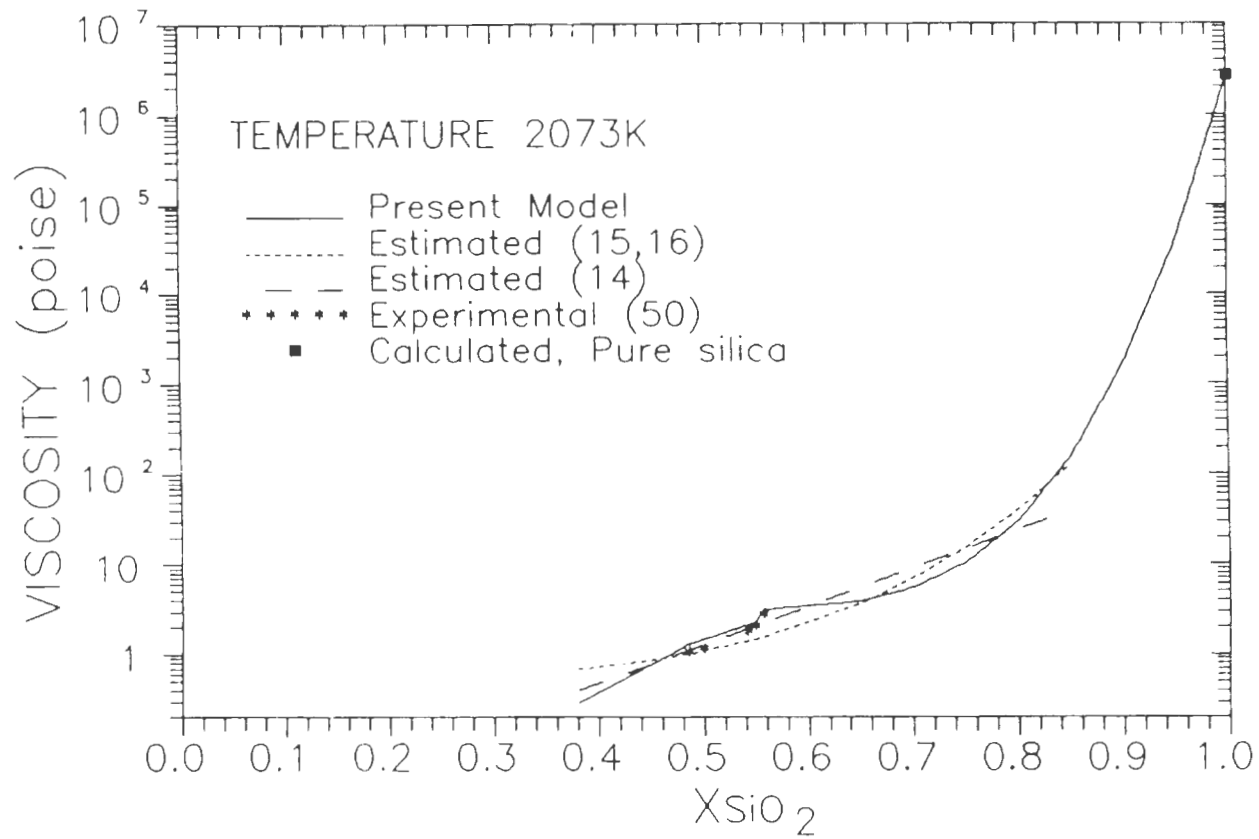


Fig.13—EXPERIMENTAL AND PREDICTED VISCOSITIES OF MgO—SiO₂ MELTS

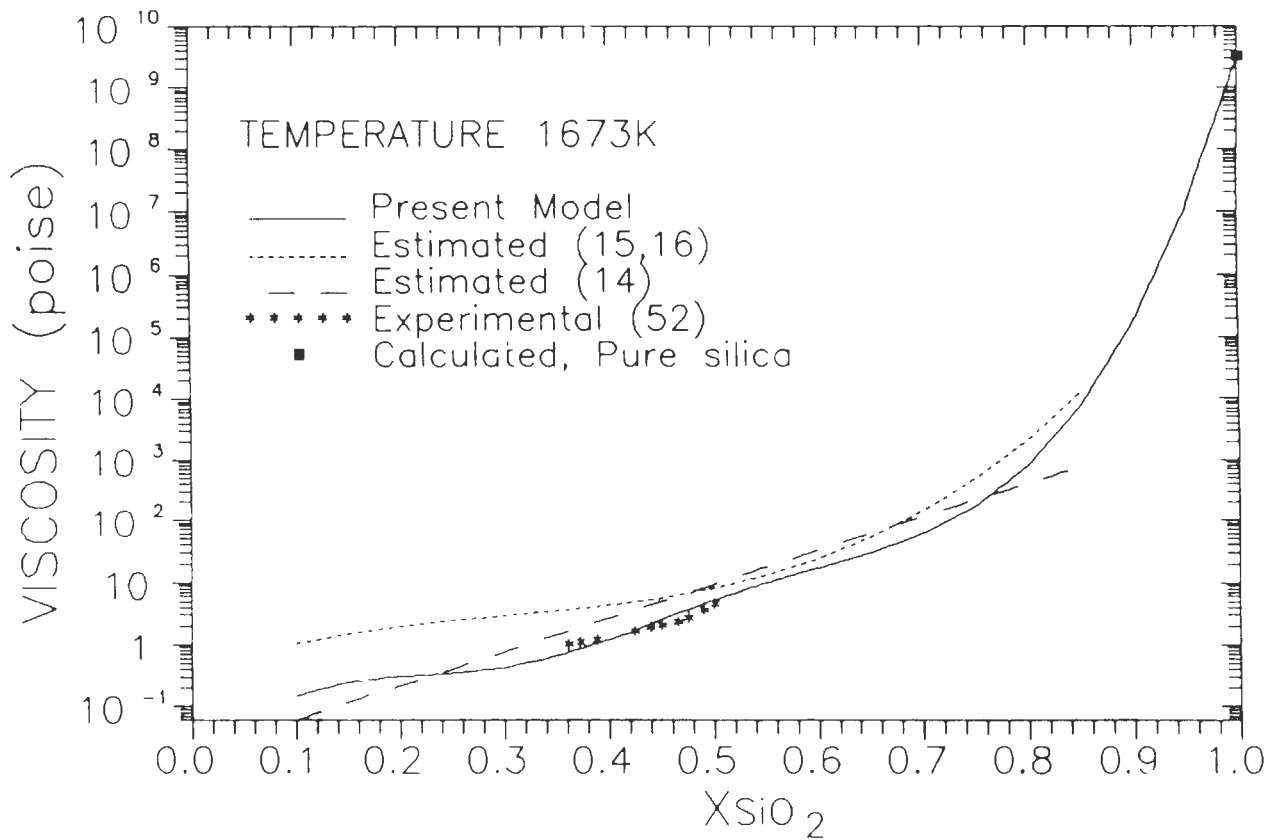


Fig.14—EXPERIMENTAL AND PREDICTED VISCOSITIES OF MnO—SiO₂ MELTS.

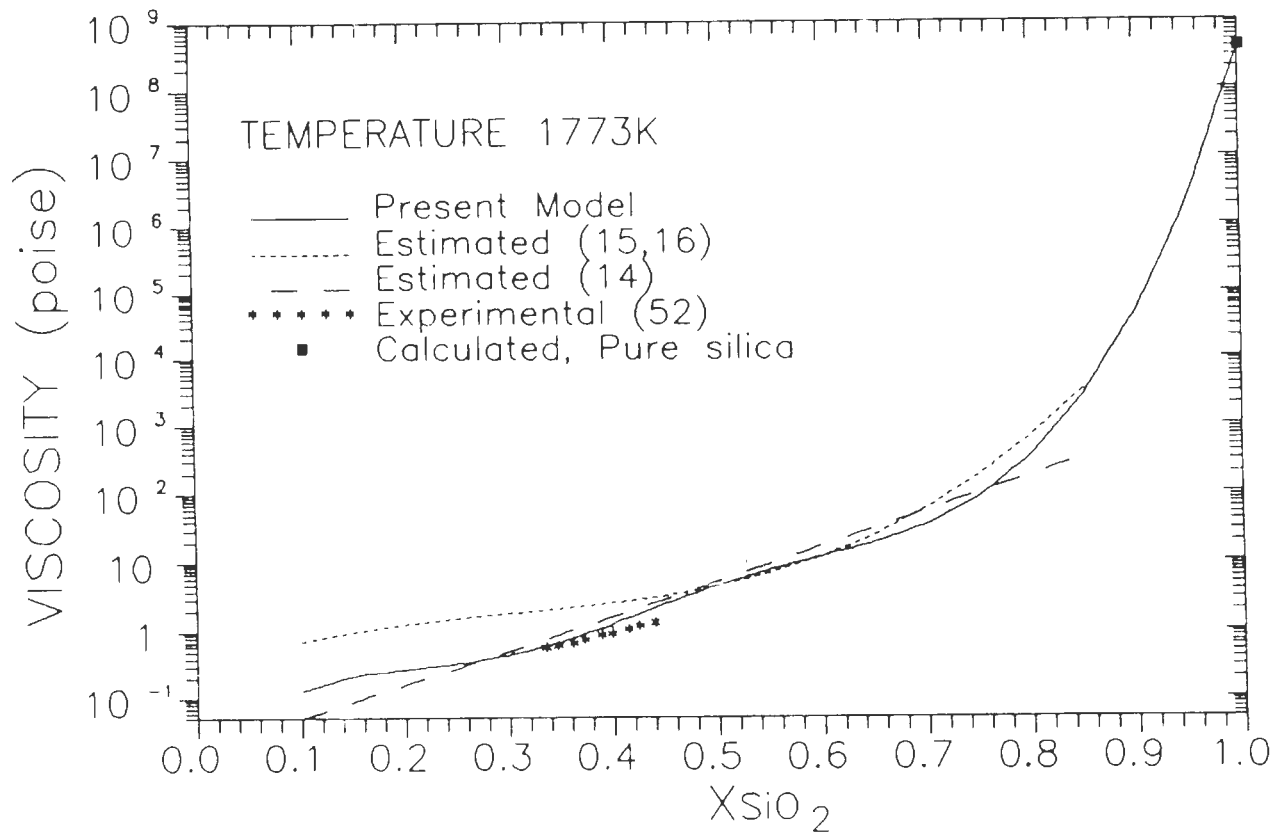


Fig.15—EXPERIMENTAL AND PREDICTED VISCOSITIES OF MnO-SiO₂ MELTS.

seen between the experimental and calculated data. The average deviation is 8% in the case of the present model. The corresponding average percentage deviations in the case of Riboud et al. (14) and Urbain et al. (15,16) are 24.8% and 38.5% respectively. The upper limit for the Riboud et al. (14) and Urbain et al. (15,16) models is $0.85X_{SiO_2}$, which is the same as in the $CaO-SiO_2$ and $MgO-SiO_2$ systems but the lower limit is set at $0.1 X_{SiO_2}$.

THE BaO-SiO₂ SYSTEM:

Viscosity data for this system have been those that were determined by Bockris et al. (50) and Mizoguchi et al. (54) in the temperature range of 1773 to 2073K and X_{SiO_2} of 0.50 to 0.85. The data compiled (50,48) by Bottinga et al. (5) have also been used. The entire range of experimental data lies in the liquid region of the BaO-SiO₂ phase diagram (49). Bockris et al. (50) have used Molybdenum crucibles and bobs at lower temperatures, but at temperatures above 2173K, serious reactions between the melt and Mo occurred and they were forced to use W coated crucibles. The predicted and experimental data have been shown in Figures 16 to 22. In this system the free energy data for solid silicate has been used. The average percentage deviations in the case of the present model is -3.6% while the Riboud et al. (14) and Urbain et al. (15,16) models give average percentage deviations of 6% and 2.1%. The

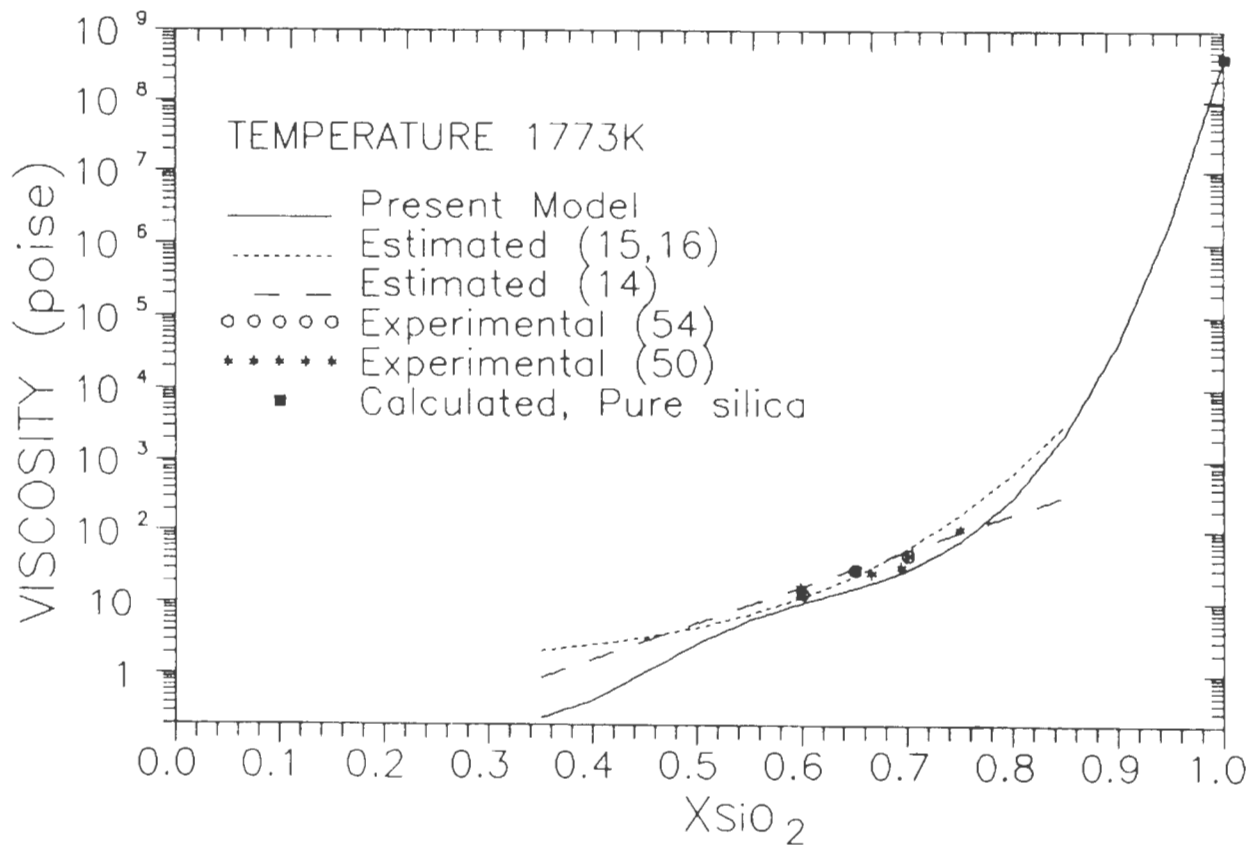


Fig.16-EXPERIMENTAL AND PREDICTED VISCOSITIES OF BaO-SiO₂ MELTS

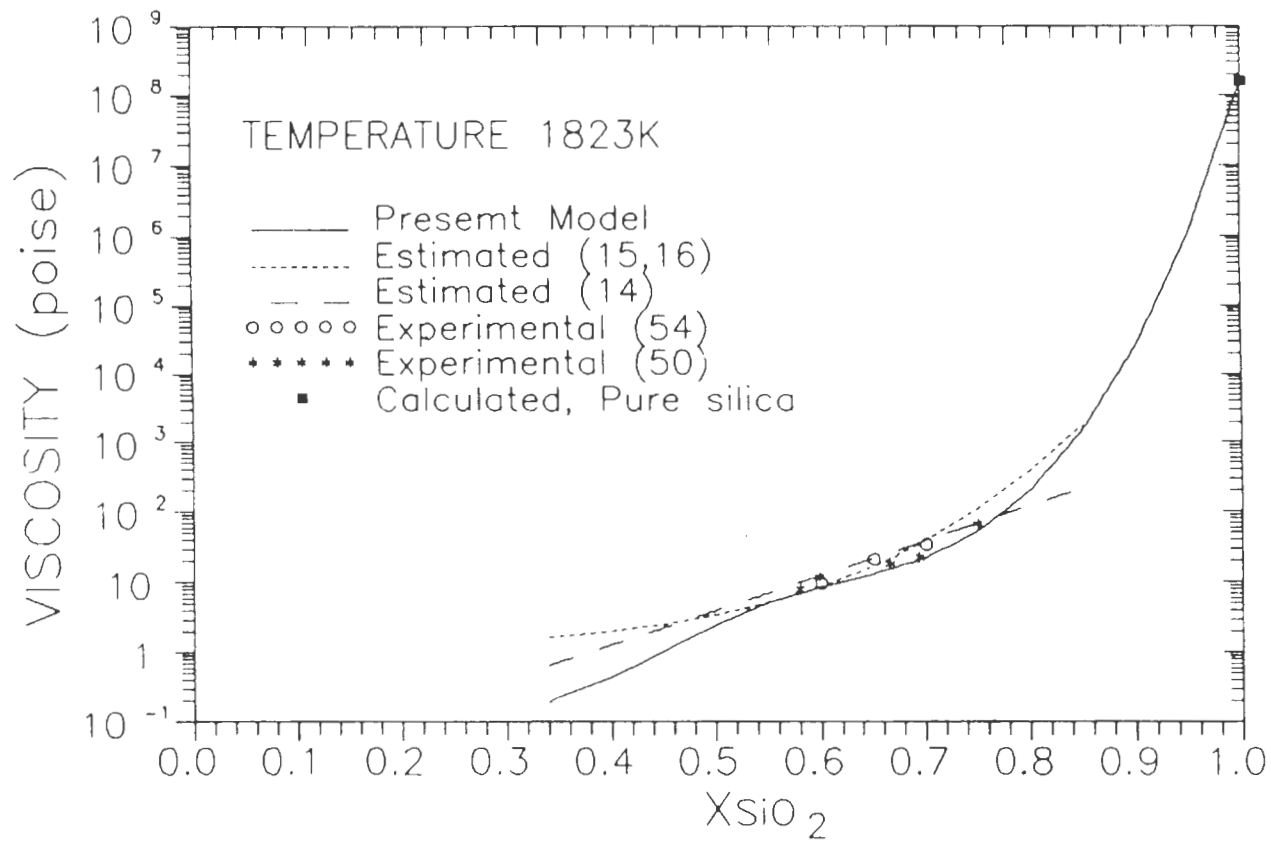


Fig.17—EXPERIMENTAL AND PREDICTED VISCOSITIES OF BaO-SiO₂ MELTS

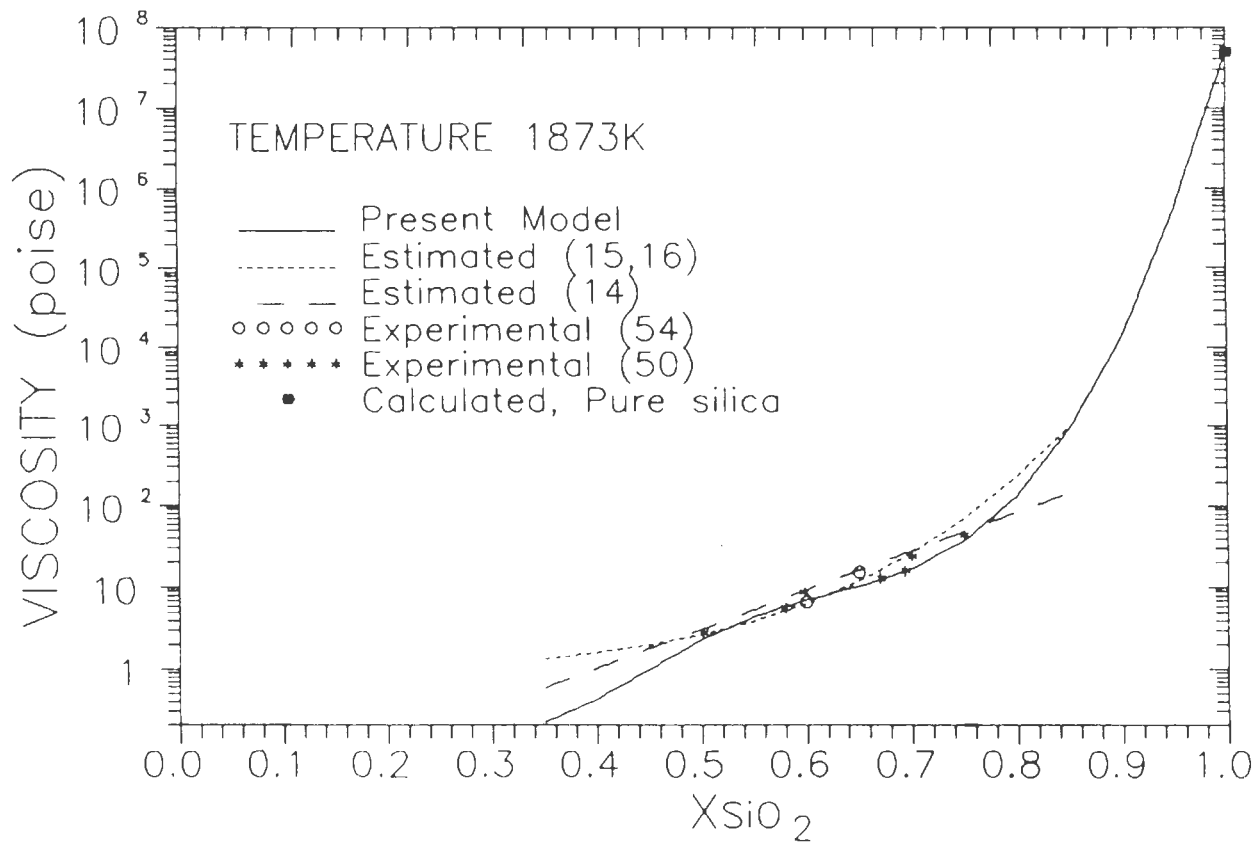


Fig.18—EXPERIMENTAL AND PREDICTED VISCOSITIES
OF BaO—SiO₂ MELTS

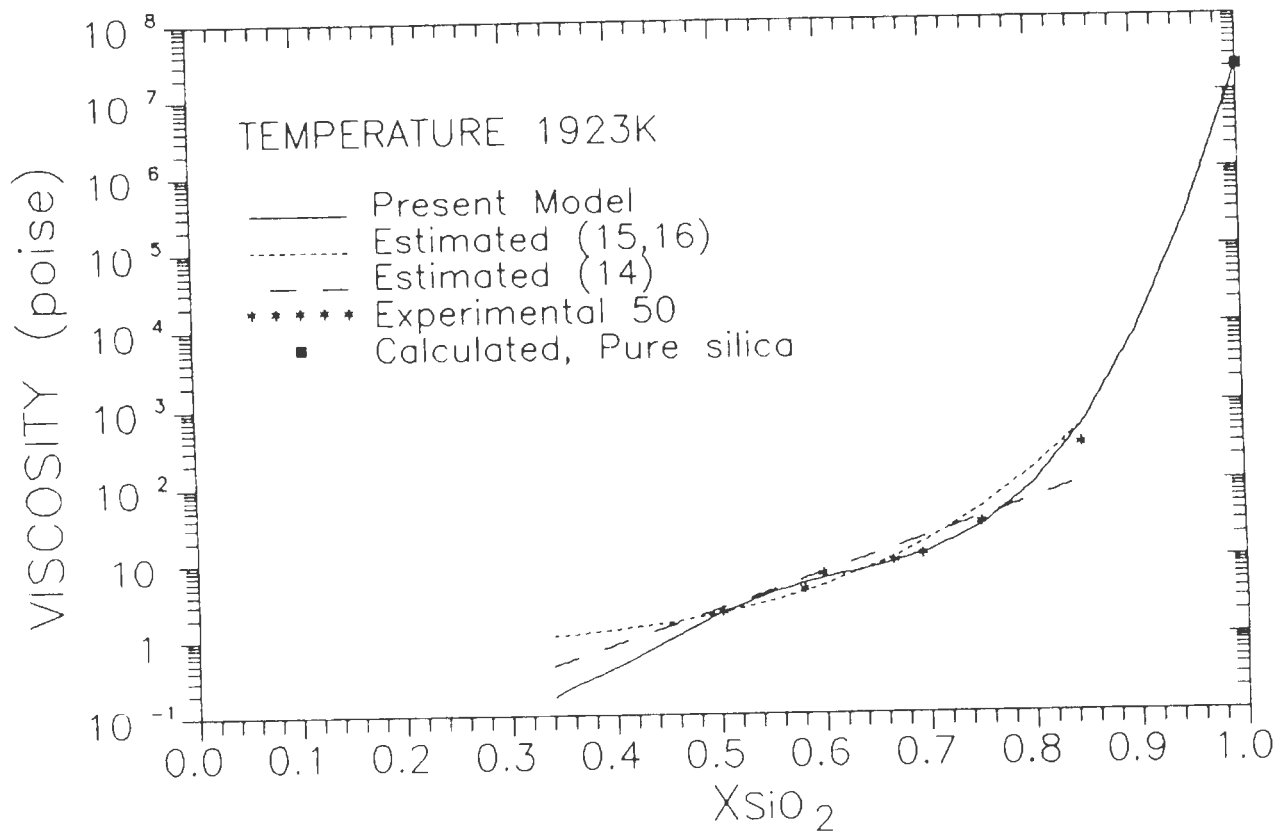


Fig.19—EXPERIMENTAL AND PREDICTED VISCOSITIES OF BaO-SiO₂ MELTS

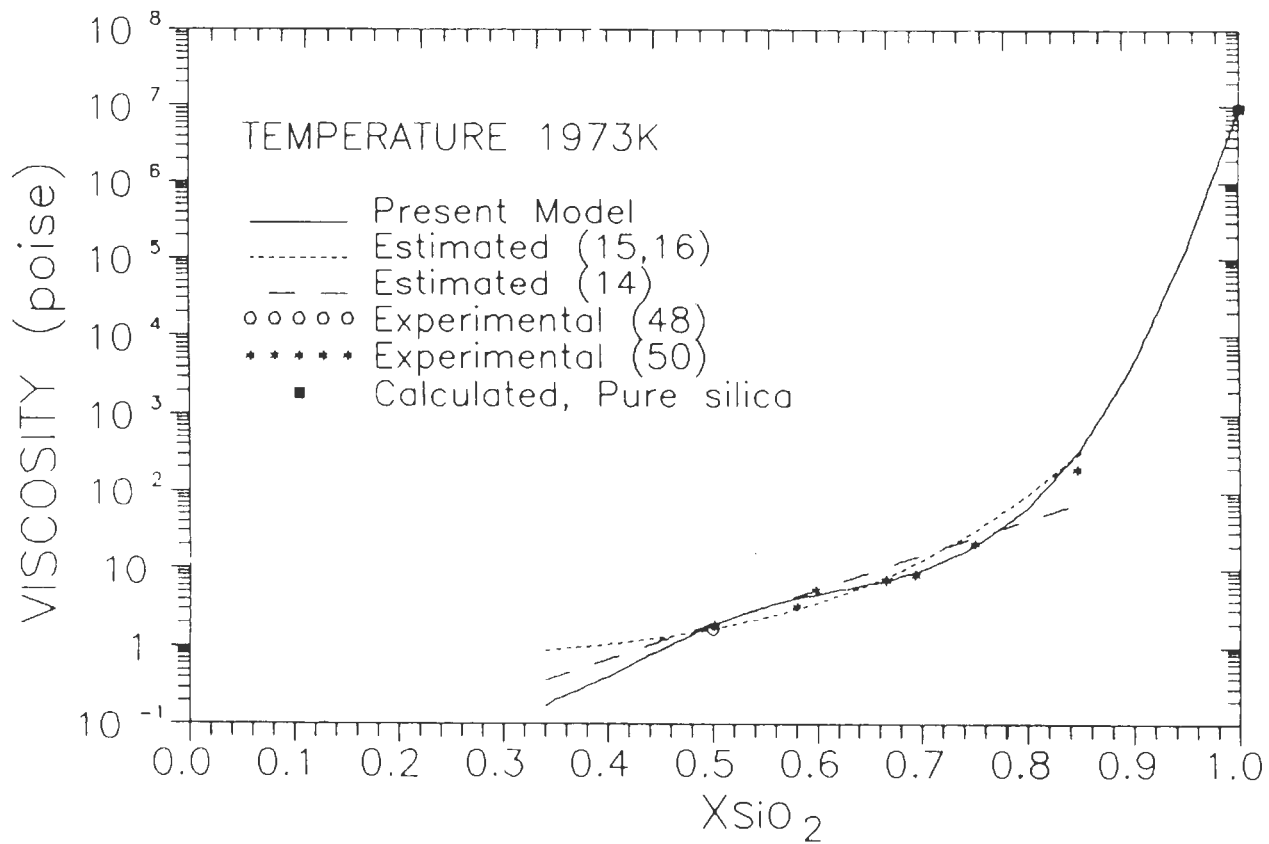


Fig.20—EXPERIMENTAL AND PREDICTED VISCOSITIES OF BaO-SiO₂ MELTS

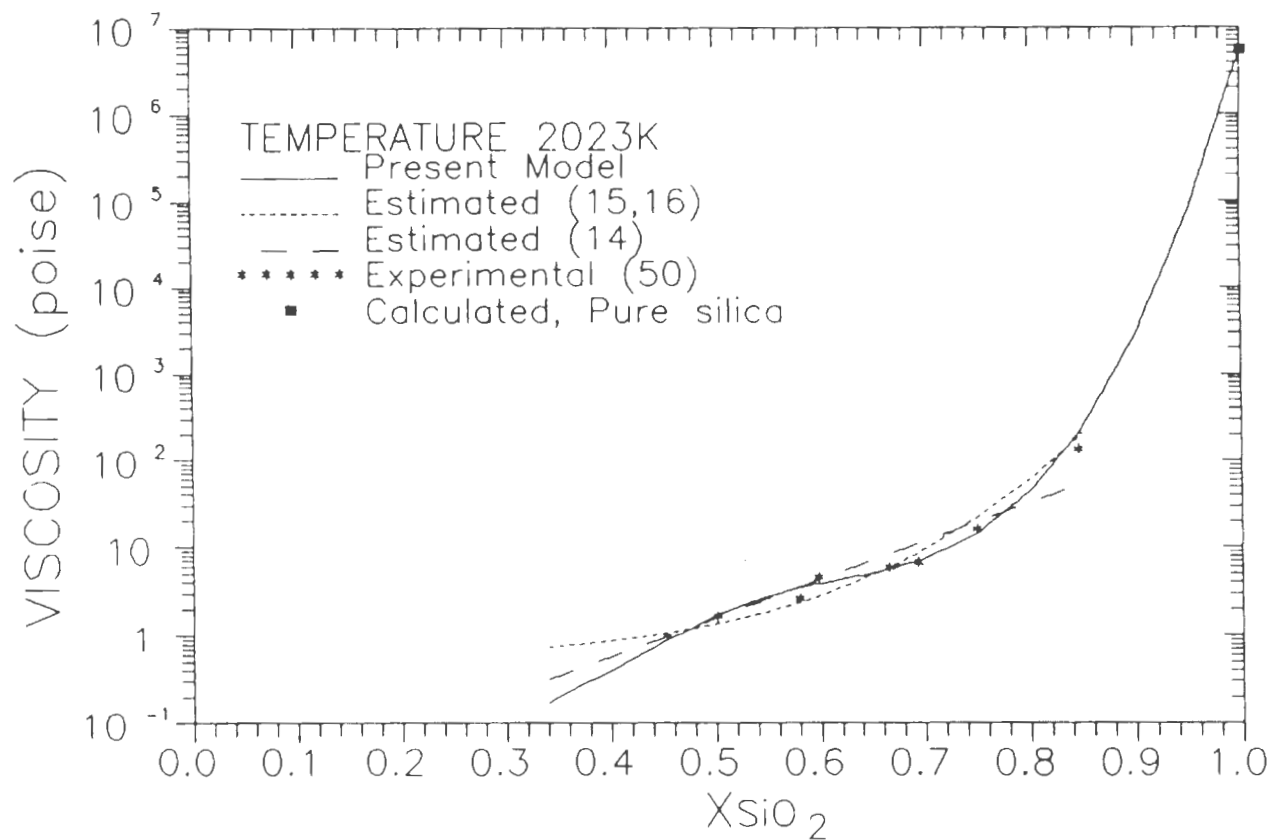


Fig.21—EXPERIMENTAL AND PREDICTED VISCOSITIES OF BaO-SiO₂ MELTS

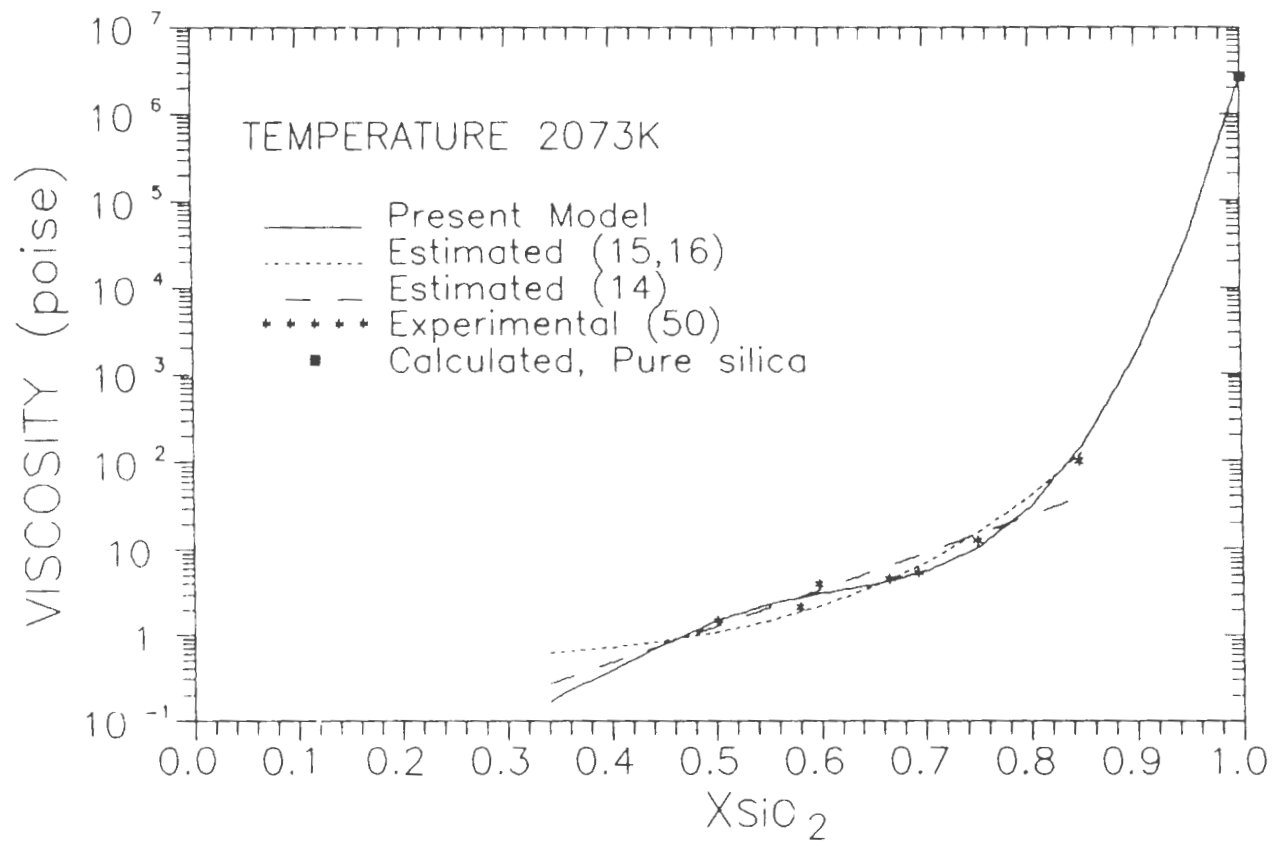


Fig.22—EXPERIMENTAL AND PREDICTED VISCOSITIES OF BaO-SiO₂ MELTS

upper limit for the Riboud et al. (14) and Urbain et al. (15,16) models are set at the same values as mentioned above and the lower limit is set at $0.34XSiO_2$.

THE SrO-SiO₂ SYSTEM:

The data for this system was obtained from the same sources as the BaO-SiO₂ system in the range 0.5 to 0.8 XSiO₂ and 1773-2073K. At lower temperatures in this range the melt lies in the two phase region at low silica mole fractions (49) and errors could arise as a result. The crucibles and bobs used were made of Mo and at temperatures higher than 2173K, crucibles coated with W were used. The data are plotted together with the predicted viscosities in Figures 23 to 28 for the temperature range 1773 to 2073K. The agreement is good with average percentage deviations of -4% in the case of the present model, 5% in the Riboud et al. model and 3% in the Urbain et al. model. The upper and lower limits for the other two models, are set at almost the same values as in the case of the BaO-SiO₂ system. Free energy of solid silicate has been used in this system also.

The FeO-SiO₂ SYSTEM:

Data have been collected from various sources in the composition range $0.1 < XSiO_2 < 0.42$ and the temperature range of 1523 to 1673K. Mills and Keene (39) have compiled the data

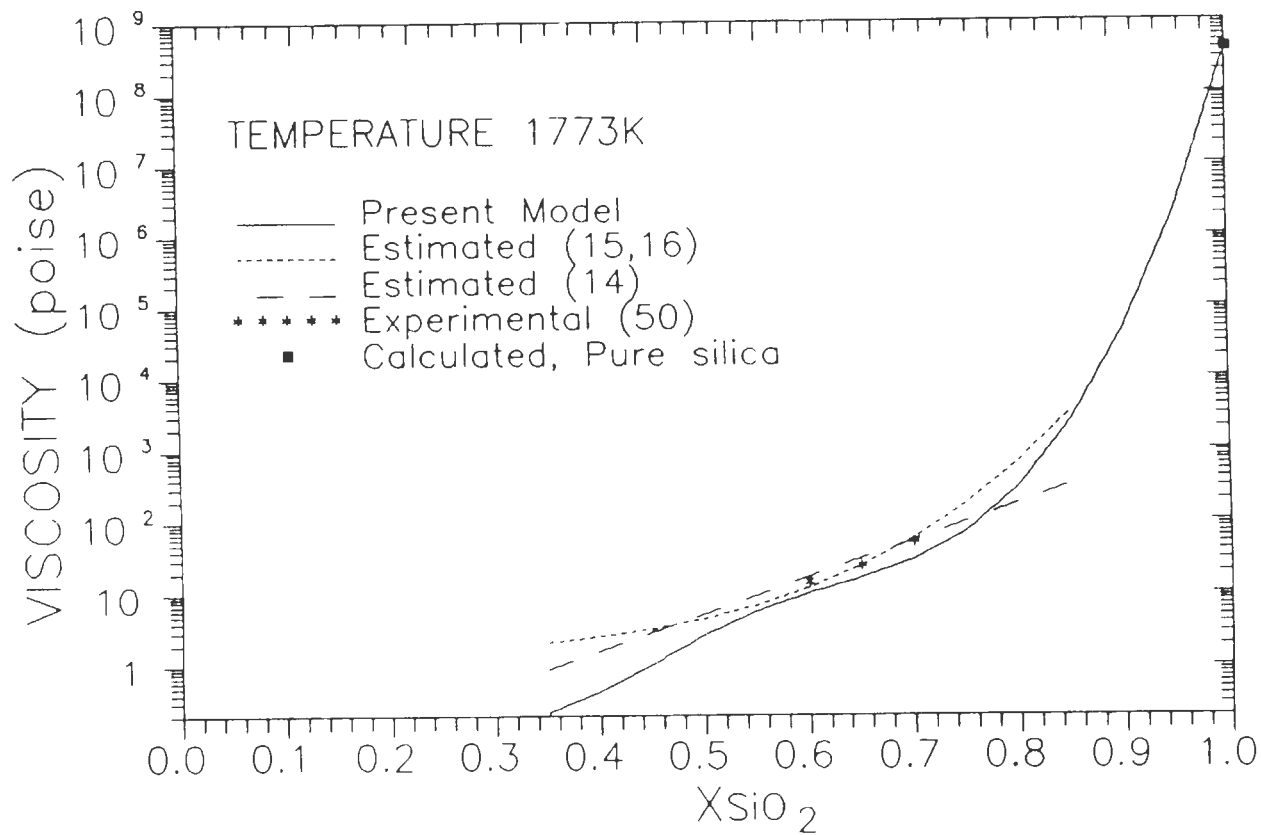


Fig.23—EXPERIMENTAL AND PREDICTED VISCOSITIES OF SrO-SiO₂ MELTS

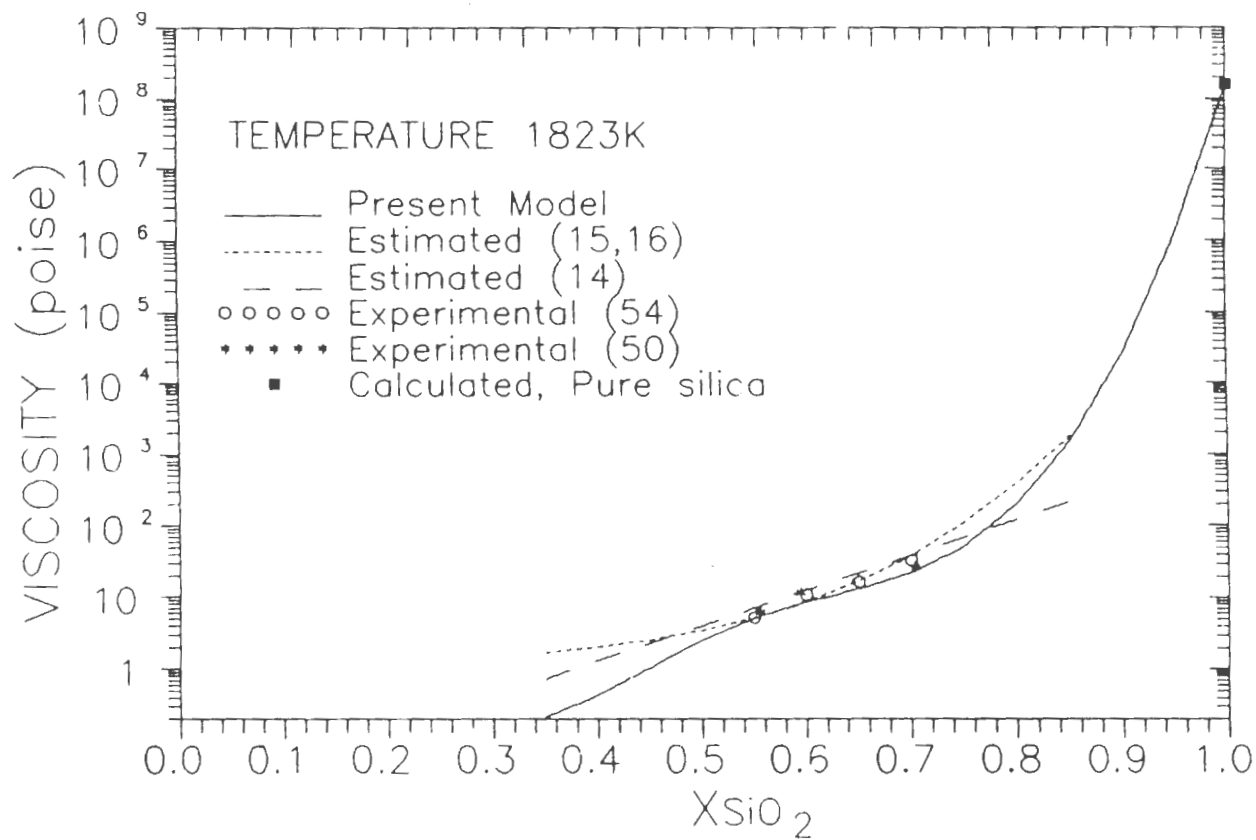


Fig.24—EXPERIMENTAL AND PREDICTED VISCOSITIES OF SrO-SiO₂ MELTS

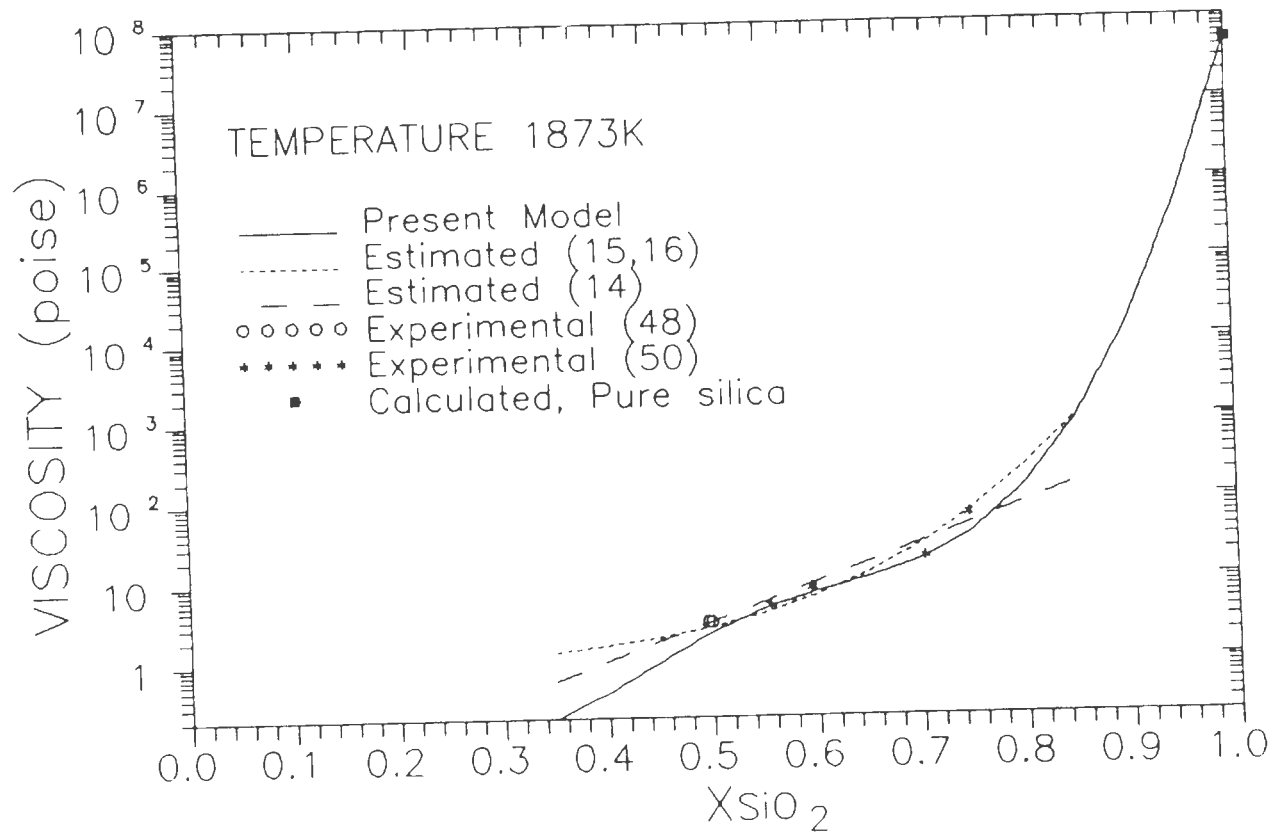


Fig.25—EXPERIMENTAL AND PREDICTED VISCOSITIES OF SrO-SiO₂ MELTS

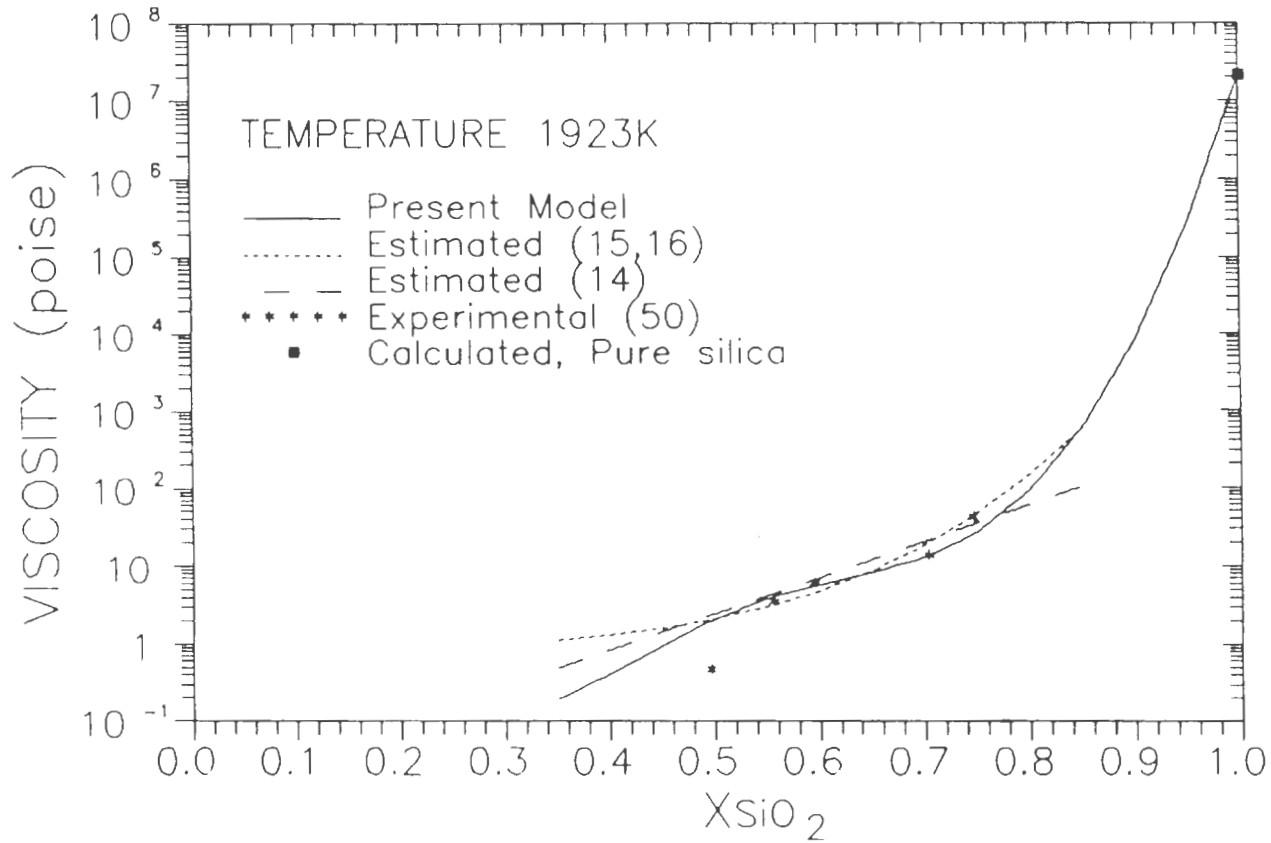


Fig.26—EXPERIMENTAL AND PREDICTED VISCOSITIES OF SrO-SiO₂ MELTS

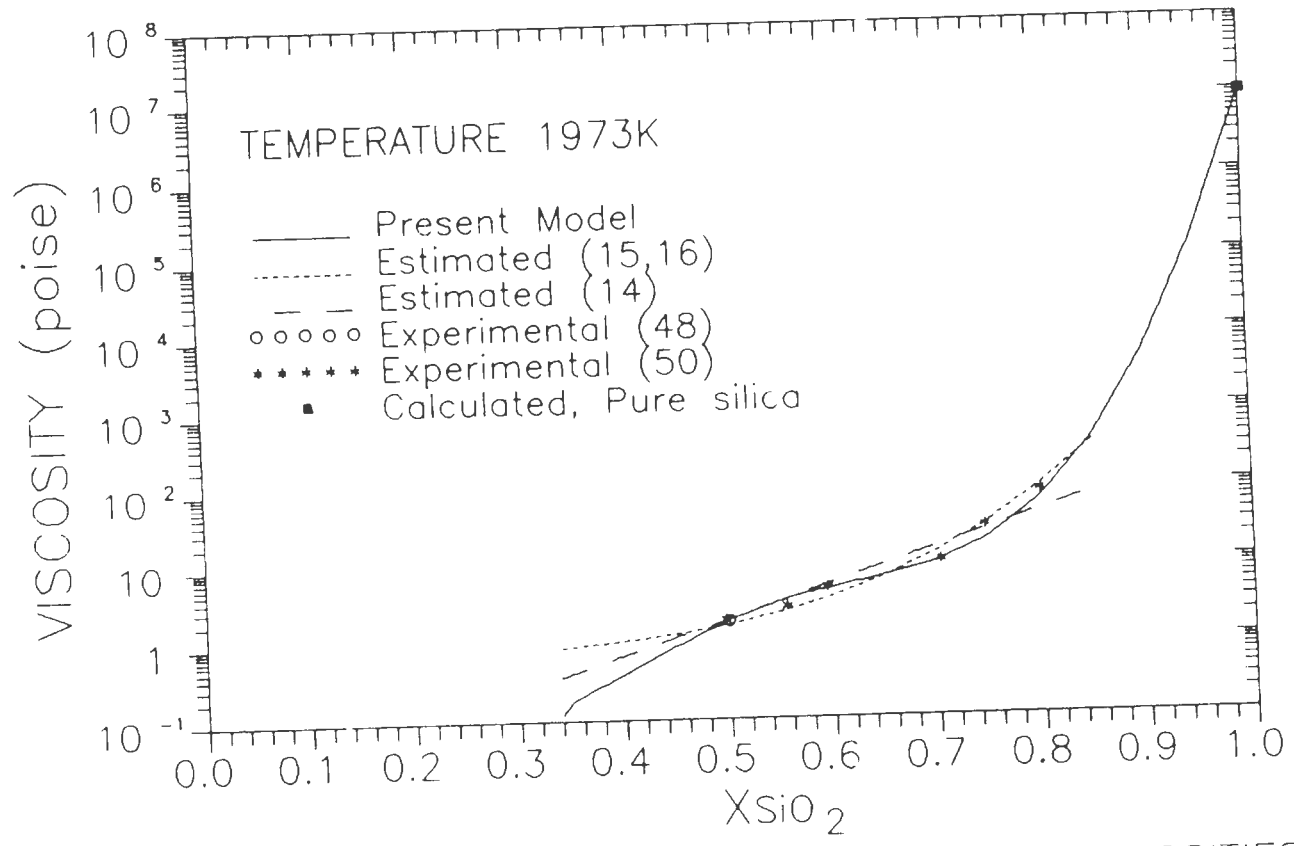


Fig.27-EXPERIMENTAL AND PREDICTED VISCOSITIES OF SrO-SiO₂ MELTS

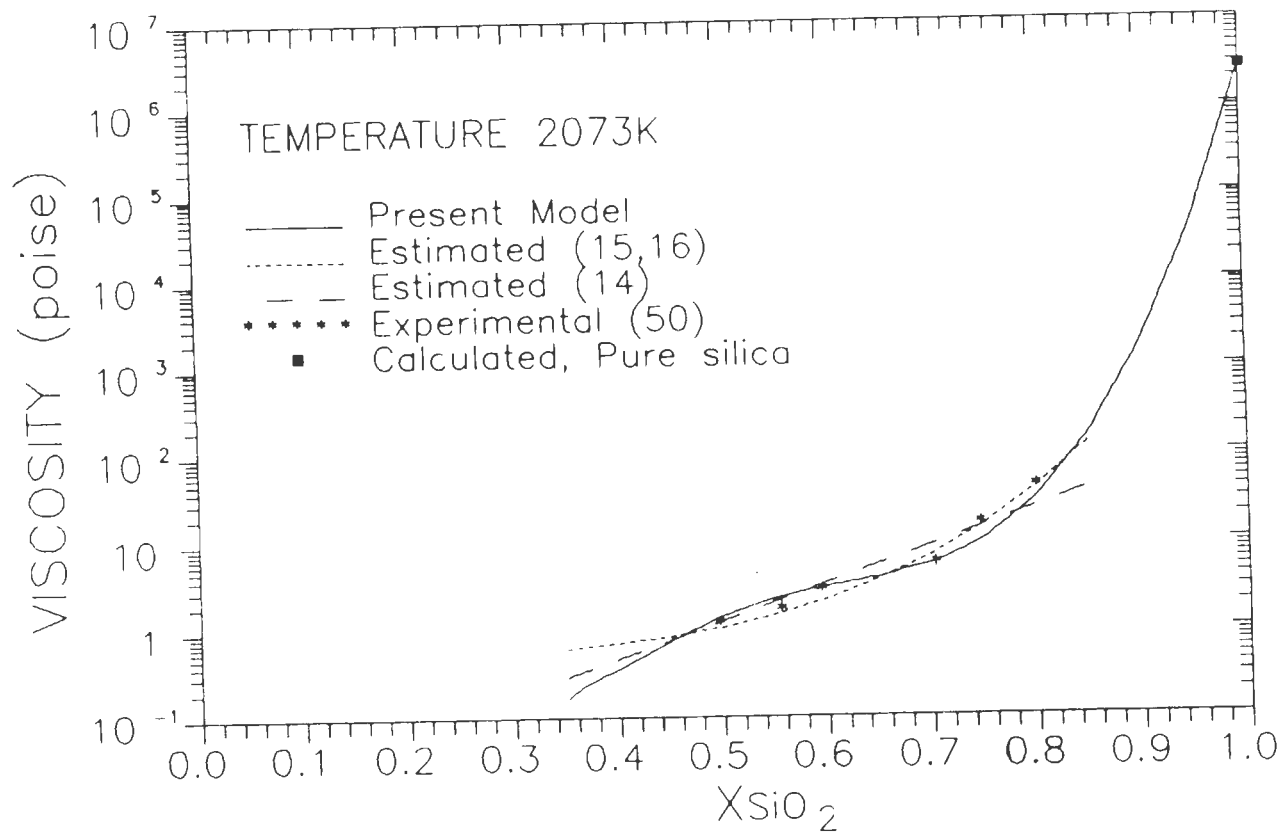


Fig.28—EXPERIMENTAL AND PREDICTED VISCOSITIES OF SrO-SiO₂ MELTS

of various investigators at 1573 (55-62) and 1673K (56,57,60,61). Some of the data at 1673K was read from the paper by Urbain et al. (63). Data at other temperatures of 1523 and 1623K were obtained from Shiraishi et al. (57) in the composition range of 0.117 to 0.423 X_{SiO_2} . The viscosity values were calculated for this system, by considering that the melt was made up of only SiO_2 and FeO , that is, all the FeO and small quantities of Fe_2O_3 , present in the melt was considered to be the total FeO content of the melt. The Fe_2O_3 and the elemental iron occur mainly due to the fact that most of the measurements were made using iron crucibles and bobs. The modified Urbain (16) model considers FeO to act as a modifier while Fe_2O_3 to be an amphoteric. However, as mentioned earlier, the melt is assumed to be made up of only FeO as the metal oxide and this has been assumed in the Urbain et al. (15,16) model too. The viscosity values estimated using this model and also the Riboud et al. (14) model are too high especially at high silica contents. The upper limit for these two models have been set at 0.85 X_{SiO_2} as this is, in general, the upper limit of the available experimental viscosities for $MO-SiO_2$ type of melts. The proposed model was tried in the composition range of 0.1 to 1 X_{SiO_2} and in the temperature range of 1523-1673K. The data of Shiraishi et al. (57) was seen to give the best fit with the model predicted data at all temperatures.

A number of investigators have tried to determine the amount of solid phases in equilibrium with liquid FeO. Bowen and Schairer (64) have determined the percentages at the liquidus temperature. Schuhmann and Ensio (65) have experimentally determined this in three temperature regions of approximately 1261, 1315 and 1365 K. Kaiura et al. (59) and Bodnar et al. (60) studied the effect of the $\text{Fe}_2\text{O}_3/\text{FeO}$ ratio on the viscosity. Based on the oxygen potential data Kaiura et al. (59) have concluded that the curve of viscosity as a function of $\text{Fe}_2\text{O}_3/\text{FeO}$ ratio shows a very slight decrease at a fixed SiO_2 content (weight pct.) while according to Bodnar et al. (60) there is an increase in slag viscosity. As seen from figure 29, there is an increase in viscosity. The predicted data gives good agreement with the experimental data of Kaiura et al. at (59) 25wt pct. silica but the agreement at 35 wt pct. silica shows a discrepancy of about 7.8%. Although there is a general agreement of the predicted values with that of Bodnar et al. (60), the predicted viscosity values do not agree with the experimental values. A probable reason could be the amount of solids in the liquid melt is not known and the variation between the experimental and calculated data would probably be a result of this. Using Roscoe's (20) expression (1-5) for the effect of solids on the viscosity, considering 0.22 volume fraction solids in the melt, the experimental viscosity would increase from 0.75 poise to 1.8 poise which would be close to

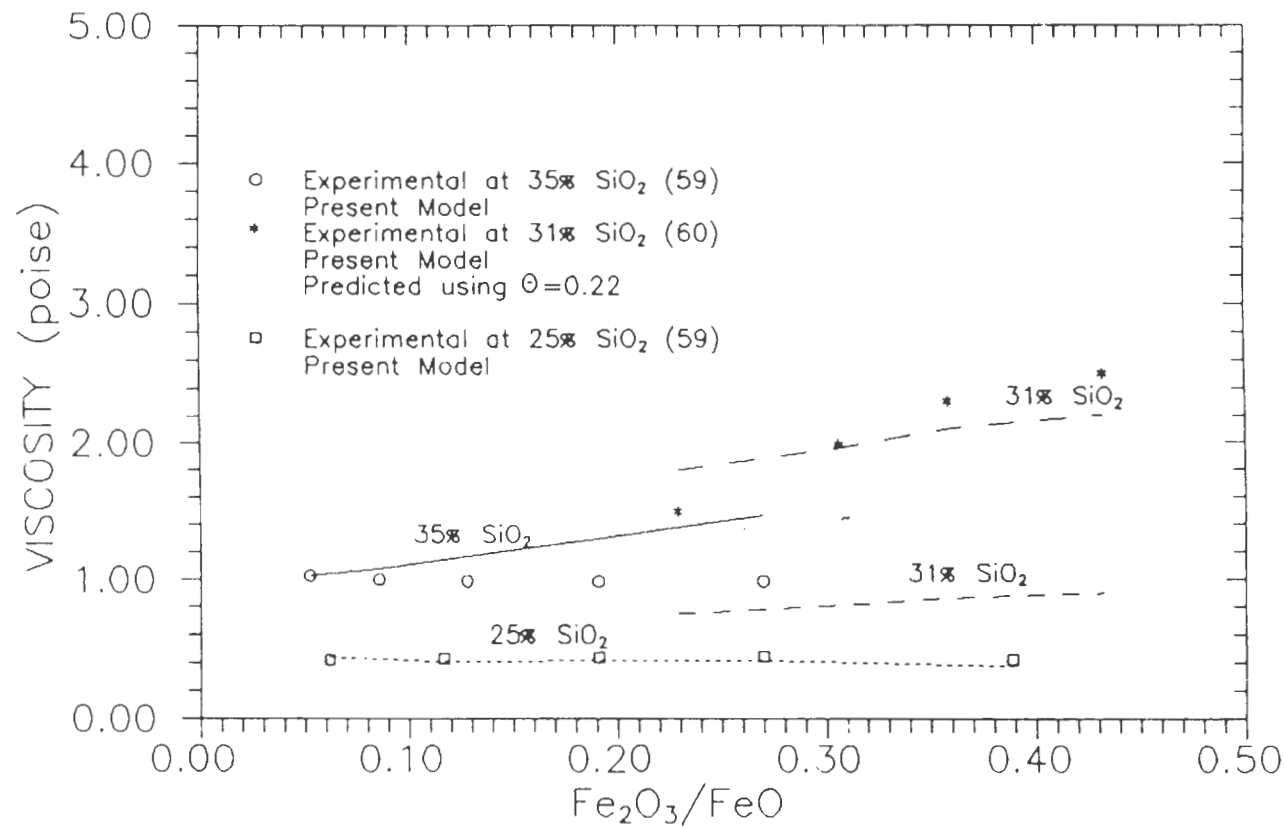


Fig.29—EFFECT OF Fe₂O₃/FeO RATIO ON THE VISCOSITIES AT 1573K

the experimental viscosity of 1.5 poise. Similarly, all other experimental data of Bodnar et al. (60) could be predicted quite accurately considering 0.22 volume fraction solid in the melt. The extent of the effect the solids have on the viscosity can be gathered from this.

The present model gives excellent agreement with experimentally determined data as seen in figures 30 to 33, with the average percentage deviation being -9% while the corresponding deviations in the Riboud et al. (14) and Urbain et al. (15,16) models are 39% and 89% respectively. It however, like other proposed models has the drawback that it does not show the peak in the viscosity composition curve for melts containing approximately 30% SiO₂ which corresponds to the fayalite composition. According to Shiraishi et al. (57) this peak occurs at 29.5%SiO₂ and proposed that this is due to the formation of fayalite clusters in the melt. Kaiura et al. (59) concluded that this is due to the presence of a high concentration of Fe²⁺ ions in the melt. However, this phenomenon was not experimentally observed for any other binary metal oxide silicate systems and needs further verification.

The present model predicts the viscosity values for a given binary system in the range of pure silica to 0.1 XSiO₂. In the case of CaO-SiO₂, MgO-SiO₂, BaO-SiO₂ and SrO-SiO₂

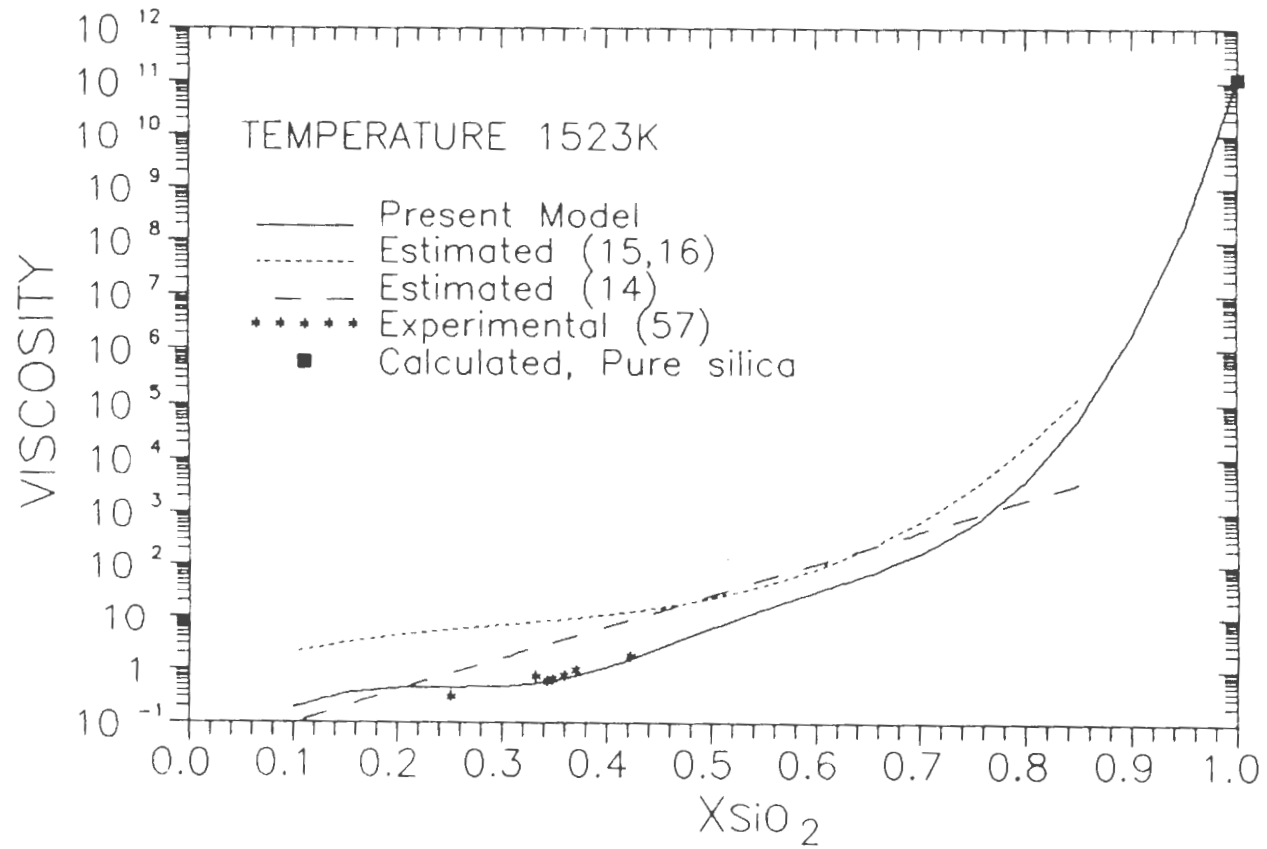


Fig.30—EXPERIMENTAL AND PREDICTED VISCOSITIES OF FeO-SiO₂ MELTS.

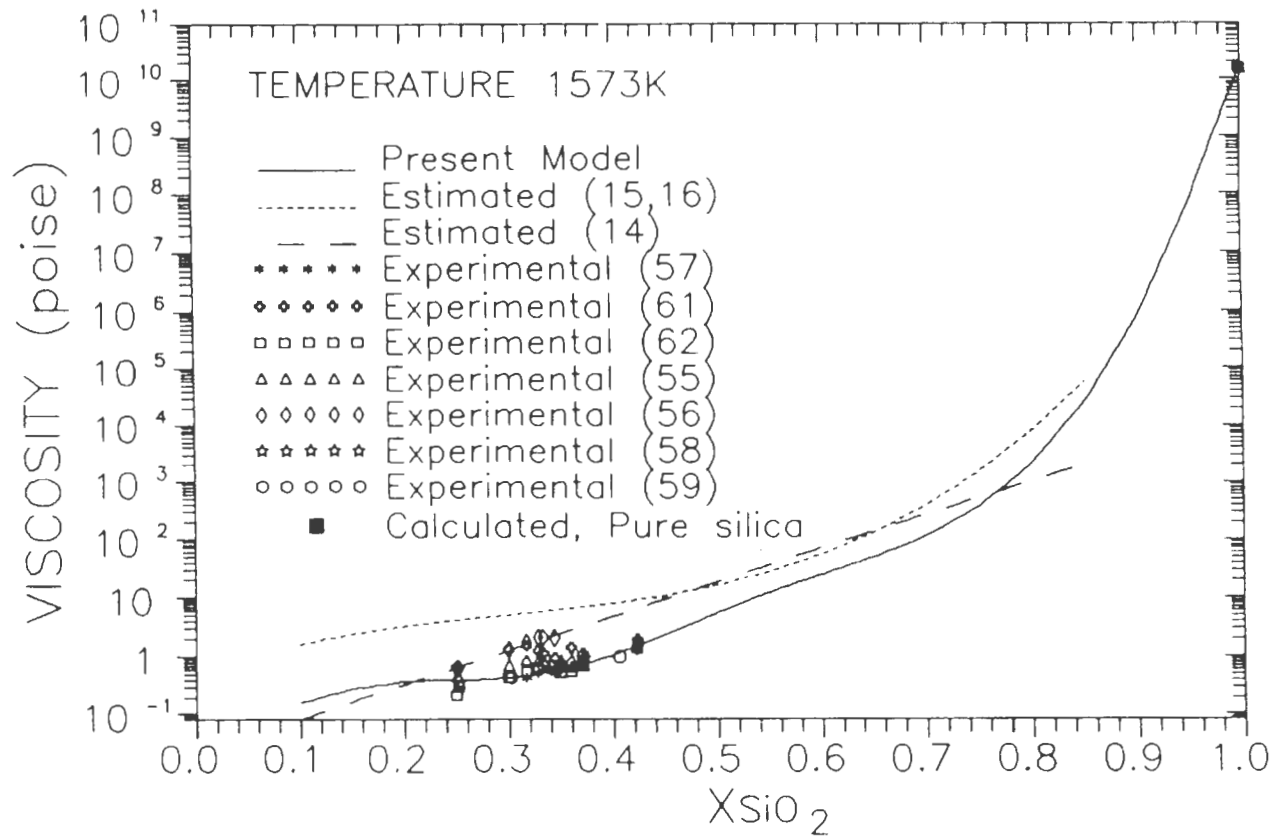


Fig.31—EXPERIMENTAL AND PREDICTED VISCOSITIES OF FeO—SiO₂ MELTS.

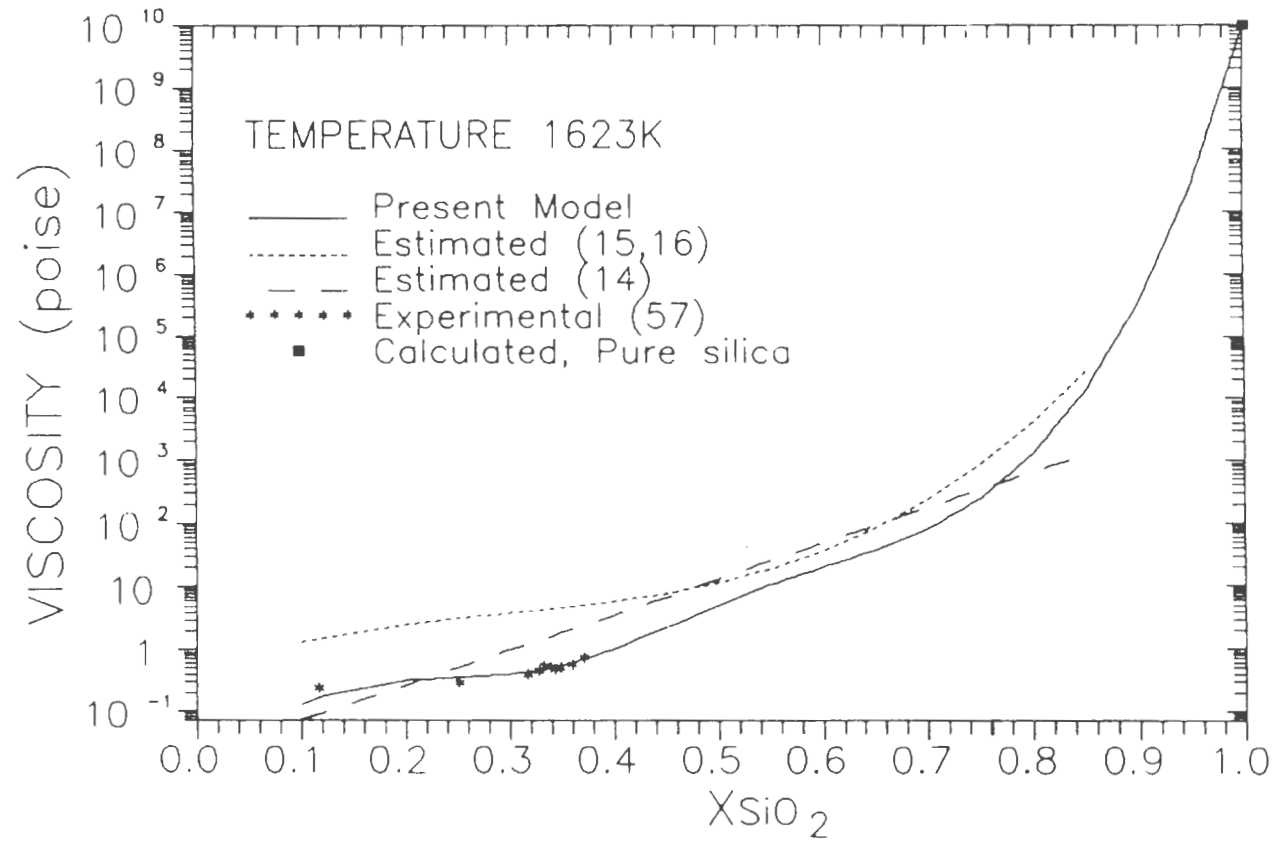


Fig.32—EXPERIMENTAL AND PREDICTED VISCOSITIES OF FeO-SiO₂ MELTS.

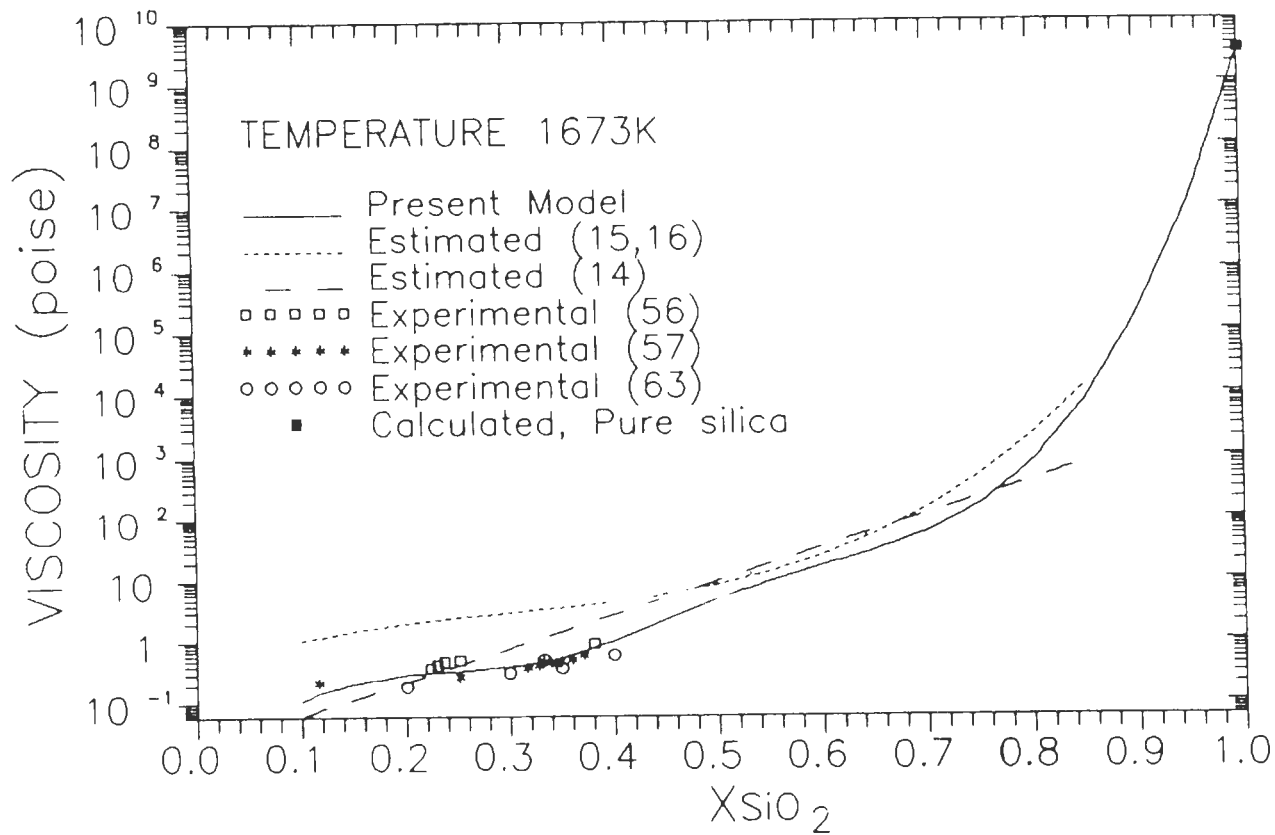


Fig.33—EXPERIMENTAL AND PREDICTED VISCOSITIES OF FeO—SiO₂ MELTS.

systems, a sharp decrease in viscosity values were observed at about $0.35XSiO_2$. The mean chain lengths (m) for CaO-SiO₂, MnO-SiO₂ and FeO-SiO₂ systems as shown in Table 2 have been calculated as a function of composition (66).

TABLE 2. Mean Chain Lengths (m) for several silicate systems at 1773K and $0.4XSiO_2$ (66)

| System | m |
|----------------------|------|
| CaO-SiO ₂ | 2.00 |
| MnO-SiO ₂ | 2.27 |
| FeO-SiO ₂ | 3.90 |

From these calculations it could be seen that for a fixed composition at the same temperature the mean chain length was the lowest for the CaO-SiO₂ system, and largest for FeO-SiO₂. The sharp decrease of the curve in the case of CaO-SiO₂ system, which can be attributed to the smaller value of m may indicate that the silicate network structure is broken (23,28) and a large number of SiO₄⁴⁻ tetrahedra exist below this $XSiO_2$ value. The MgO-SiO₂ system is also expected to behave similarly. The sharpness of the drop was lower for BaO-SiO₂

and SrO-SiO₂, and almost negligible for MnO-SiO₂, and FeO-SiO₂ systems. The drastic drops in the viscosity values in the case of CaO-SiO₂, MgO-SiO₂, BaO-SiO₂ and SrO-SiO₂ systems impose restrictions in the experimental determinations of viscosities in the range $0 < X_{SiO_2} < 0.34$. However, the model predicts viscosity values that are in excellent agreement with the experimental values in the FeO-SiO₂ (figs. 29 to 32) and MnO-SiO₂ systems (figs. 14 and 15) upto nearly pure metal oxide melts. Thus, the viscosity values predicted by our model in the low silica region of the other systems also are expected to be correct.

3.3 M₂O-SiO₂ TYPE OF SYSTEMS:

THE Na₂O-SiO₂ SYSTEM:

The viscosity values have been experimentally determined in the range of X_{SiO_2} 0.85 to 0.41 in a wide temperature range of 1373 to 1823K. Most of the experimental data are from Bockris et al. (50) and Mizoguchi et al. (40). Some others are from the compilations of Bottinga et al. (5) who have compiled the data of Shartsis et al. (67), Bockris et al. (50) and Heidtkamp et al. (68). The entire range of available data lies in the liquid region (49). Molybdenum crucibles and bobs were used to make the measurements by Bockris et al. (50). The agreement with the experimental data is excellent as seen from

figures 34 to 43 with the deviation being about 1.6%. The predicted values, using the present model gives almost comparable agreement with the experimental data, when compared to the values predicted by the Riboud et al. (14) where the average percentage deviation is -2.3%. But the values predicted by the Urbain et al. (15,16) model are not in good agreement with the experimental data and the average percentage deviation was calculated to be 87%. The upper and lower limits have been set at 0.85 and 0.35 mole fraction silica for the Riboud et al. (14) and Urbain et al. (15,16) models.

THE K_2O-SiO_2 SYSTEM:

The viscosities were predicted in the composition range of 0.83 to 0.74 mole fraction silica and in the temperature range of 1373 to 1673K. All of the experimental data were from the investigations of Bockris et al. (50). At lower temperatures there is a possibility of the melt being in the two phase region (presence of solids) at higher mole fractions of silica. Mo crucibles and bobs have been used to measure viscosities. The plots for this system are shown in figures 44 to 50. There was fairly good agreement between the experimental and calculated data with the deviation being about -25% in the case of the present model. The models of Riboud et al. (14) and Urbain et al. (15,16) show deviations

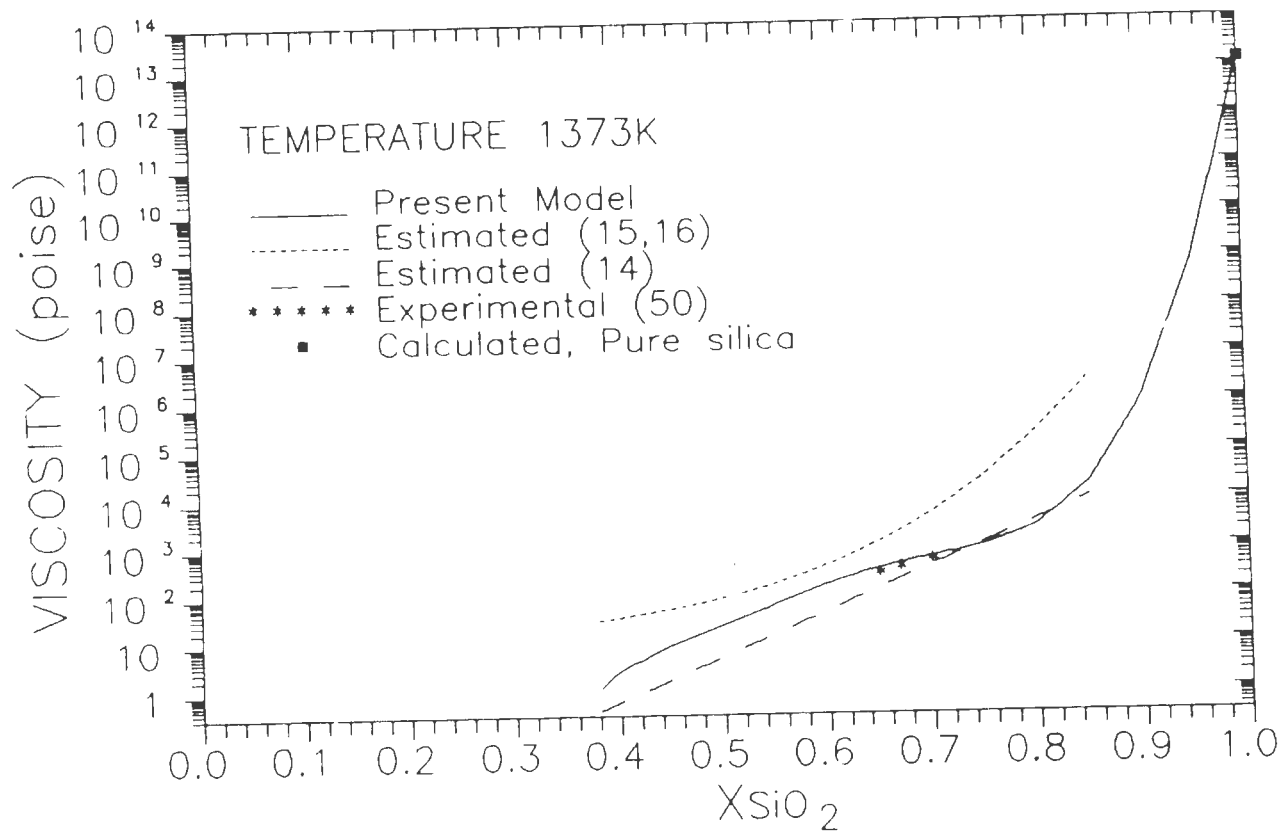


Fig.34—EXPERIMENTAL AND PREDICTED VISCOSITIES OF Na_2O-SiO_2 MELTS

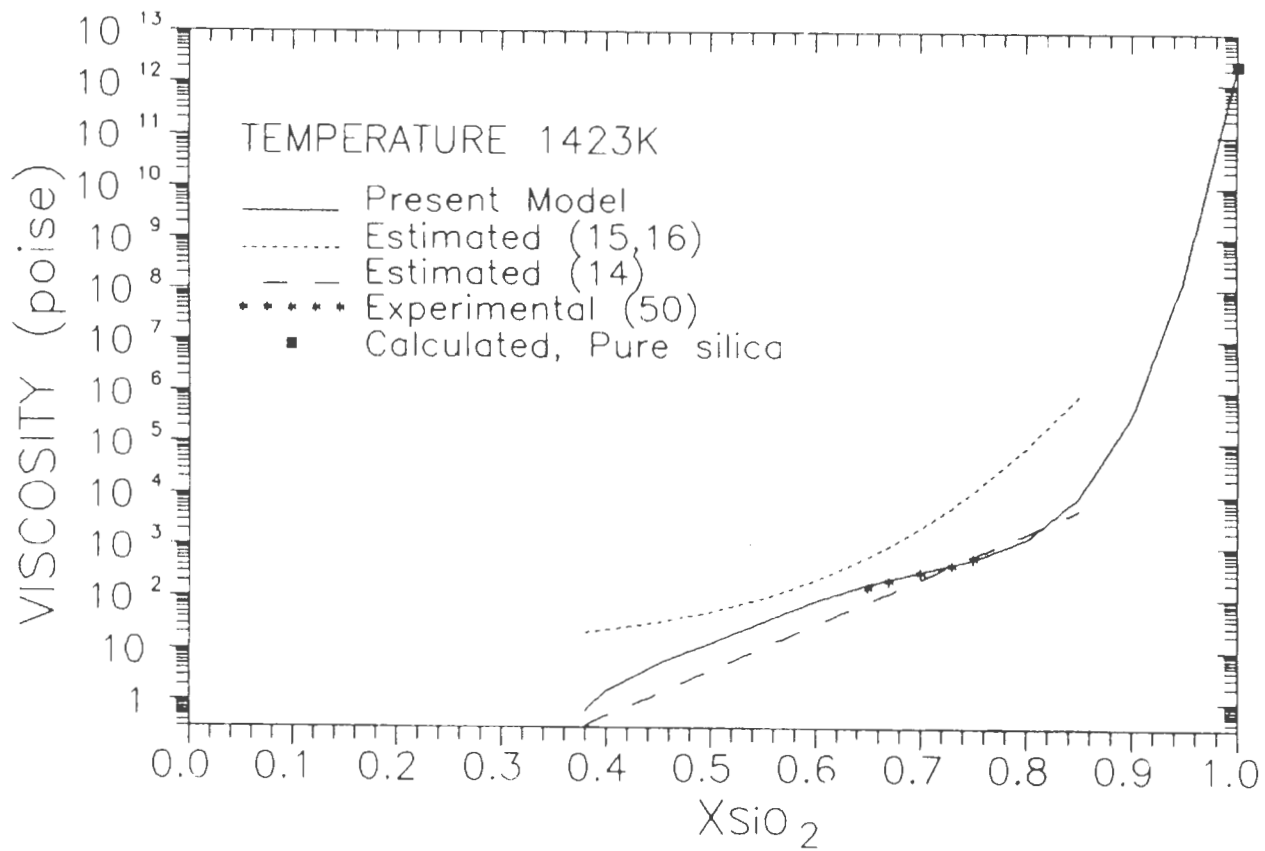


Fig.35--EXPERIMENTAL AND PREDICTED VISCOSITIES OF Na₂O-SiO₂ MELTS

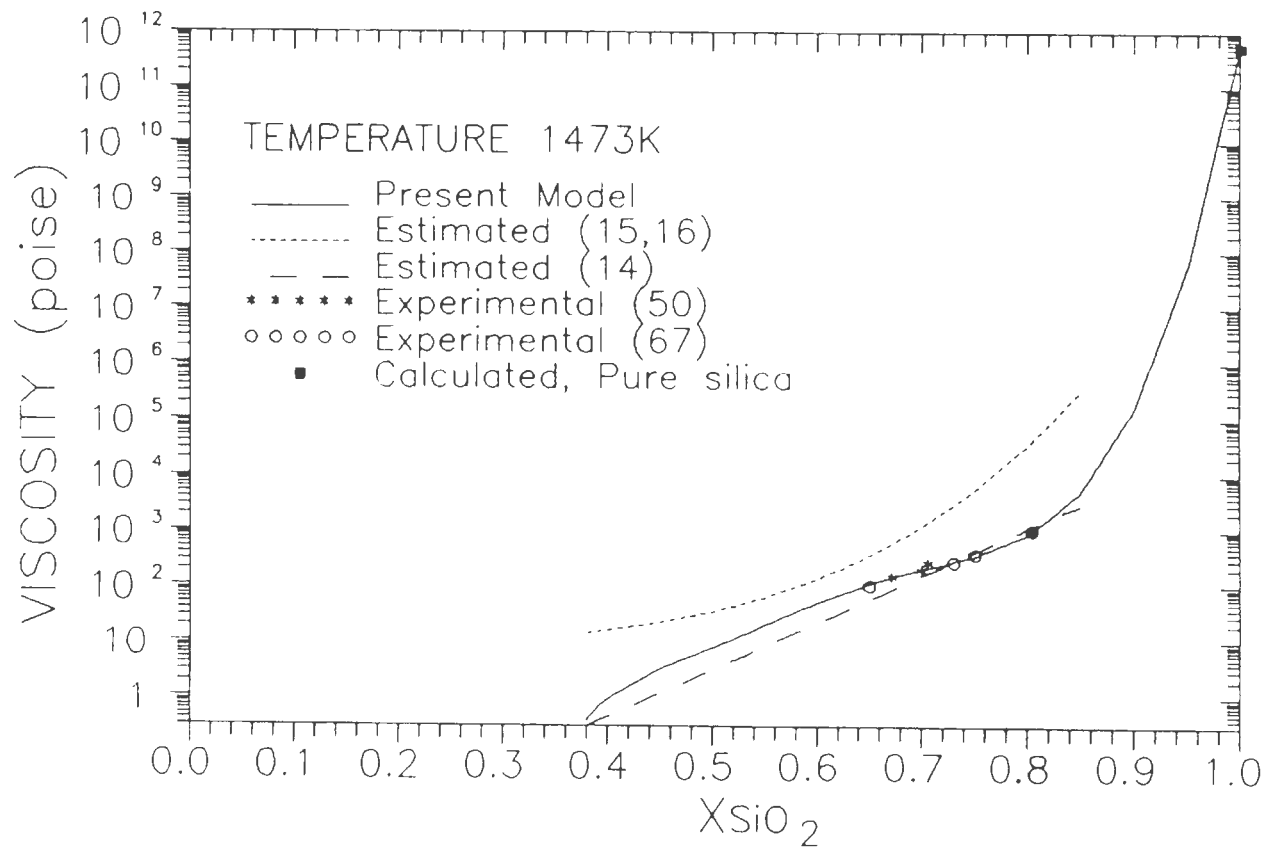


Fig.36—EXPERIMENTAL AND PREDICTED VISCOSITIES OF Na_2O-SiO_2 MELTS

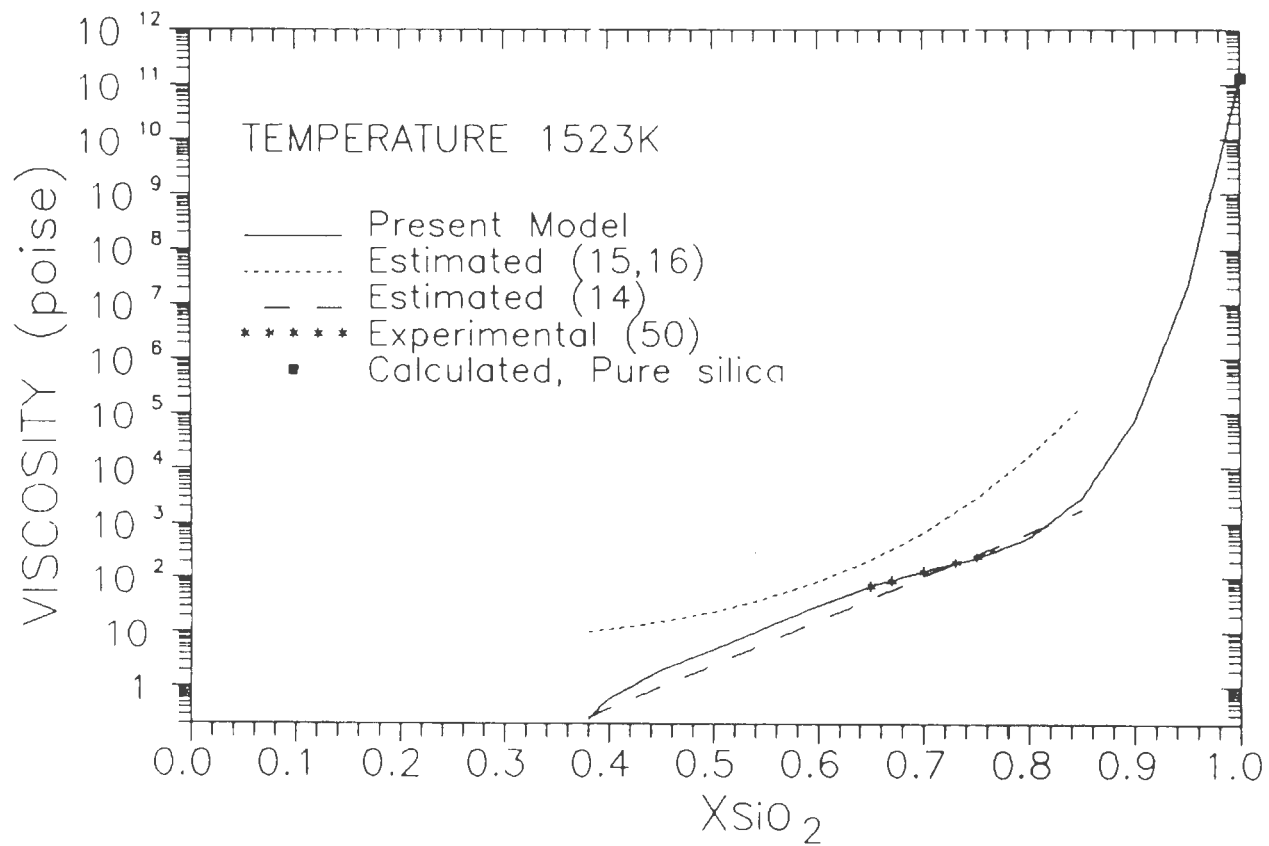


Fig.37—EXPERIMENTAL AND PREDICTED VISCOSITIES OF Na_2O-SiO_2 MELTS

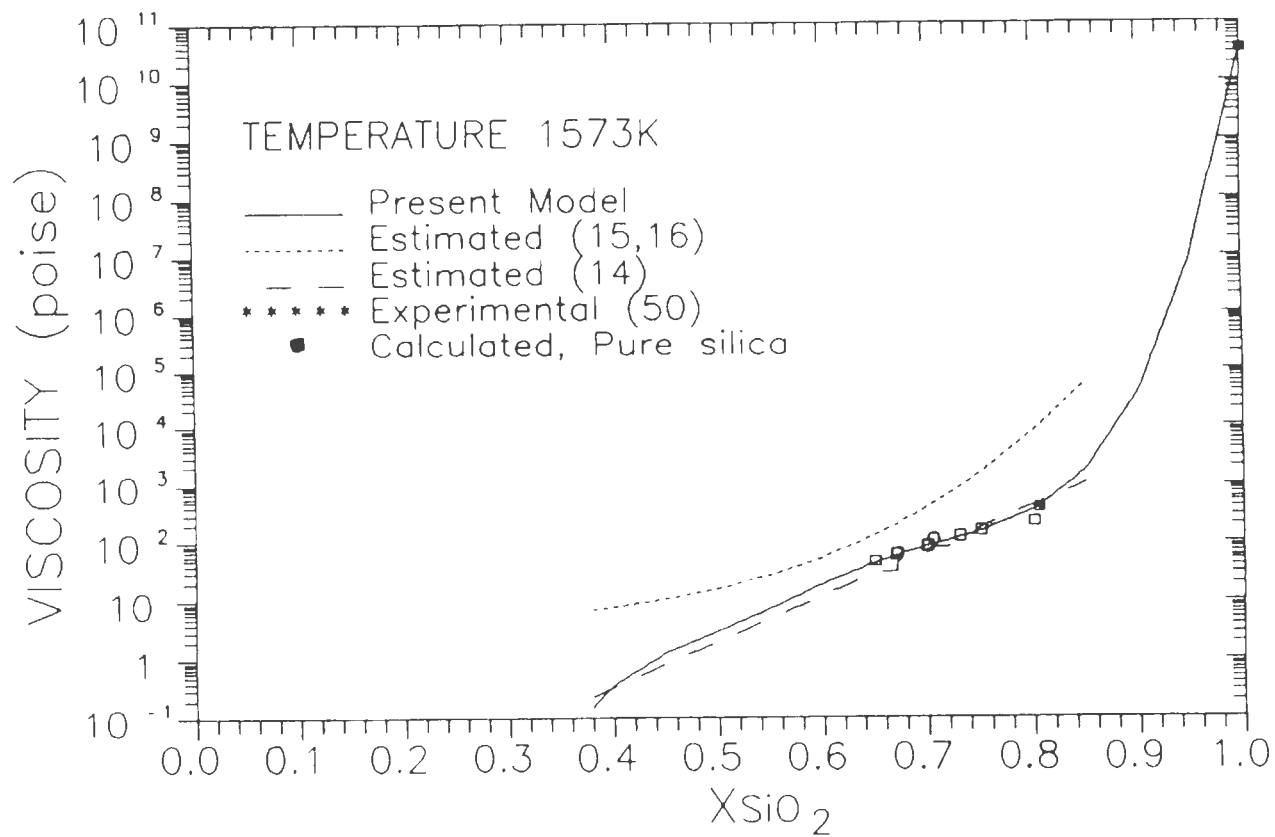


Fig.38—EXPERIMENTAL AND PREDICTED VISCOSITIES OF Na₂O—SiO₂ MELTS

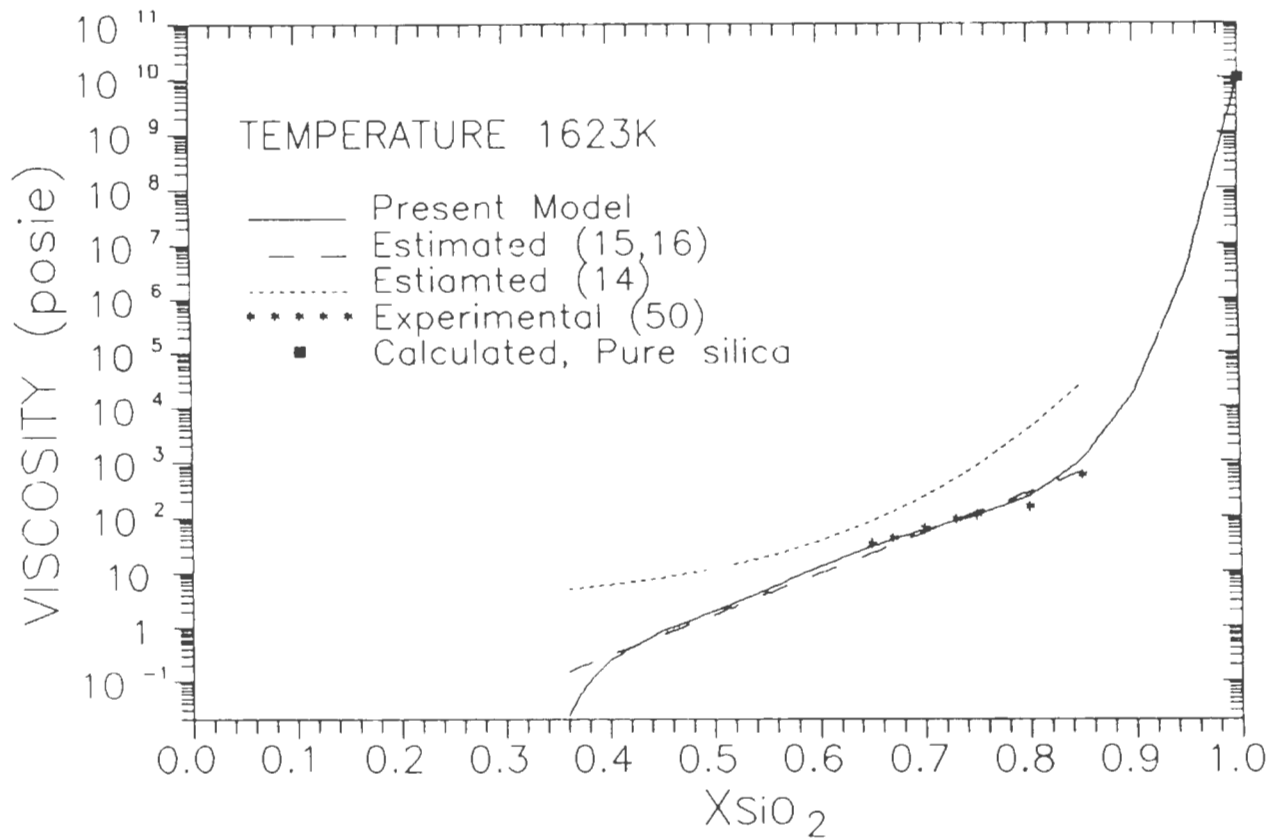


Fig.39—EXPERIMENTAL AND PREDICTED VISCOSITIES OF Na_2O-SiO_2 MELTS

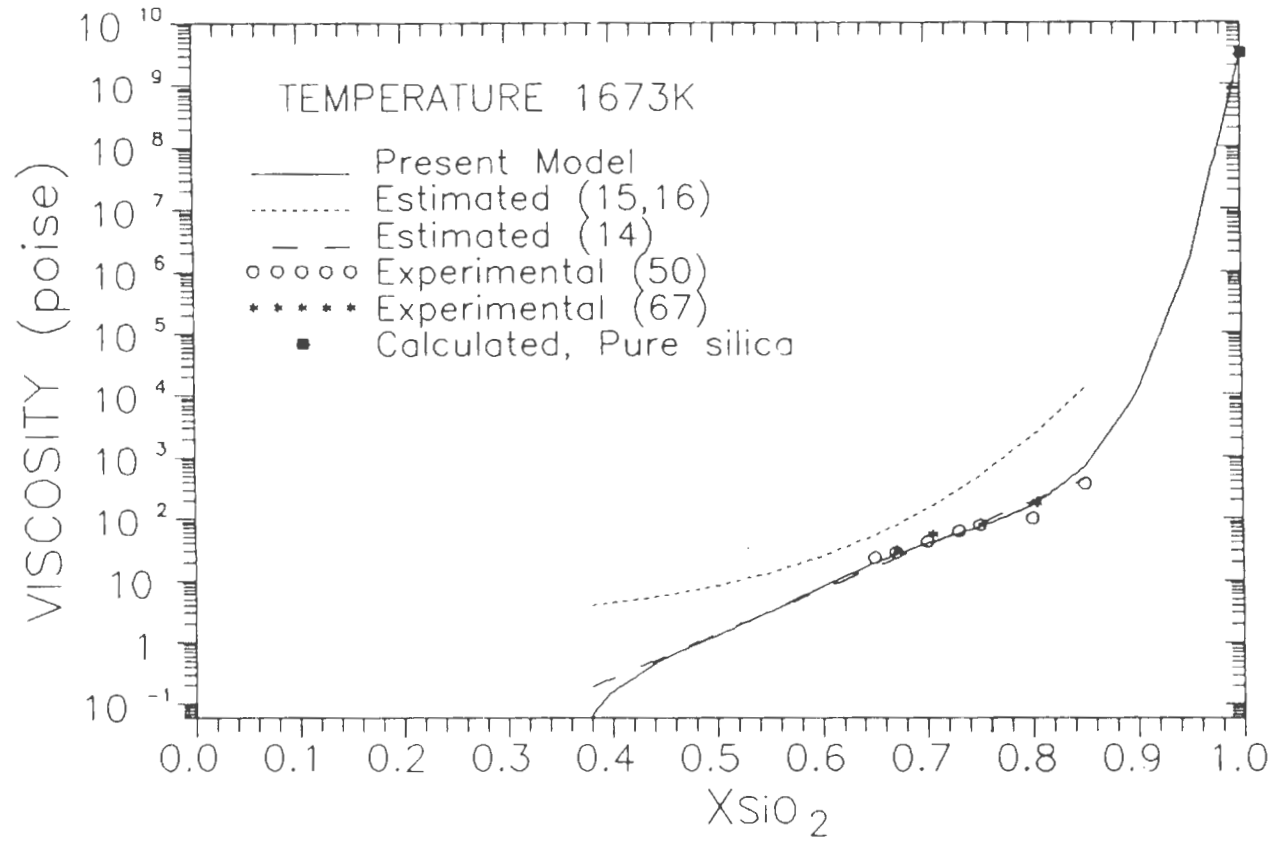


Fig.40—EXPERIMENTAL AND PREDICTED VISCOSITIES
OF Na_2O-SiO_2 MELTS

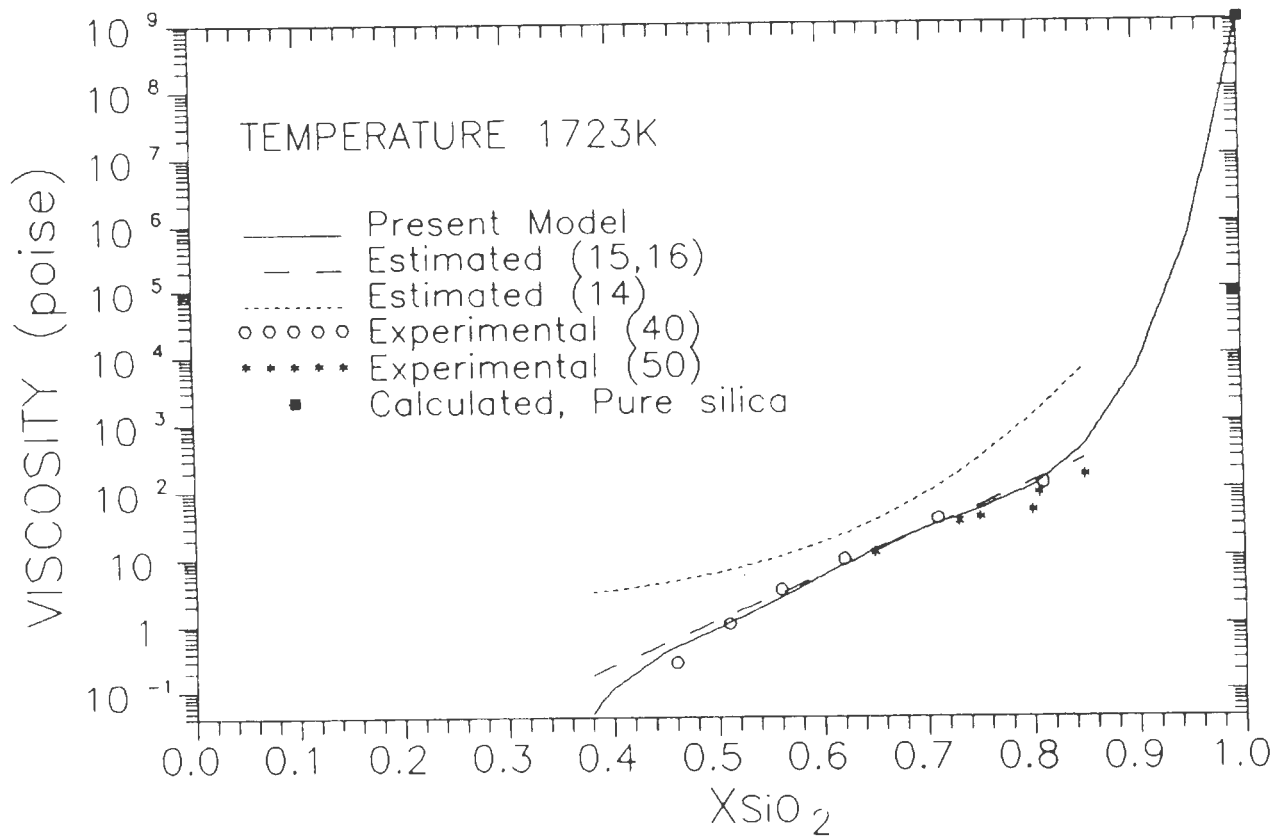


Fig.41—EXPERIMENTAL AND PREDICTED VISCOSITIES OF Na_2O-SiO_2 MELTS

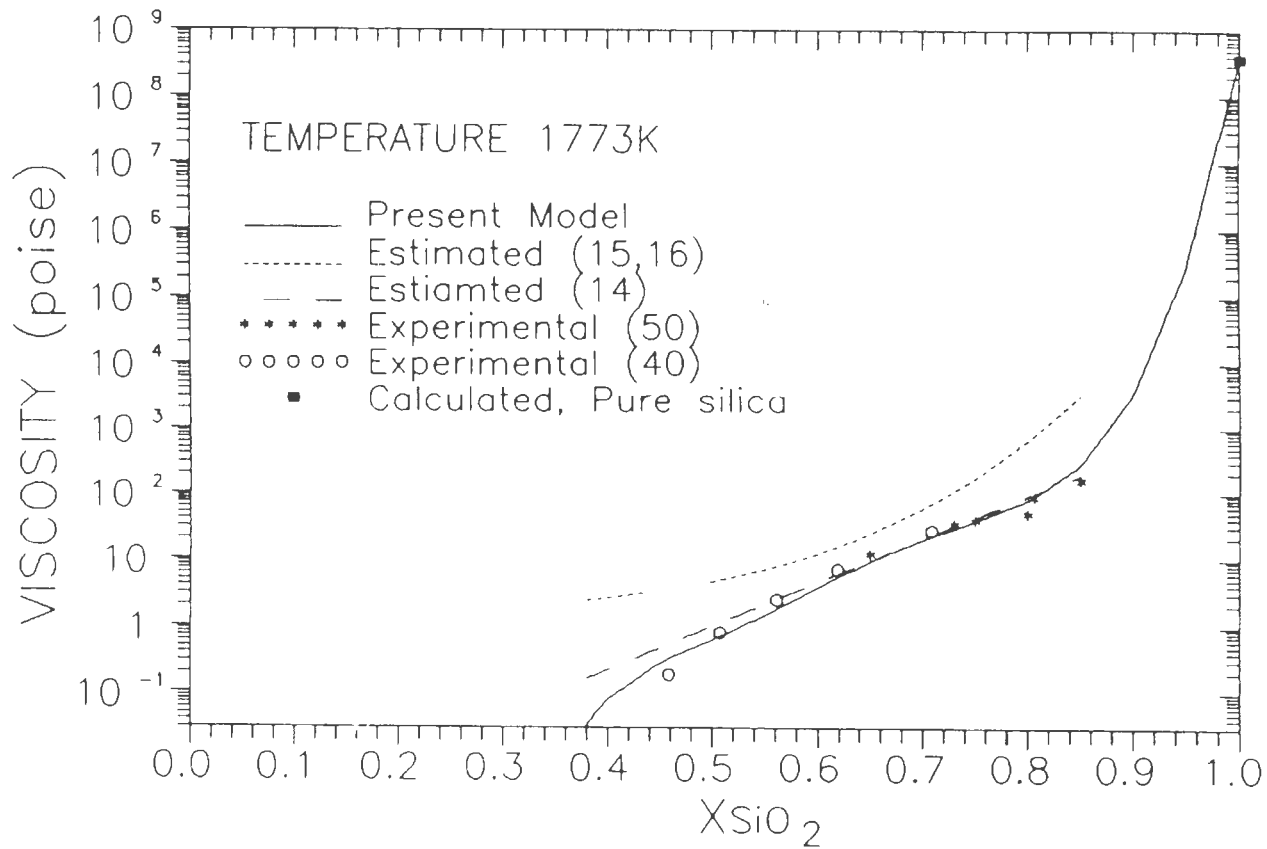


Fig.42—EXPERIMENTAL AND PREDICTED VISCOSITIES OF Na₂O—SiO₂ MELTS

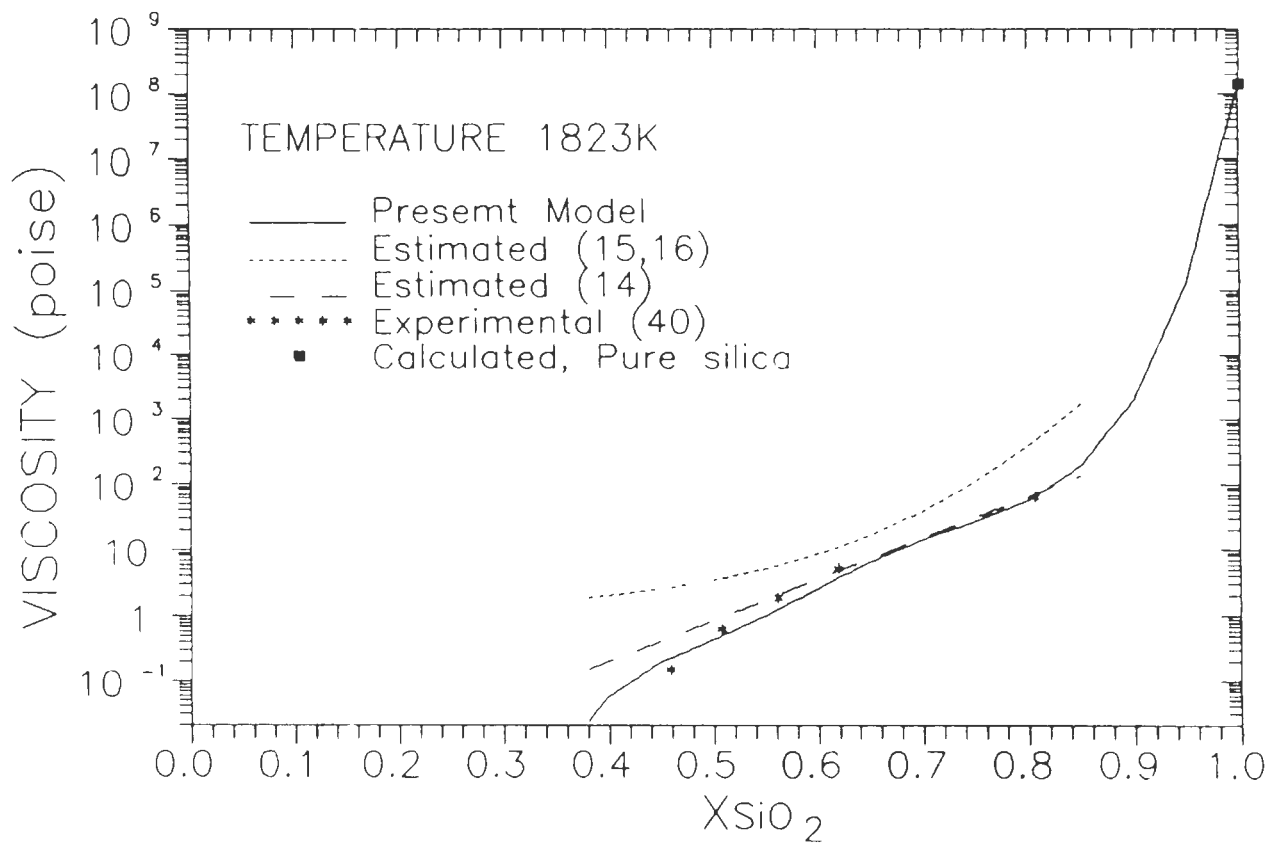


Fig.43—EXPERIMENTAL AND PREDICTED VISCOSITIES OF Na₂O—SiO₂ MELTS

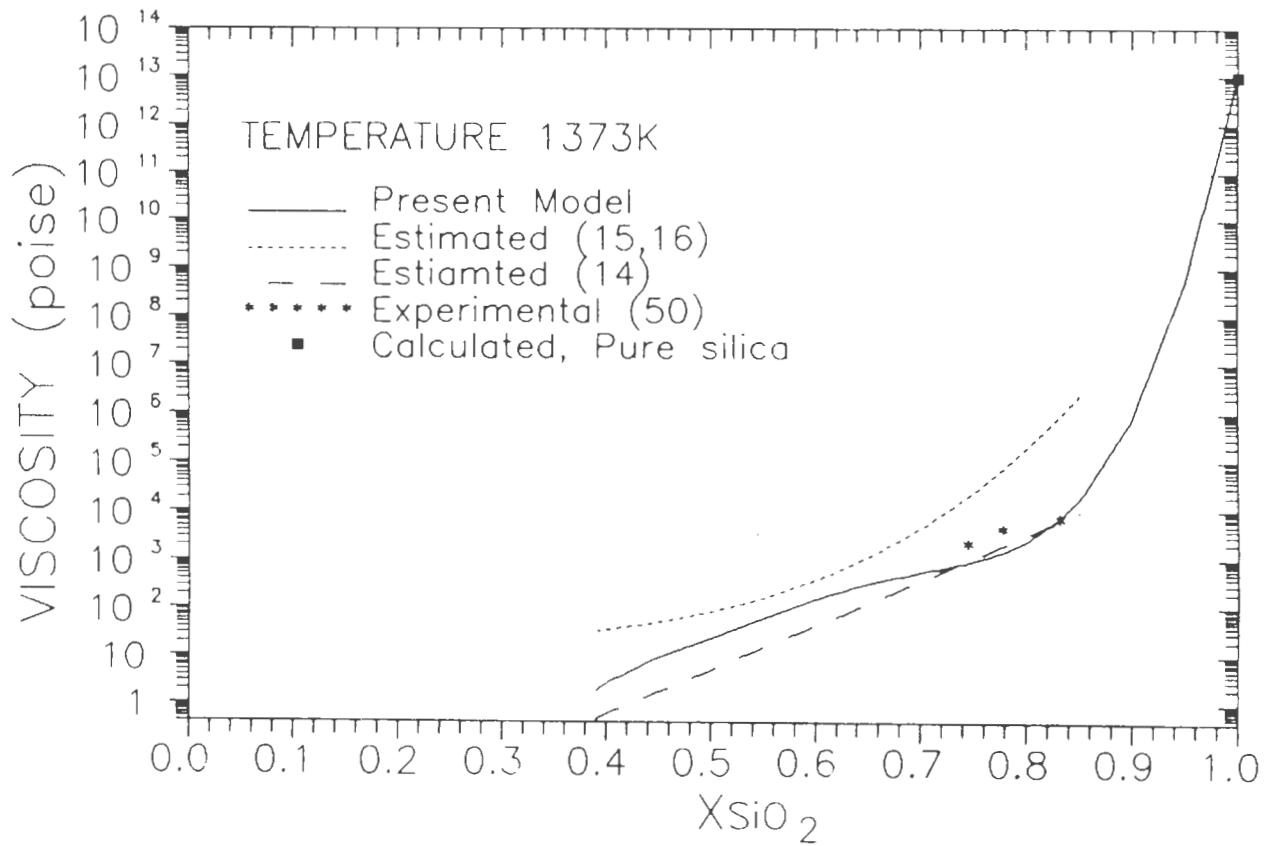


Fig.44—EXPERIMENTAL AND PREDICTED VISCOSITIES OF K₂O-SiO₂ MELTS

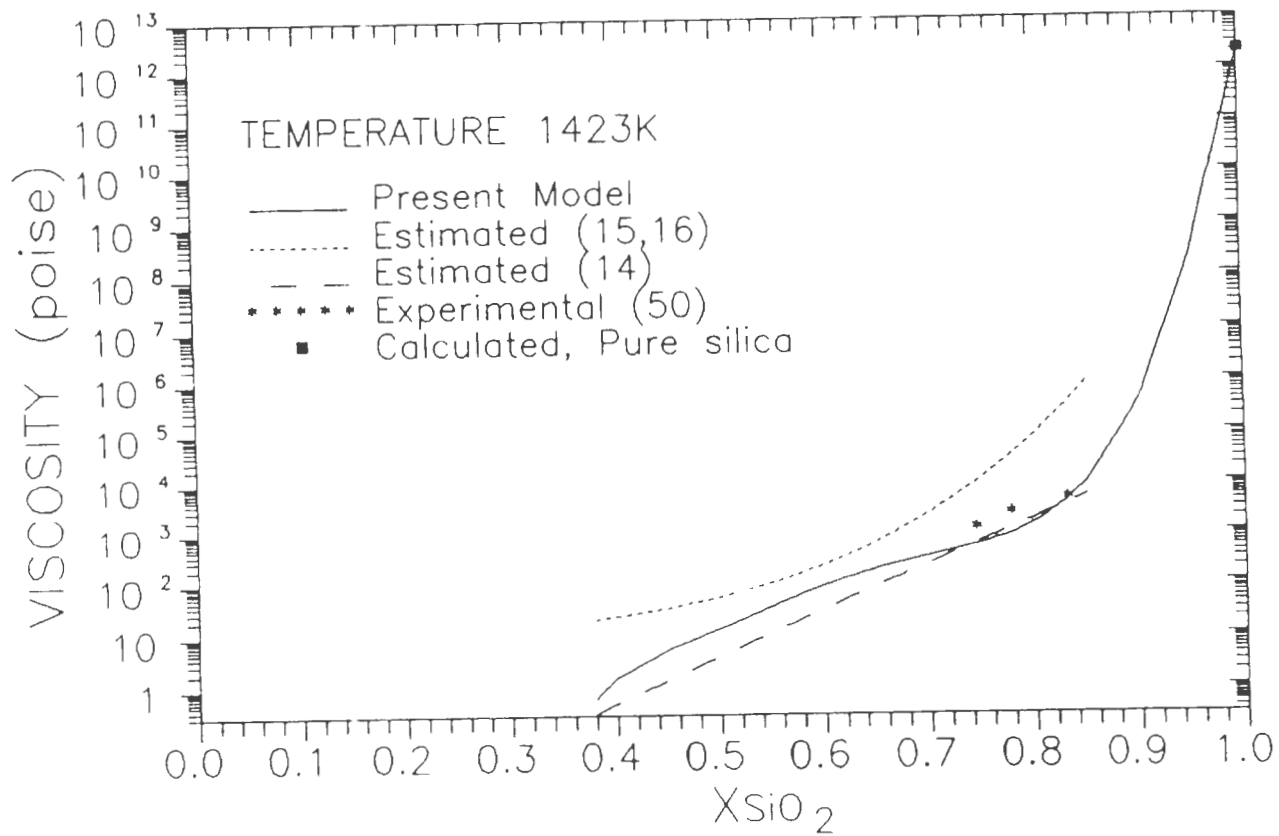


Fig.45--EXPERIMENTAL AND PREDICTED VISCOSITIES OF K₂O-SiO₂ MELTS

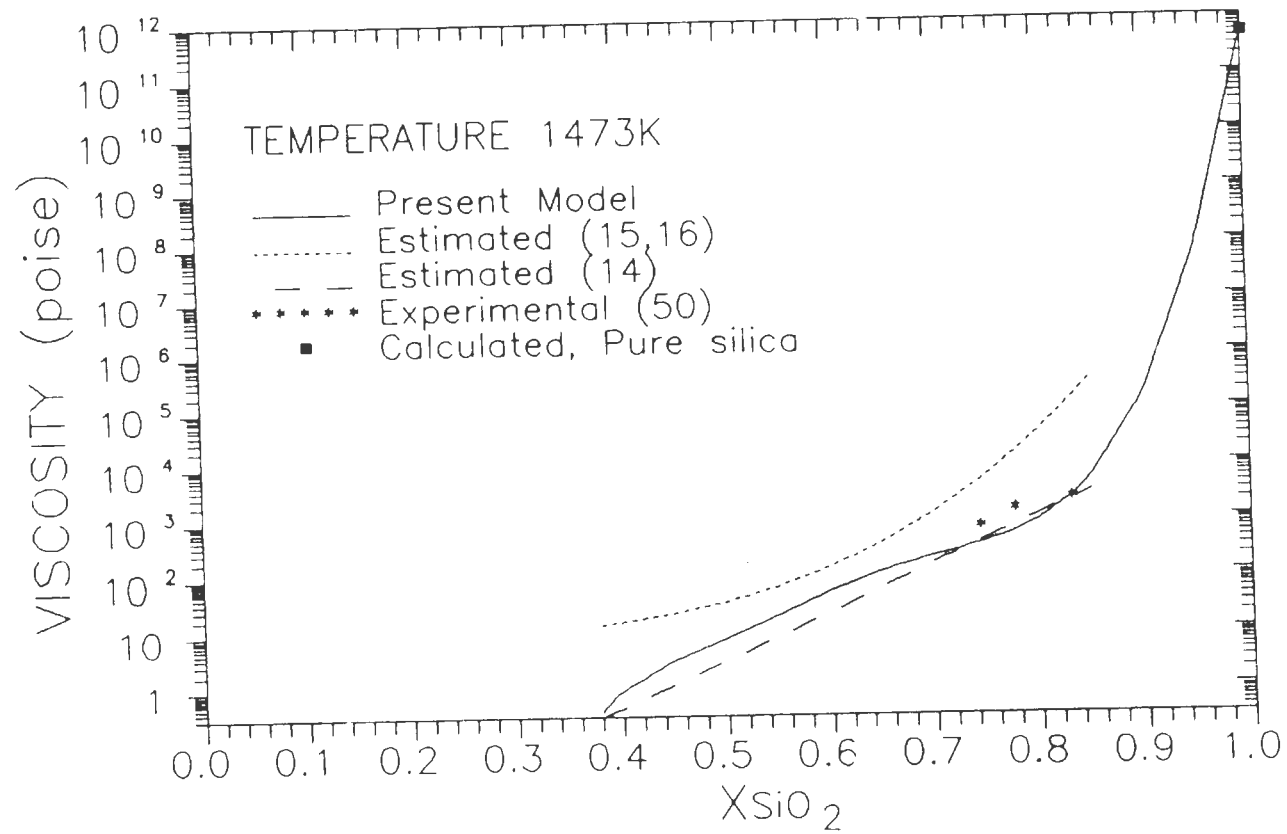


Fig.46—EXPERIMENTAL AND PREDICTED VISCOSITIES OF K₂O—SiO₂ MELTS

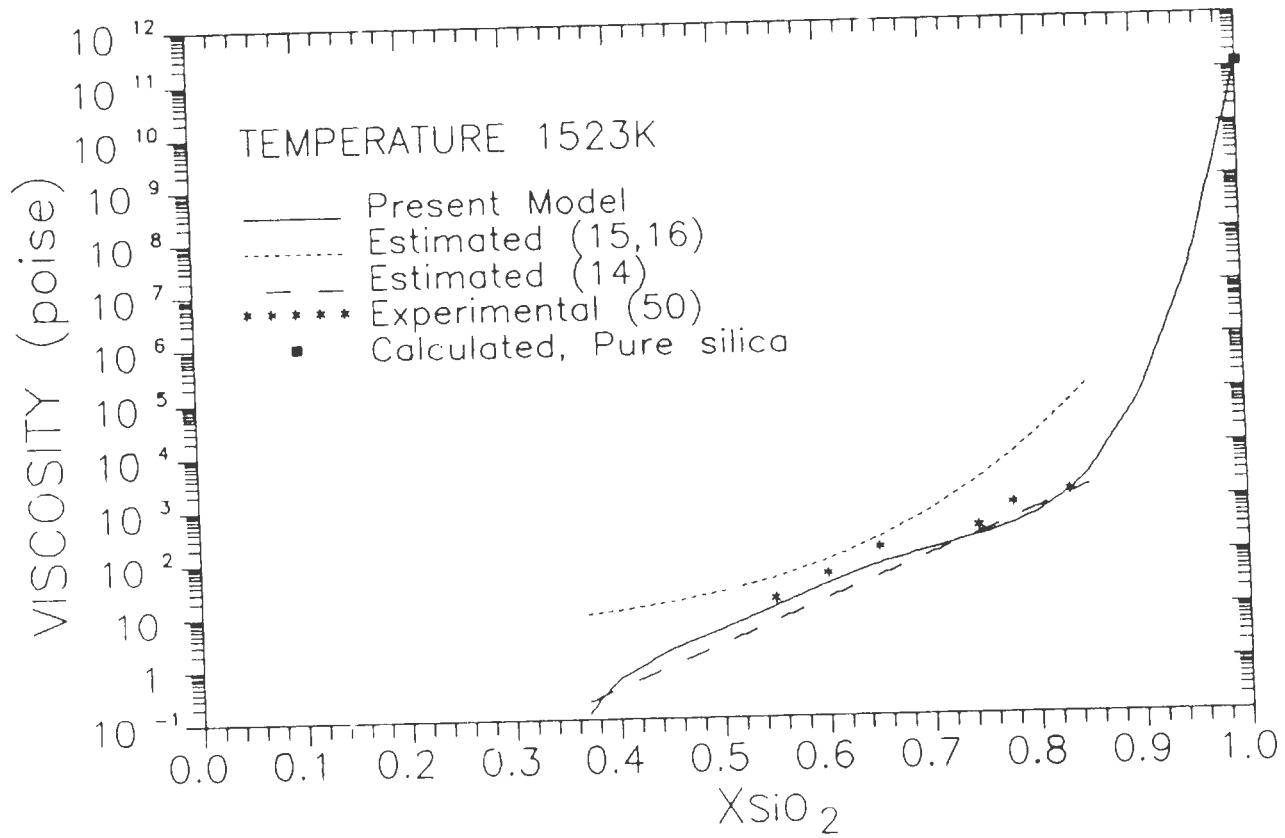


Fig.47—EXPERIMENTAL AND PREDICTED VISCOSITIES OF K₂O—SiO₂ MELTS

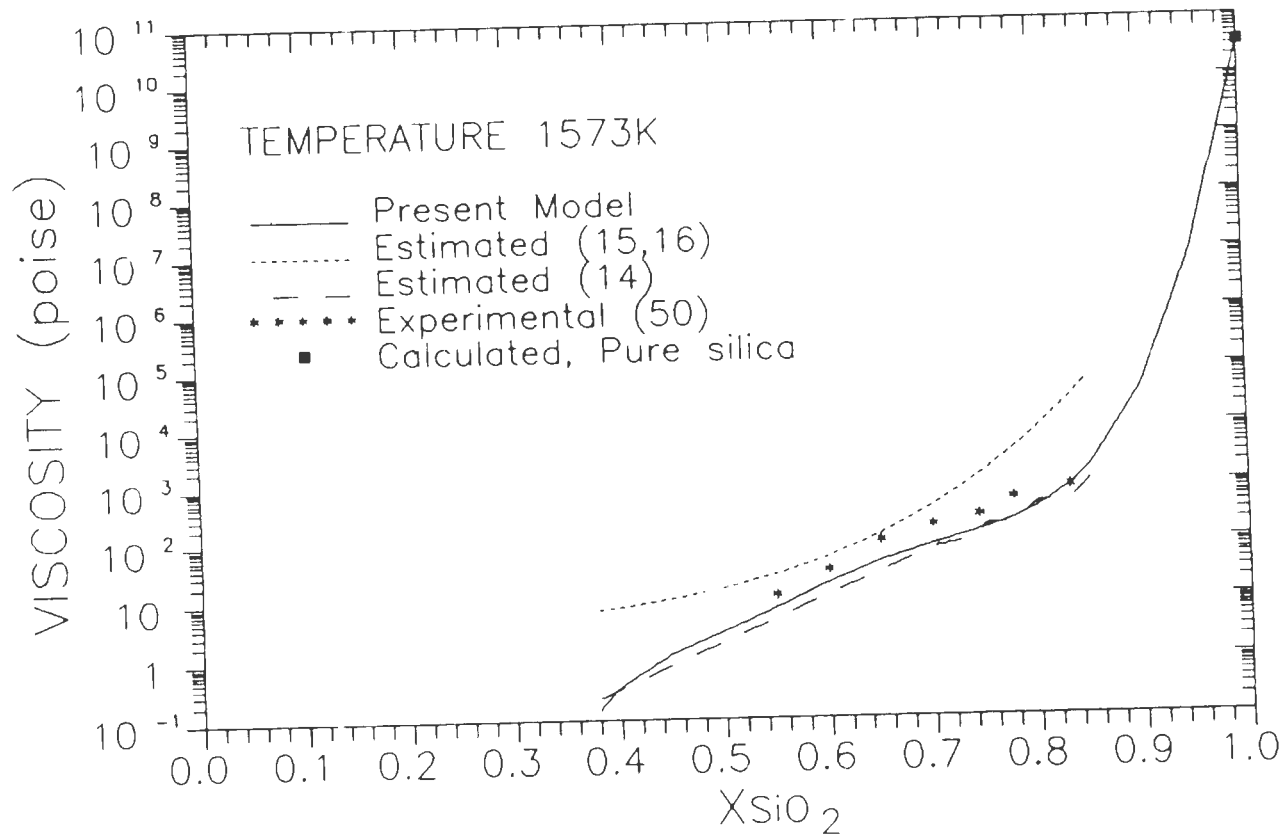


Fig.48—EXPERIMENTAL AND PREDICTED VISCOSITIES OF K_2O-SiO_2 MELTS

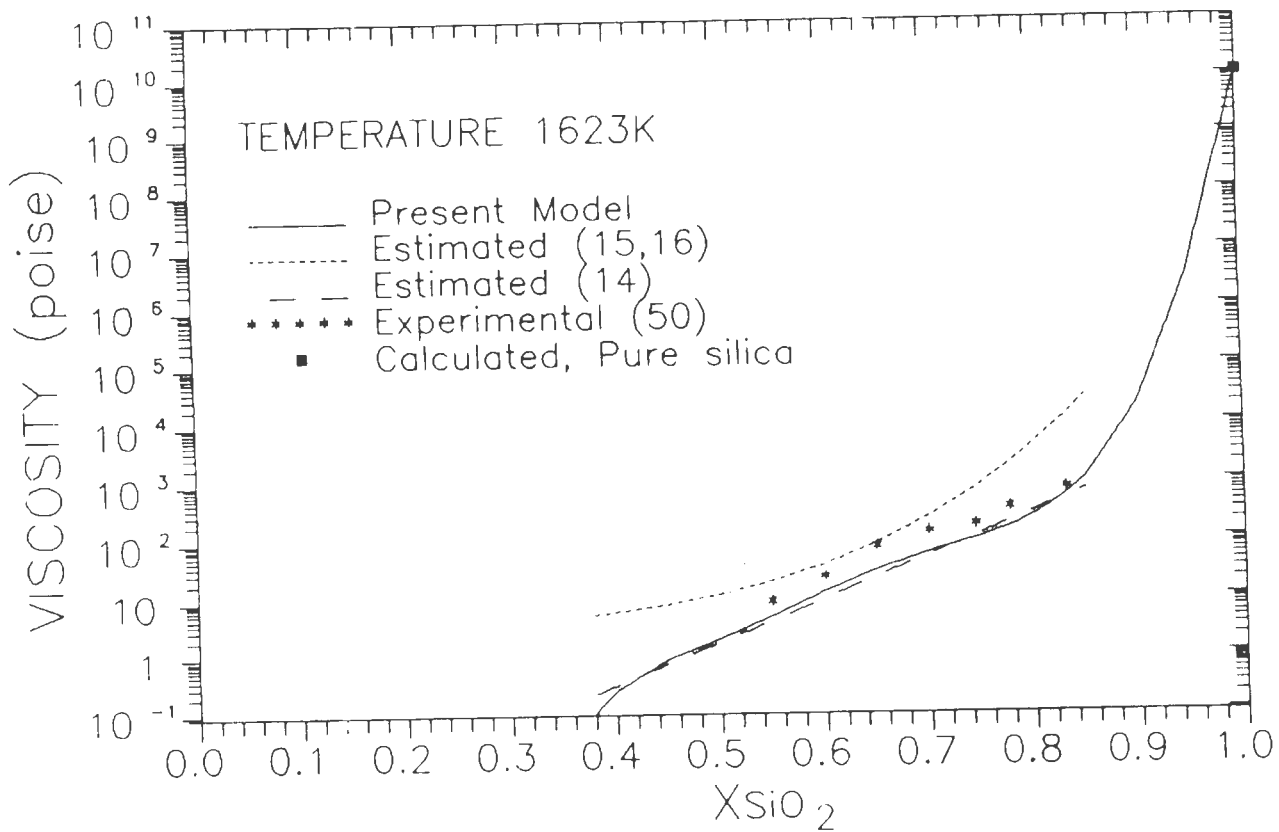


Fig.49—EXPERIMENTAL AND PREDICTED VISCOSITIES OF K₂O—SiO₂ MELTS

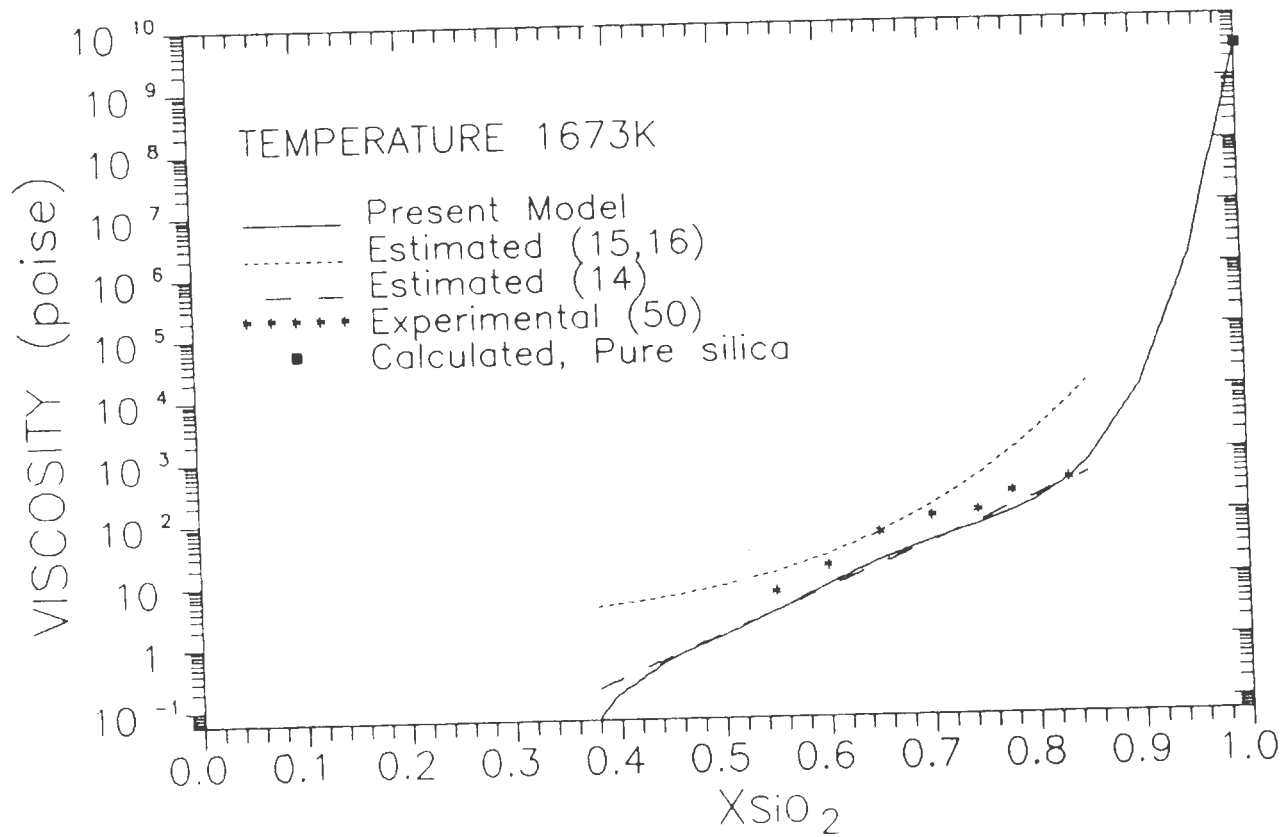


Fig.50—EXPERIMENTAL AND PREDICTED VISCOSITIES OF K₂O—SiO₂ MELTS

of -29% and 80%. These two models have been used in the range of 0.85 to 0.35 mole fraction silica. As can be seen from the average percentage deviations the Urbain et al. (15,16) model predicted values that are not in very good agreement with the experimental data in this system also.

THE $\text{Li}_2\text{O-SiO}_2$ SYSTEM:

Viscosity data was available in the composition range of 0.81 to 0.45 mole fraction silica with the temperature varying in the range 1423 to 1773K. The experimental data is from Bockris et al. (50) mainly, and some others are from Bottinga et al. (5) who have compiled the data of Shartsis et al. (67) and Bockris et al. (50). Values from Mizoguchi et al. (54) have also been used. At lower temperatures (upto 1473K) and also at higher temperatures there is a possibility that the viscosity data at the low silica mole fractions maybe in error due to the effect of solids. Mo crucibles and bobs have been used to measure viscosities. There is a fairly good agreement with the experimental data in the entire temperature range as seen from figures 51 to 56 with the deviation being about 11% in the case of the proposed model. The model of Riboud et al. (14) gives an average percentage deviation of -0.2%. The Urbain et al. (15,16) model gives an average percentage deviation of 74% implying that the predicted values are not in good agreement with the experimental data as compared to

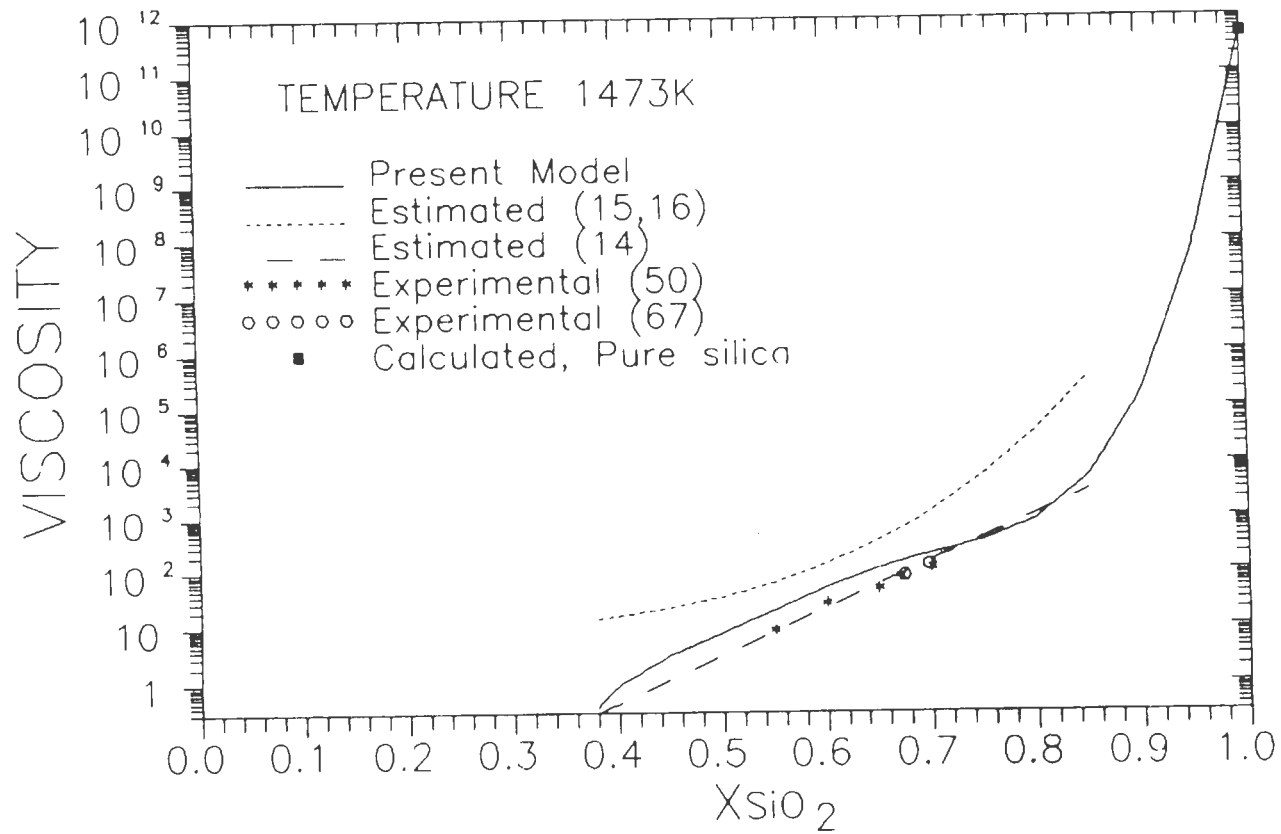


Fig.51—EXPERIMENTAL AND PREDICTED VISCOSITIES OF Li₂O—SiO₂ MELTS

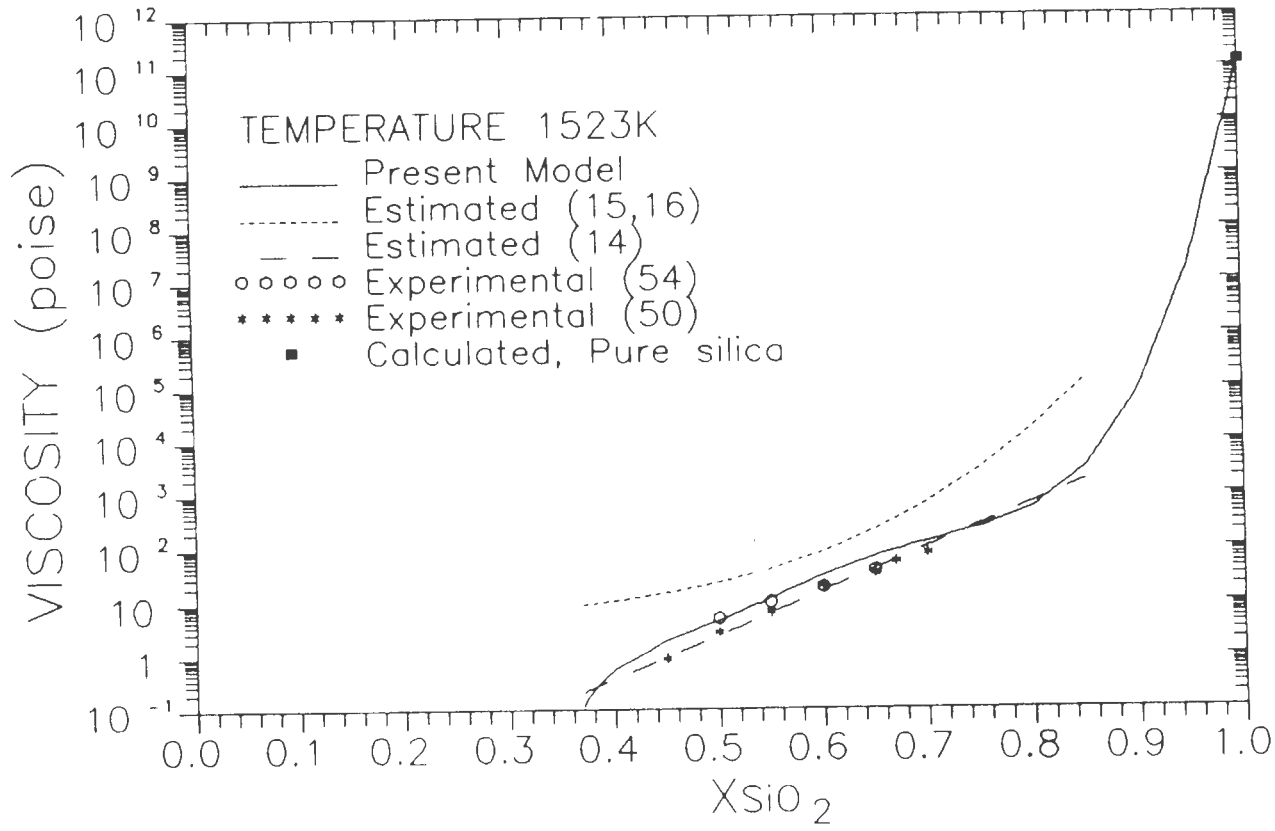


Fig.52—EXPERIMENTAL AND PREDICTED VISCOSITIES OF Li₂O—SiO₂ MELTS

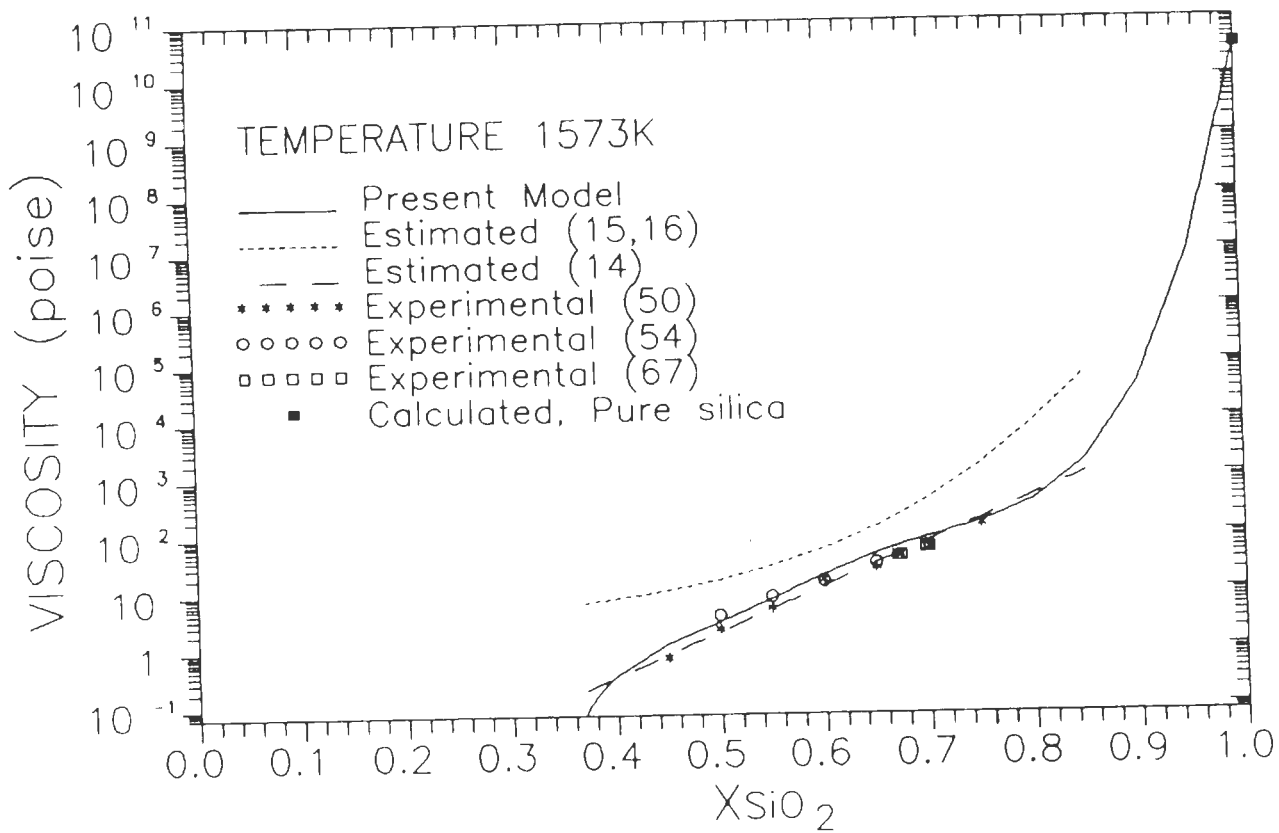


Fig.53—EXPERIMENTAL AND PREDICTED VISCOSITIES OF $\text{Li}_2\text{O}-\text{SiO}_2$ MELTS

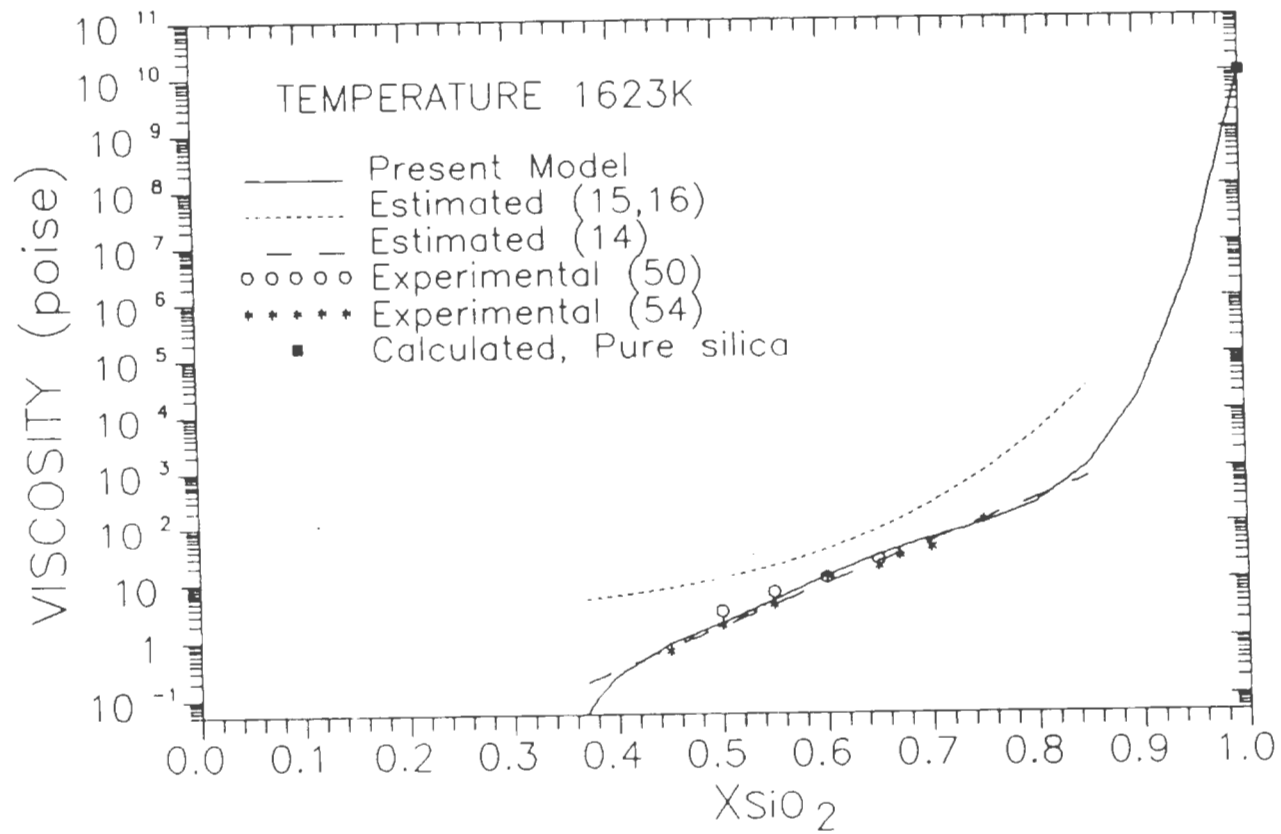


Fig.54—EXPERIMENTAL AND PREDICTED VISCOSITIES OF Li_2O-SiO_2 MELTS

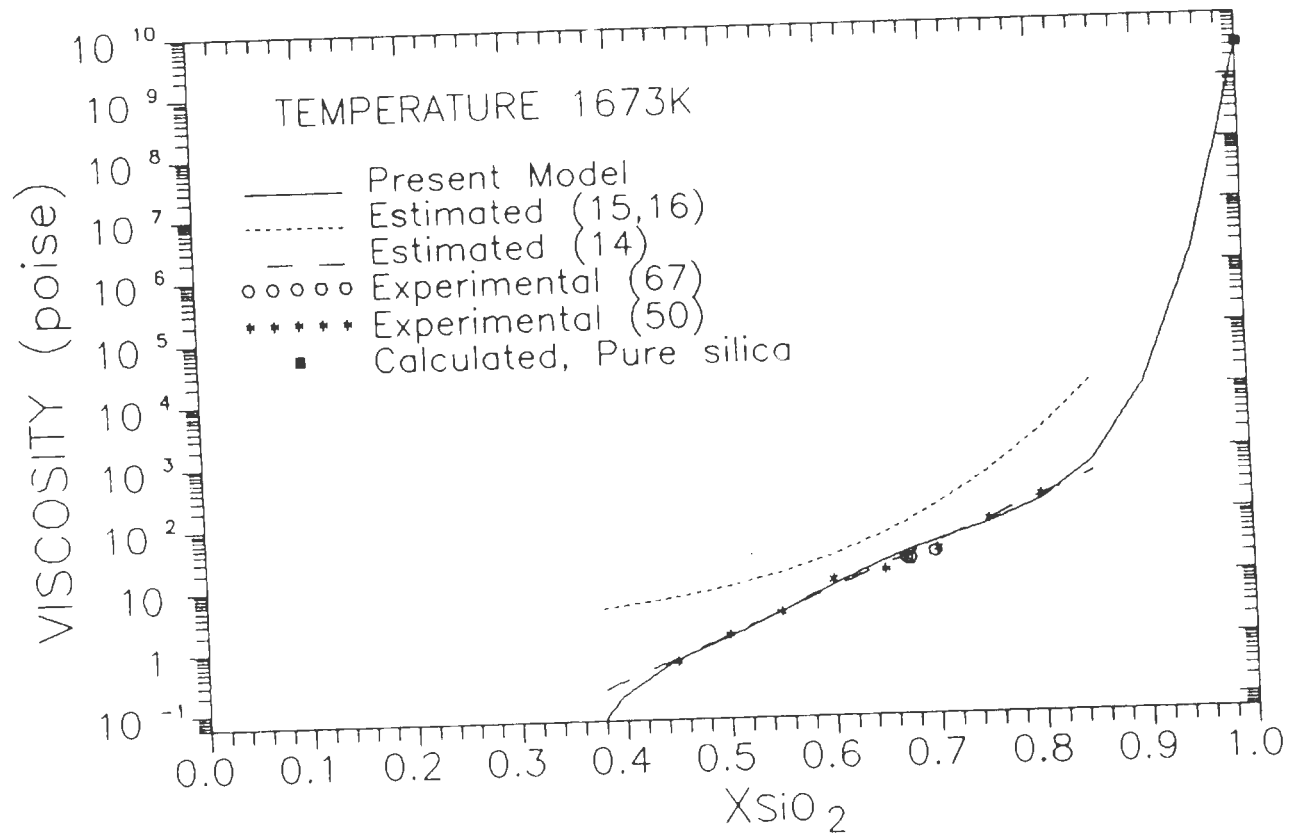


Fig.55—EXPERIMENTAL AND PREDICTED VISCOSITIES OF Li₂O—SiO₂ MELTS

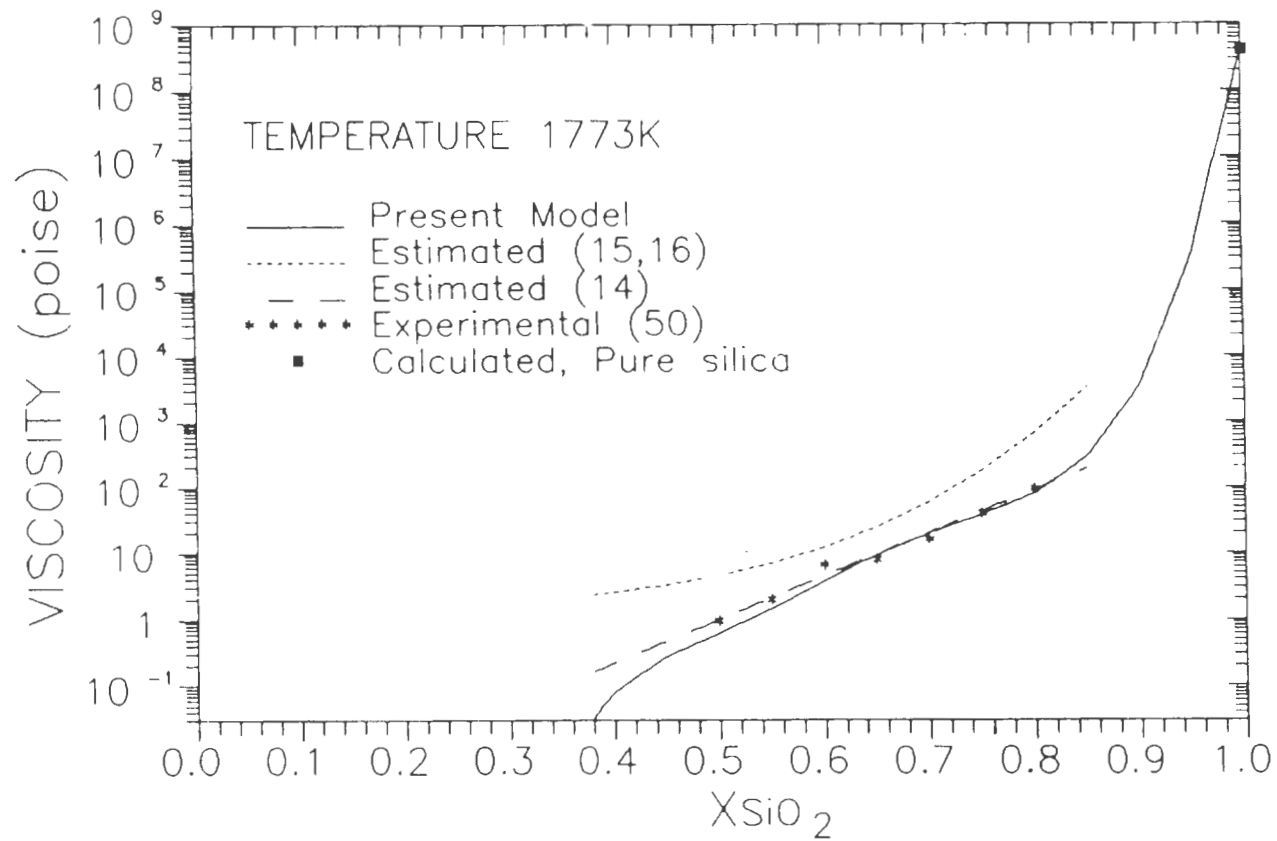


Fig.56—EXPERIMENTAL AND PREDICTED VISCOSITIES OF Li_2O-SiO_2 MELTS

the other two models.

The values predicted in the M_2O-SiO_2 systems considered here are in reasonable agreement with the experimental data. In the case of all three systems there was a sharp drop in the curve of viscosity as a function of mole fraction silica at approximately the same value of 0.35 mole fraction silica.

In general, the viscosity values can thus, be predicted in a consistent manner in all the systems. In a similar manner, it could safely be said that, it should be possible to predict viscosities in the case of other $MO-SiO_2$ and M_2O-SiO_2 type of melts where there is no experimental viscosity data available. The effect of solids in the melt could have an adverse effect on the measured viscosities, but very little investigation has been conducted on this in binary systems except on iron silicate melts.

EFFECT OF TEMPERATURE:

The variation of viscosities in the entire composition range with temperature is illustrated in figures 57 and 58. In these graphs, the viscosities have been plotted as a function of mole fraction silica, at 1423K and 1823K for the system Na_2O-SiO_2 , in figure 57 and for the system $FeO-SiO_2$, at 1523K and 1673K in figure 58. In figures 59 and 60 the variation of viscosities at particular mole fractions of silica as a function of temperature has been plotted. From these plots, it

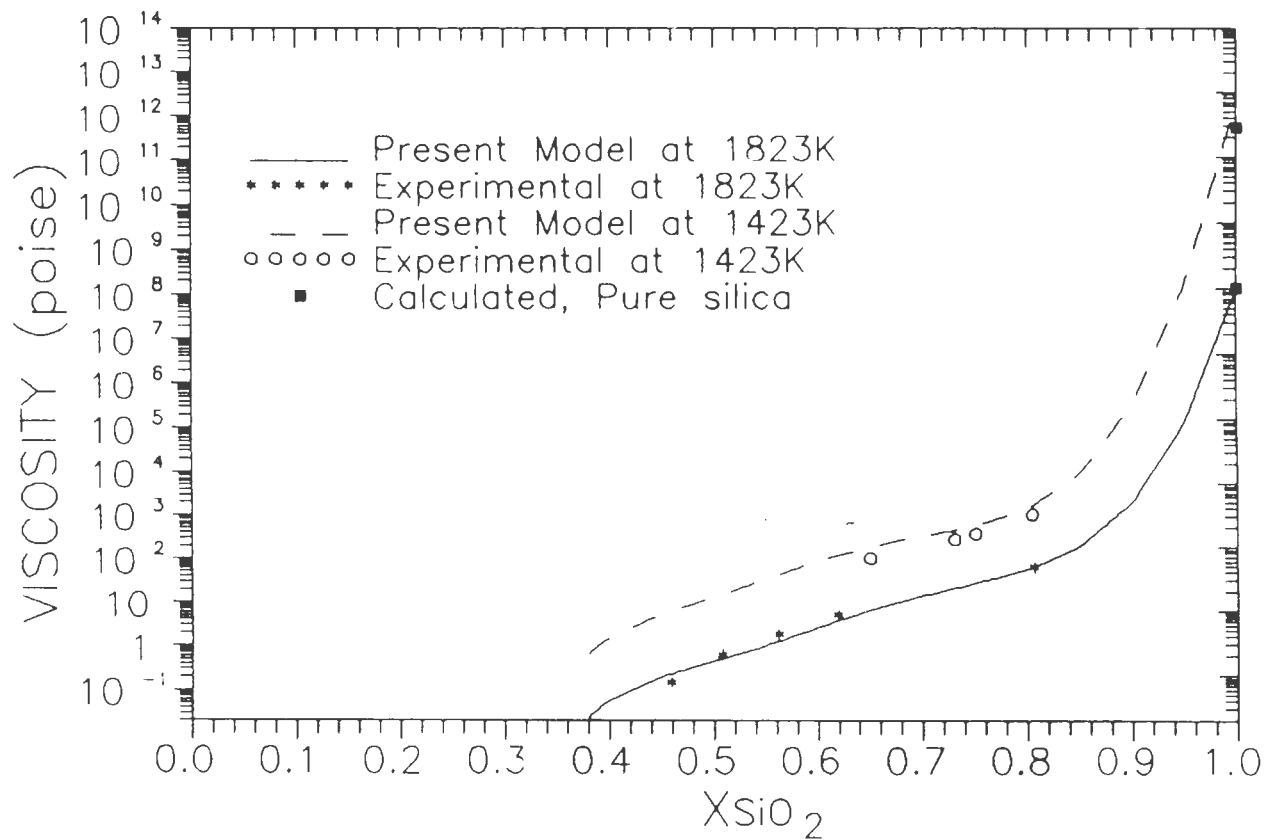


Fig.57—PREDICTED VISCOSITIES AT 1423K AND 1823K FOR THE SYSTEM Na₂O—SiO₂

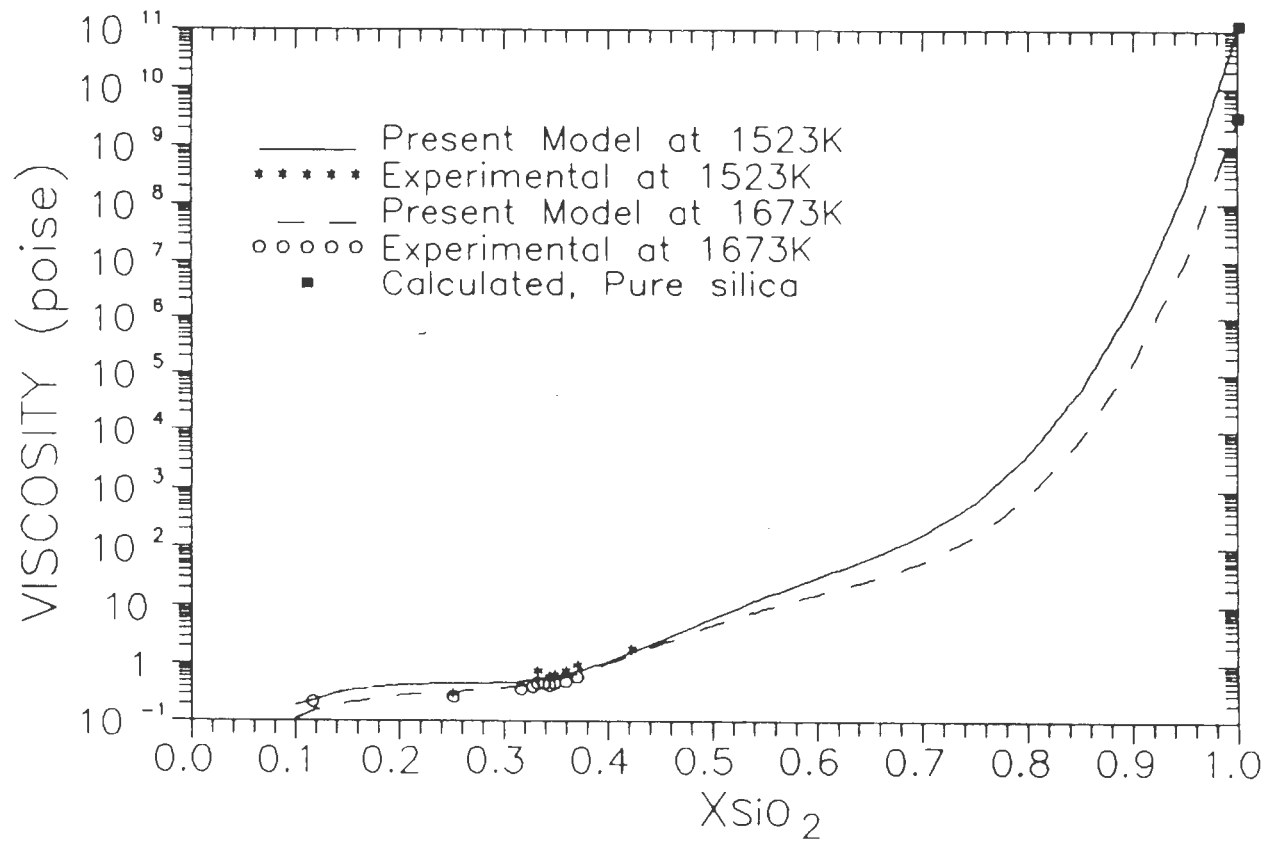


Fig.58—PREDICTED VISCOSITIES AT 1523K AND 1673K FOR THE SYSTEM FeO-SiO₂

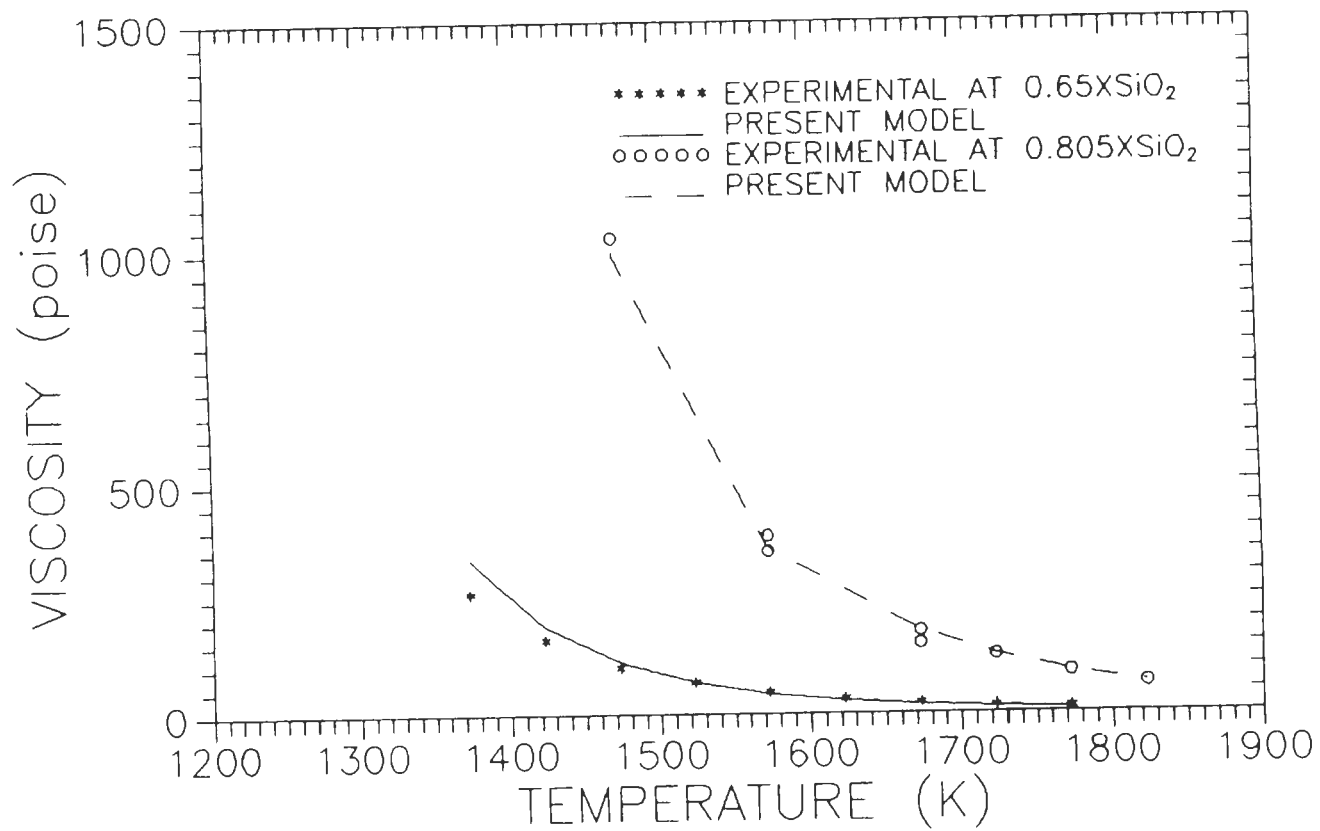


Fig.59—EFFECT OF TEMPERATURE ON VISCOSITY FOR Na₂O—SiO₂ MELTS

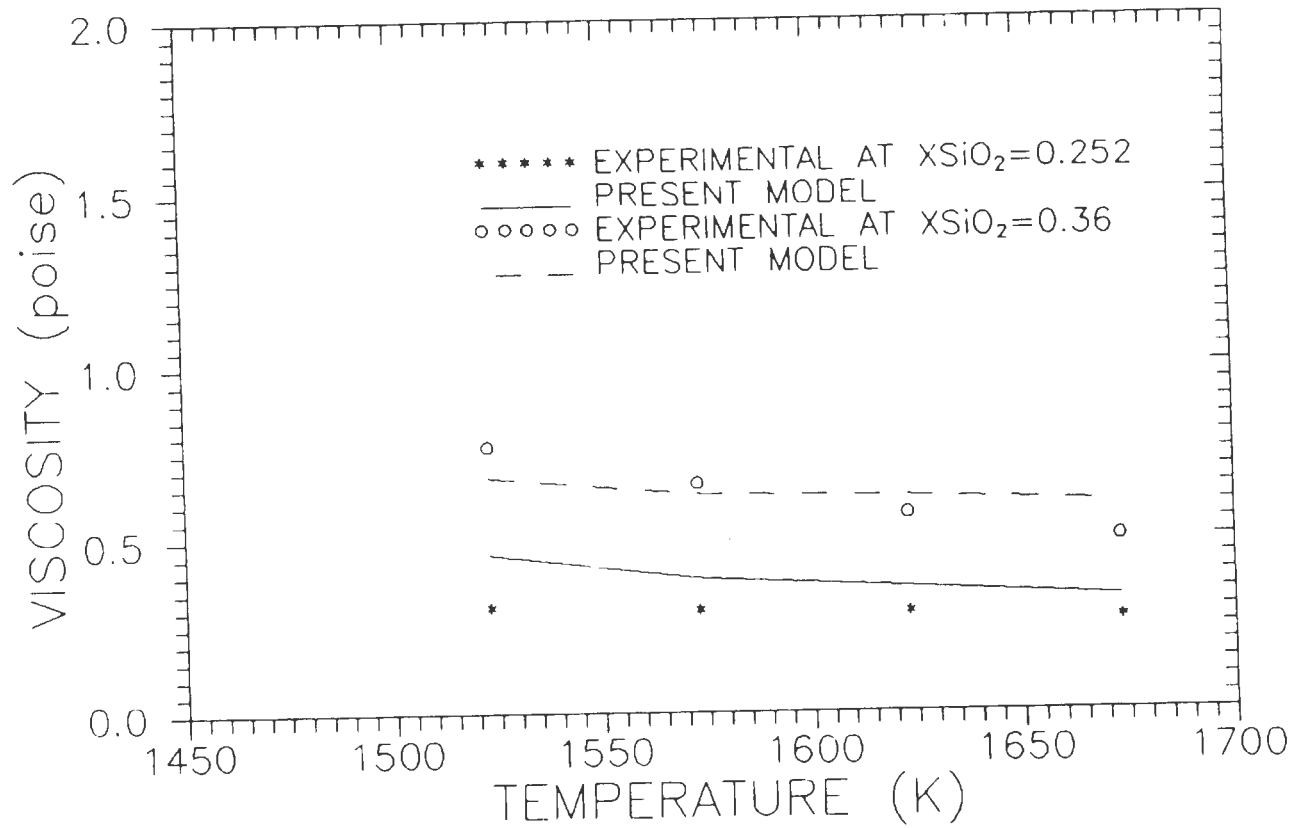


Fig.60—EFFECT OF TEMPERATURE ON VISCOSITY FOR FeO—SiO₂ MELTS

can be concluded that, as expected, temperatures have a significant effect on the viscosities of silicate melts and increase with decrease in temperature. This probably is due to appreciable change in the internal structure of a silicate slag over rather modest temperature ranges (18).

COMPARISON OF MO-SiO₂ AND M₂O-SiO₂ TYPE OF MELTS:

Figure 61 shows the plot of viscosities of iron silicate and sodium silicate melts at a fixed temperature of 1673K. Comparison of this figure with the figure 5, which shows the changes in energy in binary systems it can be concluded that the two plots are similar, in that, the drop in viscosities is much more sharp in the case of M₂O-SiO₂ melts as compared to MO-SiO₂ type of melt.

The effect that a cation has on the viscosity of a silicate melt is mainly dependent on the size of the cation. Sugihara et al. (69) have shown that in lead silicate melts, the viscosity increased with decreasing radius of the cation added in the case of MO additions (i.e. in the decreasing order as Ba²⁺, Sr²⁺, Ca²⁺, Mg²⁺, Be²⁺) while, viscosity increased with increasing radius of the cation added (Li⁺, Na⁺, K⁺, Rb⁺, Cs⁺).

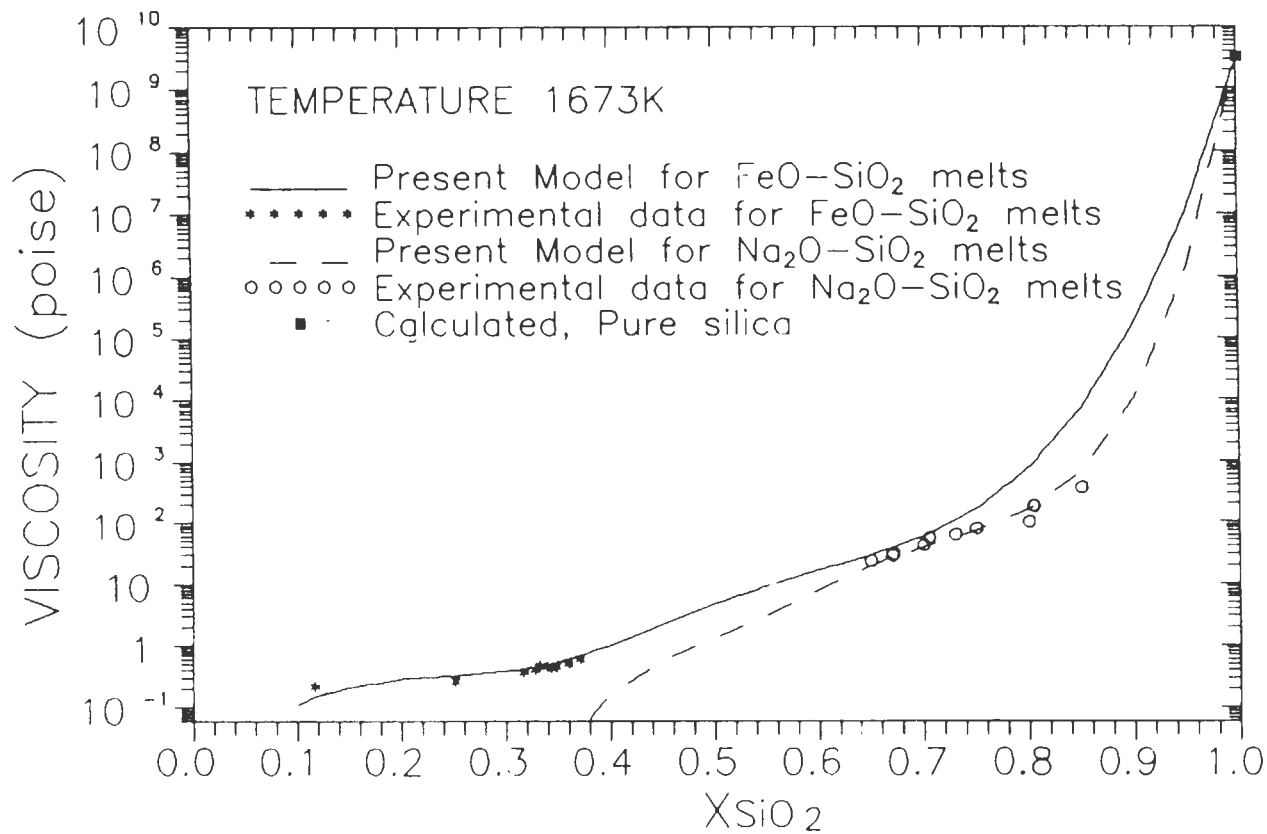


FIG. 61 - EXPERIMENTAL AND PREDICTED VISCOSITIES OF FeO-SiO₂ AND Na₂O-SiO₂ MELTS.

Table 3. Average percentage deviations for binary systems #.

| System | Composition (XSiO ₂) | Temperature K | D _p [*] | D _R [*] Percent [#] | D _U [*] |
|------------------------------------|-------------------------------------|------------------|-----------------------------|---|-----------------------------|
| CaO-SiO ₂ | 0.42-0.60 | 1773-2073 | 3.5 | 15.4 | 7.6 |
| MgO-SiO ₂ | 0.49-0.56 | 1823-2073 | -3.1 | -1.1 | -11.1 |
| MnO-SiO ₂ | 0.34-0.53 | 1673-1873 | 8.0 | 24.8 | 38.5 |
| BaO-SiO ₂ | 0.50-0.85 | 1773-2073 | -3.6 | 6.0 | 2.1 |
| SrO-SiO ₂ | 0.50-0.80 | 1773-2073 | -4.0 | 5.0 | 3.0 |
| FeO-SiO ₂ | 0.10-0.42 | 1523-1673 | -9.0 | 39.0 | 89.0 |
| Na ₂ O-SiO ₂ | 0.41-0.85 | 1373-1823 | 1.6 | -2.3 | 87 |
| K ₂ O-SiO ₂ | 0.74-0.83 | 1373-1673 | -25.0 | -29.0 | 80 |
| Li ₂ O-SiO ₂ | 0.45-0.81 | 1423-1773 | 11.0 | -0.2 | 74 |

Average Percentage deviation (APD) calculated as
 $\log(\eta_{cal}) - \log(\eta_{exp})$

* D_p APD for present model

D_R APD for Riboud model (14)

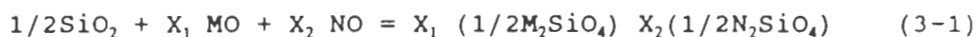
D_U APD for Urbain model (15,16)

Note: The smaller the average percentage deviation, the better is the agreement with experimental data.

3.4 TERNARY SYSTEMS:

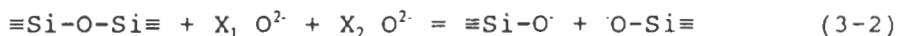
The binary model that was described in the earlier chapters was extended to ternary systems. The basic viscosity expression was the same, but the calculation of NO° and E have been modified. In this case the effect of both the cations on the silicate melt is considered. The method of calculation is described in detail in this chapter.

When Y moles of SiO_2 , M_1 moles of a metal oxide, MO and M_2 moles of another metal oxide, NO are mixed together, the reaction can be written as:



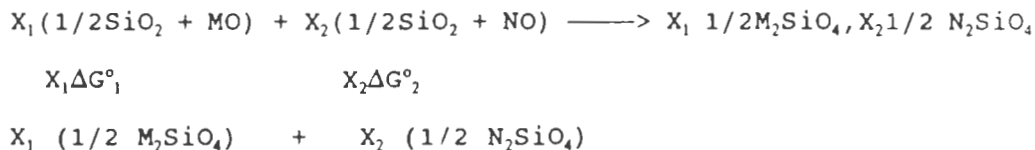
where, X_1 and X_2 are the individual fractions which can be expressed as $X_1 = M_1/(M_1+M_2)$, and $X_2 = M_2/(M_1+M_2)$.

In terms of simple electrochemical reaction, this can be written as:



The result is the breakdown of the silicate network to form oxygen atoms bonded to only one silicon atom and the metal ion stays close to it in order to maintain charge balance.

The entire cyclic process can be written as:



The total cyclic process, thus requires the consideration of the free energy changes associated with the formation of M_2SiO_4 from the interaction of MO with SiO_2 , and the formation of N_2SiO_4 as a result of the NO in the melt. In addition, these two must interact to form the reaction product of equation (3-1). The latter is small in comparison with the former two, and hence the free energy for the fore mentioned reaction can be simply written as the summation of two terms as:

$$\Delta G^\circ = X_1 \Delta G_1^\circ + X_2 \Delta G_2^\circ \quad (3-3)$$

The calculation of the term NO° followed from that for the binary systems, and involved more rigorous statistical calculations. These have been described in Hu's thesis (70). The final expression obtained was:

$$NO^\circ = [4 - 4(X_{MO} + X_{NO}) - NO^\circ] / 2[2 - (X_{MO} + X_{NO})] \quad (3-4)$$

The NO° is calculated by solving the following equation simultaneously:

$$[1 - \exp(\Delta G^\circ/RT)] (NO^\circ)^2 + [2(X_{MO} + X_{NO}) - 4] NO^\circ + 8[(X_{MO} + X_{NO})(1 - X_{MO} - X_{NO})] = 0 \quad (3-5)$$

The energy term was calculated by using the expression developed by the Flood et al (71) theory as follows:

$$\ln E_{\text{ternary}} = XM^{2+} \ln E_{MO-SiO_2} + XN^{2+} \ln E_{NO-SiO_2} \quad (3-6)$$

In this expression, the E_{MO-SiO_2} and E_{NO-SiO_2} are the energy terms of binary silicate melts and have been calculated using the same methods as described in section 2-2 (equations 2-11 to 2-16). The XM^{2+} and XN^{2+} are the "electrically equivalent

fractions" and can be expressed as

$$X_{M^{2+}} = \frac{2nM^{2+}}{2nM^{2+} + 2nN^{2+}} \quad (3-7)$$

$$X_{N^{2+}} = \frac{2nM^{2+}}{2nM^{2+} + 2nN^{2+}} \quad (3-8)$$

where $2nM^{2+}$ and $2nN^{2+}$ are the numbers of equivalent of the cations M^{2+} and N^{2+} in the solution.

Once the E_{ternary} is calculated, the NO° and E are substituted into the viscosity expression (equation 1-4) and the viscosities thus calculated.

Thus, the method described above can be used in calculating the viscosities of various binary combinations of M_2O and MO metal oxides with the silica melt. The method of calculation described above has been applied to various $MO-NO-SiO_2$ type of melts. The systems considered are $CaO-MnO-SiO_2$ system at various temperatures, $CaO-MgO-SiO_2$ at 1773K, ' FeO '- $MnO-SiO_2$ 1673K and CaO -' FeO '- SiO_2 at 1673K. The ternary plots are shown in figures 62 to 66 and some of the predicted viscosities using the proposed model, the models of Riboud et al and Urbain et al, along with the experimental data are shown in tables 5 to 8.

The results of the individual systems are discussed below.

CaO-MnO-SiO₂ SYSTEM:

Model predicted values are compared with the experimental data Segers et al (72) at temperatures of 1673-1773K and those of Kawahara et al (73) at 1823K. The agreement of the model with experimental data is quite good when compared to the values predicted by the Riboud et al (14) and Urbain et al (15,16) models, as seen from Tables 4 and 5. The model predicted isoviscosity contours are shown in Figures 62 to 64.

Segers et al (72) reports viscosity data for melts containing large amounts of CaO, despite their high melting points and their great chemical reactivity towards even Pt-20% rhodium alloy that they have used in their investigations. This could lead to a considerable amount of error in the experimental viscosities.

The liquidus temperatures in this system are those determined by Glasser (74). There is a large range of compositions with melting points lower than the temperature at which the liquidus contours are drawn and they extend from the binary CaO-SiO₂ system to the binary MnO-SiO₂ system for molar fractions of silica between 0.35 to 0.5.

CaO-MgO-SiO₂ SYSTEM:

Experimental data for this system have been taken from Mills and Keene (39) who have reported the data of Gulyai

Table 4. Calculated and Experimental Viscosities of CaO-MnO-SiO₂ system at 1673K^{*}.

| SiO ₂ (mole pct.) | MnO | CaO | η_{exp} | η_{R} (Poise) | η_{U} | η_{P} |
|---------------------------------|-----|-----|---------------------|------------------------------|-------------------|-------------------|
| 50 | 30 | 20 | 5.0 | 9.5 | 8.3 | 3.5 |
| 45 | 35 | 20 | 2.5 | 5.1 | 5.8 | 1.6 |
| 45 | 45 | 10 | 2.5 | 5.1 | 5.8 | 1.96 |

Table 5. Calculated and Experimental Viscosities of CaO-MnO-SiO₂ system at 1773K^{*}.

| SiO ₂ (mole pct.) | MnO | CaO | η_{exp} | η_{R} (Poise) | η_{U} | η_{P} |
|---------------------------------|-----|-----|---------------------|------------------------------|-------------------|-------------------|
| 40 | 30 | 30 | 0.8 | 1.6 | 2.6 | 0.6 |
| 40 | 40 | 20 | 0.8 | 1.6 | 2.6 | 0.97 |
| 40 | 50 | 10 | 3.6 | 5.3 | 4.6 | 2.9 |
| 50 | 10 | 40 | 3.5 | 5.3 | 4.6 | 3.2 |
| 50 | 20 | 30 | 3.0 | 5.3 | 4.6 | 3.5 |

* η_{R} Predicted values using Riboud et al. model(14)

η_{U} Predicted values using Urbain et al. model(15,16)

η_{P} Predicted values using the Present proposed model

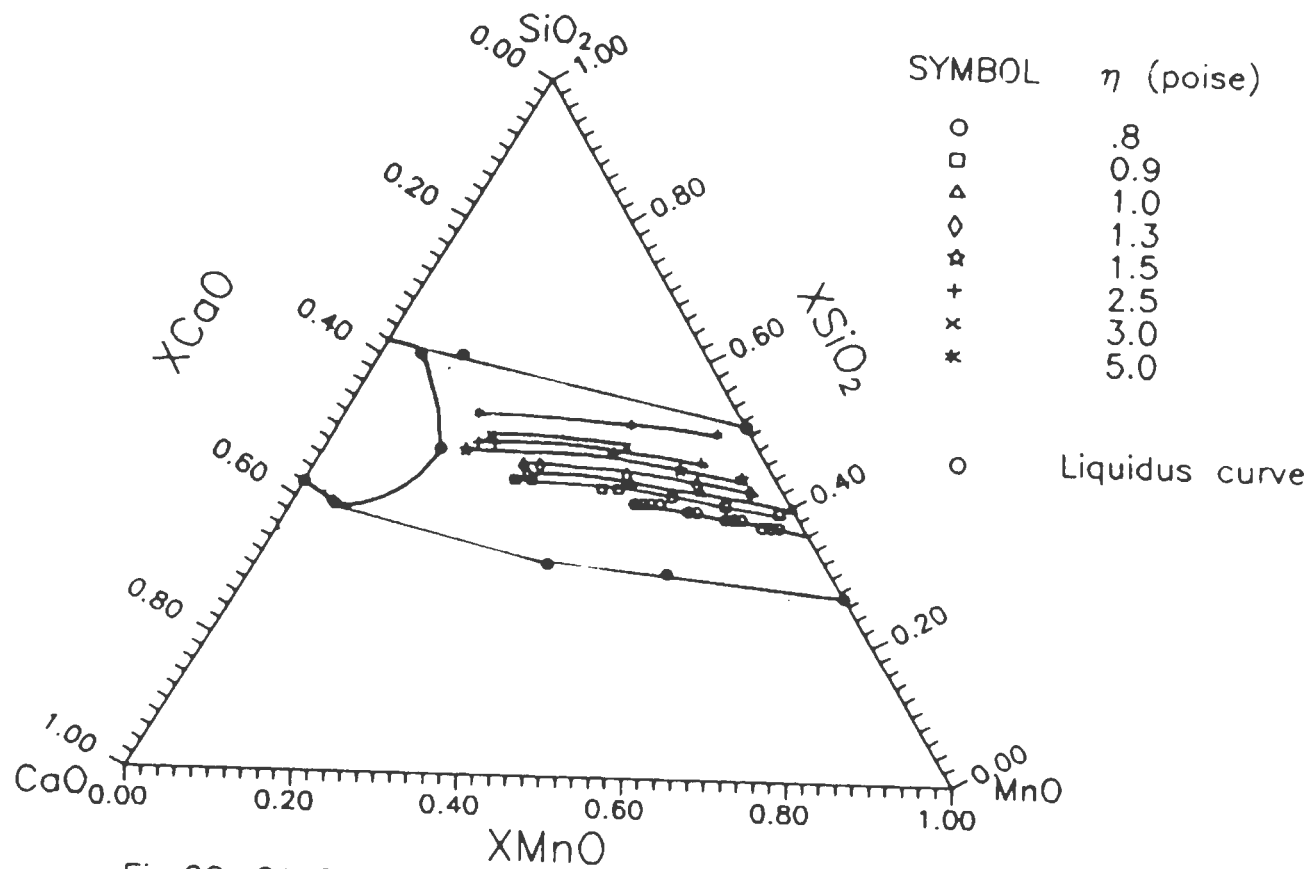


Fig.62-CALCULATED VISCOSITIES OF CaO-MnO-SiO₂ MELTS AT 1673K

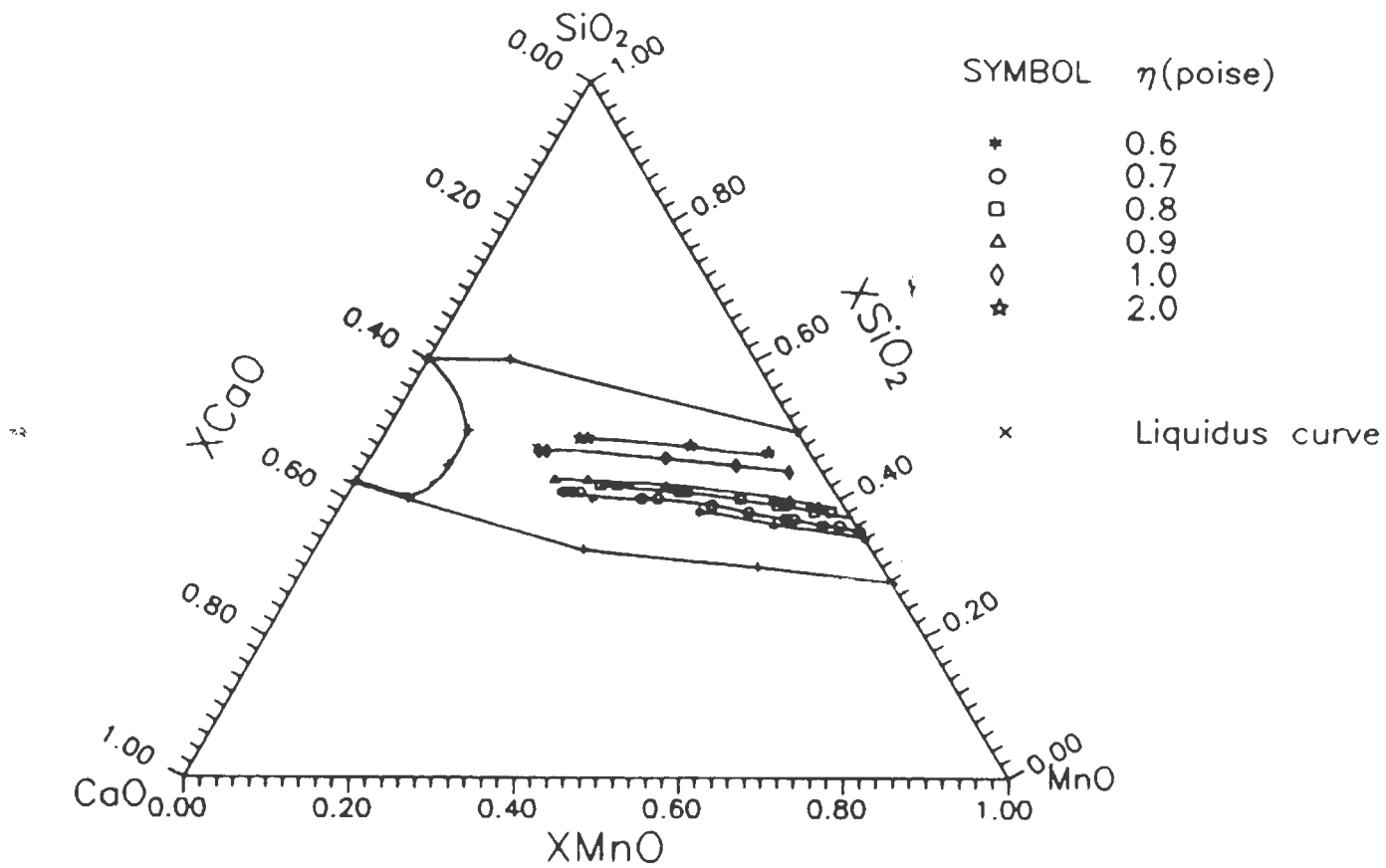


Fig.63—CALCULATED VISCOSITIES OF CaO—MnO—SiO₂ MELTS AT 1723K

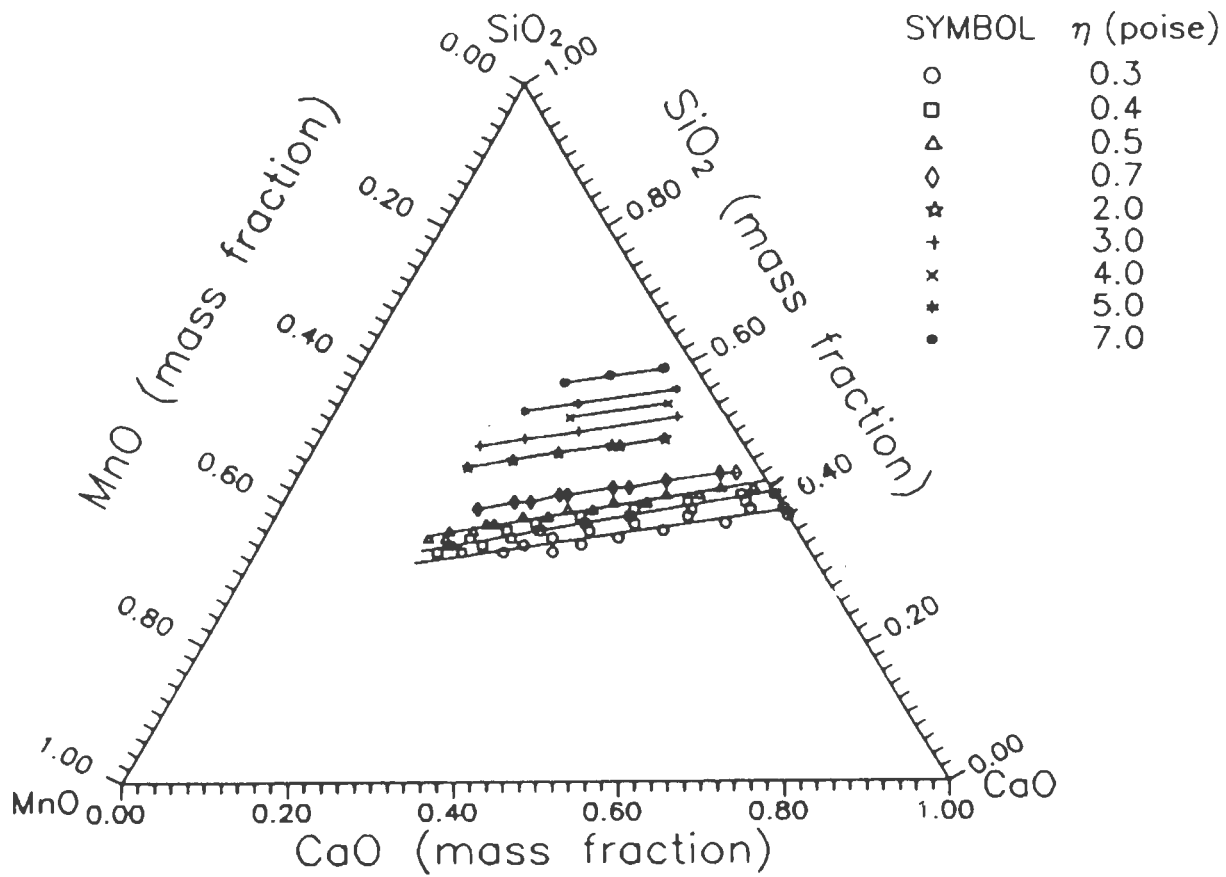


Fig.64—CALCULATED VISCOSITIES OF CaO—MnO—SiO₂ MELTS AT 1823K

(75) and Machin and Yee (76) at 1773K. There is considerable amount of disagreement in the experimental data reported by these two investigators. The shape of the model predicted viscosity contours agree with the contours of Machin and Yee, as seen from Figure 65, but comparison of viscosities at the same composition shows that the viscosities predicted by using the model are slightly higher than the experimental values. But in general, the agreement is quite good. As seen from the Table 6, the values predicted by the Riboud et al (14) and Urbain et al (15,16) models are also in good agreement with the experimental values. The experimental and model predicted viscosity contours indicate that there is a slight decrease in viscosity when CaO is replaced by MgO, on a mass percent basis.

'FeO'-MnO-SiO₂ SYSTEM:

The model predicted contours are compared with those of Adolf et al (77), which Mills and Keene (39) have reported at 1673K. Iron crucibles and bobs have been used in making these measurements. According to Mills and Keene (39), the isoviscosity contours of Adolf et al (77) give a general agreement with those reported by Kozakevitch (78). But the data of Sokolov et al (79) are higher than the values of Adolf et al (77). The values predicted by the present model (figure 66 and table 7) are only in reasonable agreement with the

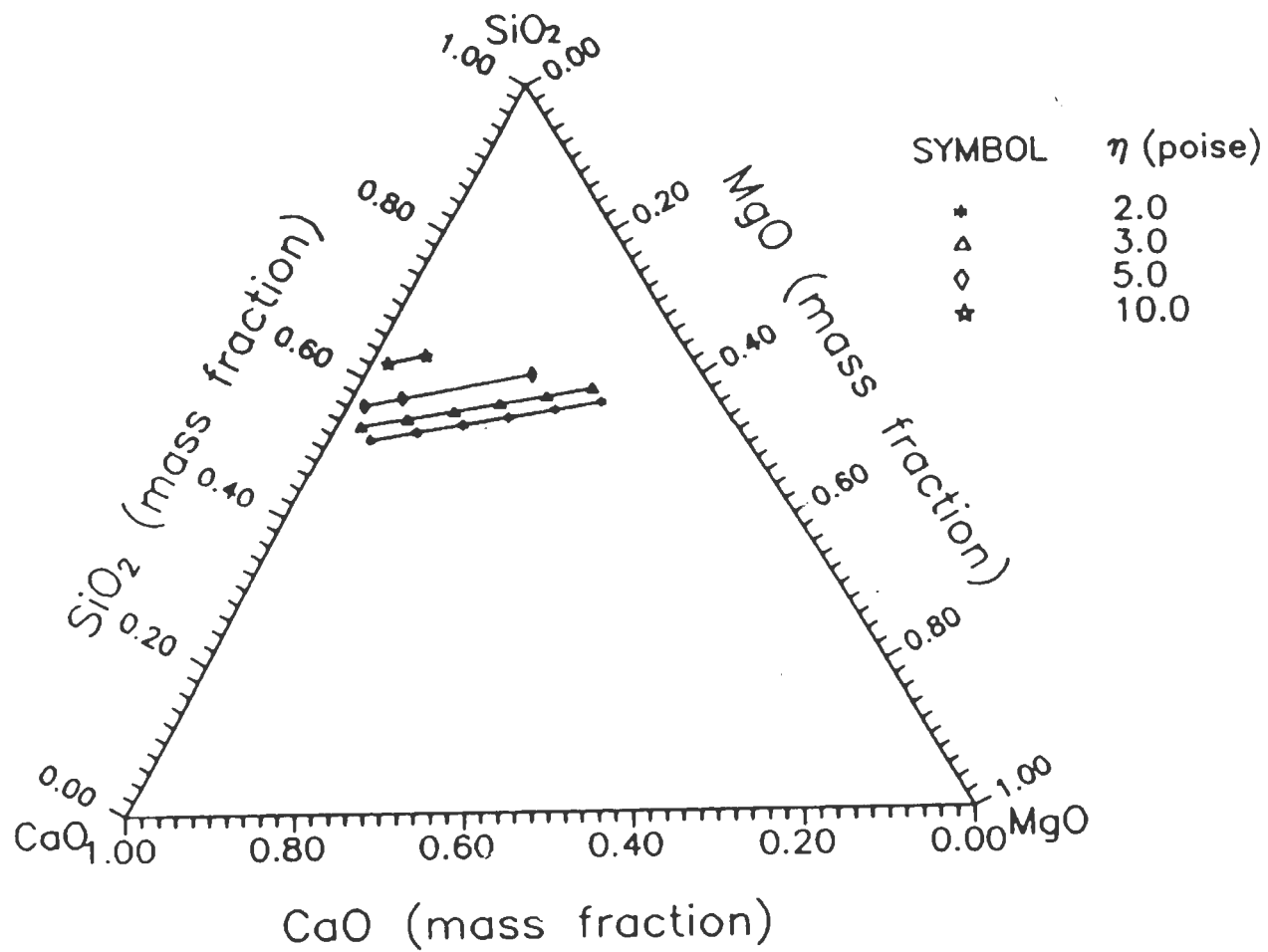


Fig.65—CALCULATED VISCOSITIES OF CaO—MgO—SiO₂ MELTS AT 1773K

Table 6. Calculated and Experimental Viscosities of CaO-MgO-SiO₂ system at 1773K*.

| SiO ₂ (mass pct.) | CaO | MgO | η_{exp} | η_{R} (Poise) | η_{U} | η_{P} |
|---------------------------------|------|------|---------------------|------------------------------|-------------------|-------------------|
| 59.2 | 33.3 | 7.5 | 10 | 10.4 | 7.5 | 6.36 |
| 55.8 | 30.8 | 13.3 | 5 | 3.4 | 5.0 | 3.39 |

Table 7. Calculated and Experimental Viscosities of FeO-MnO-SiO₂ system at 1673K*.

| SiO ₂ (mass pct.) | FeO | MnO | η_{exp} | η_{R} (Poise) | η_{U} | η_{P} |
|---------------------------------|-----|-----|---------------------|------------------------------|-------------------|-------------------|
| 20 | 60 | 20 | 0.3 | 0.32 | 2.26 | 0.32 |
| 20 | 50 | 30 | 0.5 | 0.32 | 2.26 | 0.32 |
| 40 | 50 | 10 | 1.0 | 4.6 | 5.54 | 2.01 |
| 40 | 20 | 40 | 1.0 | 4.6 | 5.54 | 2.16 |

* η_{R} Predicted values using Riboud et al. model

η_{U} Predicted values using Urbain et al. model

η_{P} Predicted values using the Present proposed model

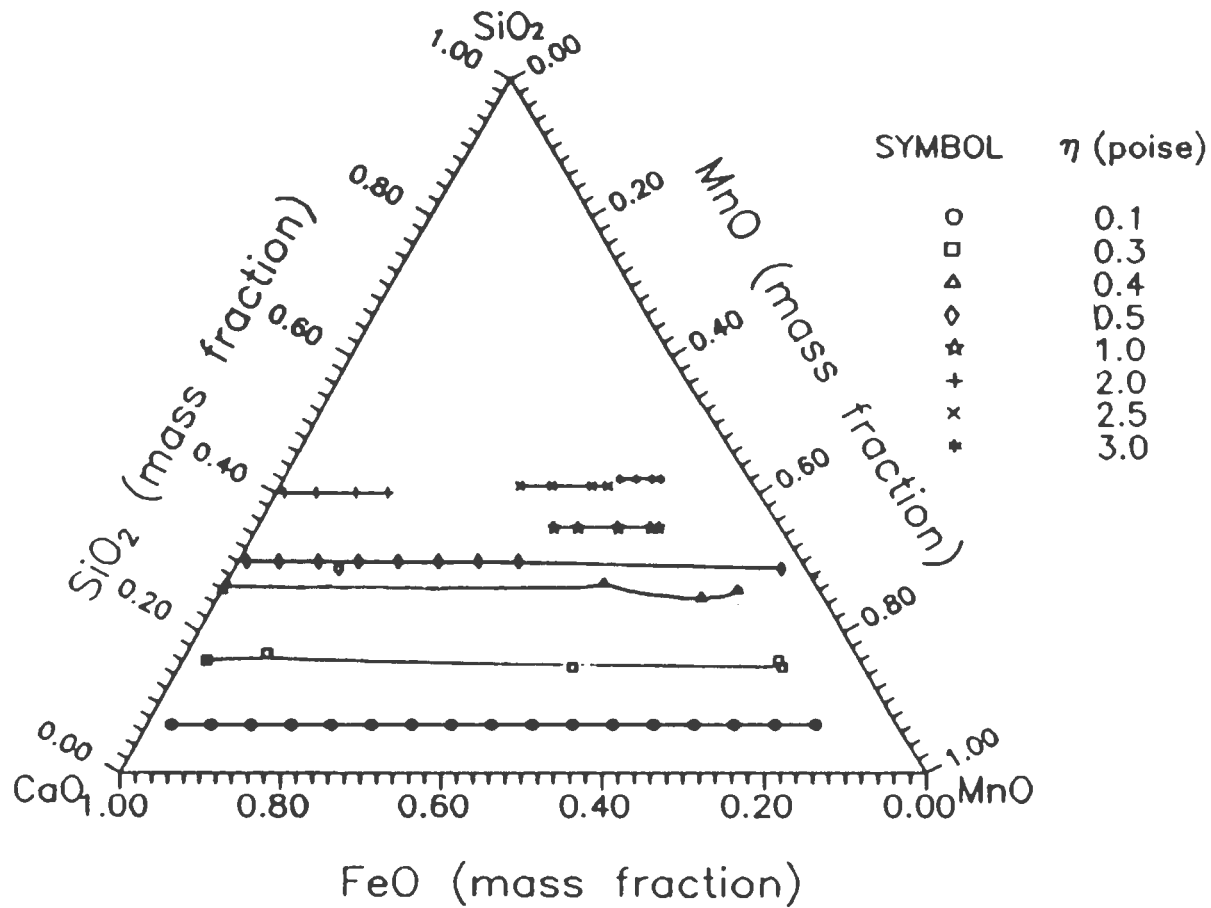


Fig.66-CALCULATED VISCOSITIES OF FeO-MnO-SiO₂ MELTS AT 1673K

experimental data with which they were compared. The model predicted does not predict the experimental isoviscosity contours, which are very similar to the liquidus curves. One possible reason could be that the melt is considered to consist of FeO as the primary iron oxide phase, but the minor amounts of other phases, like Fe_2O_3 , could increase the experimental viscosities considerably (as discussed in the binary FeO-SiO₂ system, section 3.3). The models of Riboud et al (14) and Urbain et al (15,16) also do not predict these isoviscosity contours. However, MnO-FeO solutions are considered to be ideal solutions and there should be no change in the viscosity values when one is substituted by the other (as indicated by the models), although this is not what has been experimentally observed.

CaO-'FeO'-SiO₂ SYSTEM:

The experimental values reported in Mills and Keene (39) from various investigators have been compared with the model predicted values, and the values predicted using the Riboud et al (14) model and Urbain et al (15,16) models in Table 8. The viscosity contours could not be predicted by any of the models. Mills and Keene have reported that the conditions were controlled to ensure that the iron oxide phase was predominantly present as FeO. The isoviscosity contours do not have the same shape as the liquidus temperature contours.

Table 8. Calculated and Experimental Viscosities of
CaO-FeO-SiO₂ system at 1673K*.

| SiO ₂ (mass pct.) | FeO (mass pct.) | CaO (mass pct.) | η_{expt} | η_{R} (Poise) | η_{U} | η_{P} |
|---------------------------------|--------------------|--------------------|----------------------|------------------------------|-------------------|-------------------|
| 45 | 46.3 | 8.7 | 4 | 7.73 | 7.26 | 3.17 |
| 43.7 | 26.3 | 30 | 2 | 5.68 | 1.3 | 4.89 |
| 43.7 | 30 | 26.3 | 2 | 5.82 | 1.44 | 5.12 |
| 30 | 50 | 20 | 0.5 | 3.21 | 0.29 | 1.01 |
| 30 | 38.8 | 31.2 | 0.5 | 3.1 | 0.17 | 0.91 |
| 30 | 47.5 | 22.5 | 0.5 | 3.18 | 0.27 | 0.99 |

* η_{R} Predicted values using Riboud et al. model(14)

η_{U} Predicted values using Urbain et al. model(15,16)

η_{P} Predicted values using the Present proposed model

In conclusion, it could be said that the model requires some refining in order to accurately predict experimentally determined isoviscosity contours. One possibility could be that the free energy of formation (ΔG°) of the complex compound does have a large enough value to make a difference in the NO° value. But very little information on these free energy data are available to date and would thus, require the determination of these quantities with great accuracy. As seen in the case of binary iron silicate melts (section 3.2), solids maybe playing an important role in the ternary melts also and this too may have to be accounted for. Also in general, the extent of ternary viscosity experimental data itself are few and disparate and this heavily restricts progress.

PART B.
CHAPTER 4
SPENT POTLINER STUDIES

4.1 LITERATURE REVIEW:

The spent potliner is generated during the electrolytic process (Hall-Heroult) of reducing alumina (bauxite) in the production of aluminum using a bath of molten salts, cryolite (Na_3AlF_6) and aluminum fluoride (AlF_3) in a rectangular steel cell (pot). The corrosion/erosion of the cathode (lining of the steel cell) by the molten Al metal and other chemicals destroy it and it has to be replaced after 3-5 years or longer. Approximately 40-60 tons of spent potliner is generated from each pot. It has been placed in the list of hazardous materials, because of its high concentrations of cyanide which is produced by chemical reaction between hydrogen, carbon and nitrogen. Moreover, it also contains leachable metal components like NaF and AlF_3 . Considering the fact that, on an average, there is about 190,000 tons of spent potliner produced in the U.S. annually, (80) and that there is a record of about 1.1 million tons already present, this proves to be quite a problem.

The major constituents of the SPL are carbon as graphite and sodium fluoride. Thus there are a number of valuable elements in the SPL that could be recovered. The 60% Carbon from the spent cathode was estimated to have a energy value estimated between 3,000 and 5,000 Btu/lb (81). This calorific

value could be used advantageously. Fluoride (15% or more of total material) is a valuable chemical. Substantial amounts of Cryolite could be recovered. For these reasons, many alternative methods have been investigated that address the recovery of valuable chemicals and energy resources as well as the disposal and/or destruction of spent potliner.

Blayden and Epstein (81), have made a critical review of the alternative disposal and recovery techniques. Chief amongst them are the use of SPL as a substitute for fluorspar in iron smelting and steelmaking, (83-85) and as a supplementary fuel in the cement industry (82,83). But the transportation costs have proven to be an important concern here. Fluidized bed combustion of SPL has been viewed as another disposal technique (82). But the problem of crushing in order to obtain a proper size feed to the combustor (about 100 mesh) has been a factor of concern. Other than these three disposal techniques, several recovery techniques were also considered like the cryolite recovery (82), recovery of chemical and energy values with molten salts (82), pyrohydrolysis (82) and pyrosulfolysis (82). But the limited market for cryolite, and complexity of the process of recovery of chemical and energy values have dampened further work on the first two recovery processes. The pyrohydrolysis process was suspected to cause economical problems. Moreover, some of these processes would generate waste products that would have

to be taken care of. Considering the large quantities of SPL that is being generated some other alternative method of disposal is still being researched. In the present work the preliminary studies on fixing SPL in a glassy matrix has been carried out.

4.2 GLASS FORMATION CHARACTERISTICS:

The factors involved in glass formation are considered in this section where, the general rules of glass formation, and the effect of various parameters like temperature, cooling rate and cations on glass formation are discussed.

The structural model of glass formation is based largely on that of Zachariasen (86) and Warren's (87) rules.

Zachariasen formulated some rules which concerns glass formation based on the tetrahedral coordination. According to these rules an oxide glass will be formed (86): a) if the sample contains a high percentage of cations which are surrounded by oxygen tetrahedra or by oxygen triangles b) if these tetrahedra or triangles share only corners with each other c) if some oxygen atoms are linked to only two such cations and do not form further bonds with any other cations; and d) at least three corners in each oxygen polyhedron must be shared.

Silica is a good candidate as a glass former as it satisfies these conditions very well. Figure 67a (88) shows

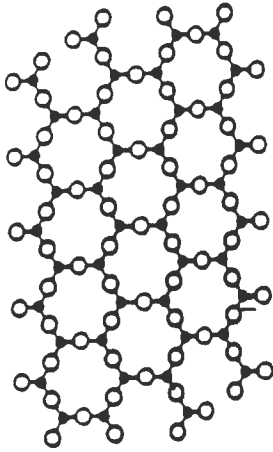


Fig. 67a -STRUCTURE OF CRYSTALLINE SILICA

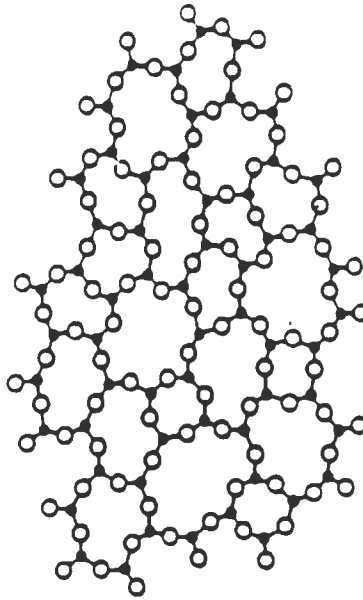


Fig. 67b -STRUCTURE OF SILICA GLASS

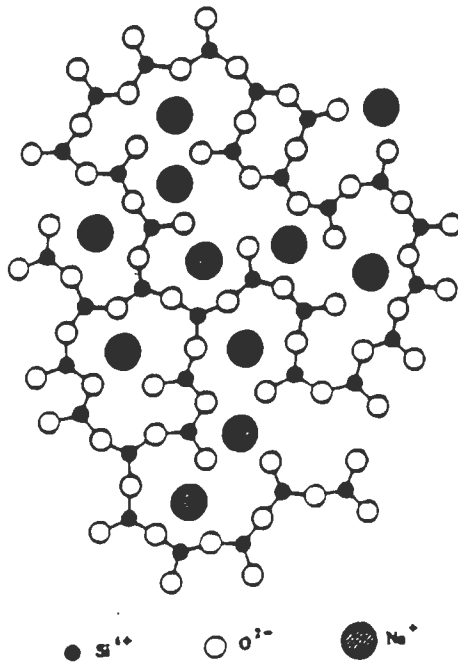


Fig. 67c) -STRUCTURE OF SODIUM SILICATE GLASS

the regular silica network structure. Here, the silicon atoms are shown as small black spheres surrounded in a tetragonal array by oxygen atoms shown as larger open spheres. This is a two-dimensional view and the fourth oxygen atoms project from the plane of the paper. Each oxygen is therefore coordinated to two silicon atoms. The structure is thus covalent and has a high melting point. Figure 67b shows the structure of a glass where the short range order is maintained but the long-range order is broken up.

Many silicates are cooled from the liquid state to form non-crystalline products. This requires that the driving force for the liquid-crystal transformation be low and that the activation energy for the process be high. The rate of nucleation for a crystalline phase forming from the liquid is proportional to the product of the energy difference between the crystal and liquid ($\Delta H_f/T_{mp}$) and the mobility of the constituents that form a crystal (which depends on the viscosity of the melt). In silicate systems, both of these factors change so as to favor the formation of glasses as the silica content increases. The limiting mobility is that of the large network-forming anions and is inversely proportional to the viscosity. Thus the product of $\Delta H_f/T_{mp}$ and $1/\eta$ can be used as one index for the tendency to form glasses on cooling.

For silica, (88), at the melting point of 1713°C, the product of $\Delta H_f/T_{mp}$ and $1/\eta$ is equal to 1.1×10^{-6} . This justifies

the fact that silica is a good glass former.

Glasses are amorphous (vitreous) solids that have formed from a liquid on cooling in a reversible process. Glass formation is a rate phenomenon that requires the understanding of the thermodynamic picture of the structure of glasses and the kinetic treatment. A liquid forms a glass, on cooling if the conditions do not permit its crystallization. The probability of nucleation, which is one of the prerequisite for crystallization (mobility of the constituents being the other) is decreased by rapid cooling, high activation energy of nucleation and low liquidus temperature. There is generally no relation between activation energy of nucleation of a substance and its thermodynamic properties including the average bond strength. There is also no valid relation between the rate of nucleation of a substance and the free-energy change of the process, that is, the difference between the energy content of the compound in its crystalline and its molten state.

EFFECT OF TEMPERATURE:

When a liquid is cooled, the melt passes through a range of temperatures. The relationships between the liquid, the crystalline and the glassy states of a material are explained by the volume-temperature diagram (figure 68) (89). On cooling the liquid, there is a discontinuous change in the volume at

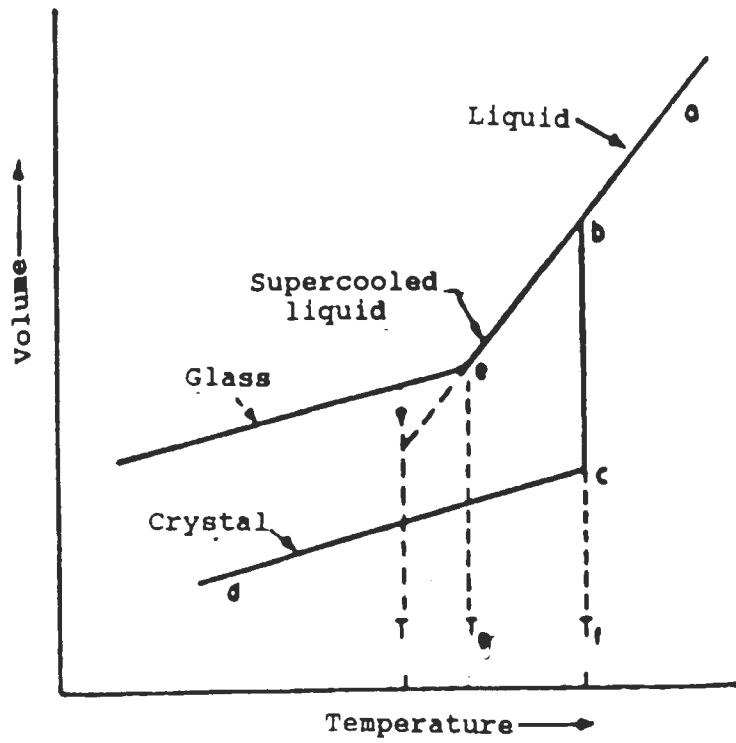


Fig.68 -EFFECT OF TEMPERATURE ON GLASS FORMATION

the melting point if the liquid crystallizes (bc). On further cooling, the crystalline substance contracts along cd. No crystallization takes place if the rate of viscous flow is sufficiently rapid. This is because the rate of viscous flow is too slow to permit atomic rearrangement. If no crystallization takes place, the volume of the liquid decreases at about the same rate as above the melting point until there is a decrease in the expansion coefficient at a range of temperatures called the glass transformation range. Below the temperature range the glass structure does not relax at the cooling rate used. The expansion coefficient for the glassy state is usually about the same as that for the crystalline solid. Below the transition temperature (T_g) the direction is changed and it continues almost parallel to the contraction curve of the crystalline form. The transformation temperature (Tammann's temperature- T_g) is thus the temperature that separates the glassy state (below T_g) from the liquid state (above T_g). If the temperature of glass is held constant at T_1 the volume decreases slowly until it reaches a point on the dotted line-this is a more stable condition and the process is called stabilization. By heating the glassy material in the annealing range, in which slow relaxation can occur, the glass structure in time approaches an equilibrium density corresponding to the supercooled liquid at that temperature. There is an increase in glass transition

temperature with increase in cooling rate (as do the specific volumes of the glasses).

Generally, glass has the tendency to return to the crystalline state, but is prevented in doing so by the extremely high viscosity. At elevated temperatures, when glass transforms into a more plastic state, either single crystals may develop or the glass crystallizes completely. A study on the system PbO-SiO_2 containing transition metal oxides indicated that the viscosity of a glass in which a part of the SiO_2 is substituted with FeO or MnO is lower than that of the base glass (90). This difference results from reduction of SiO_2 since the viscosity of the glass containing FeO is approximately the same as that of glass containing MnO .

When glasses of different compositions are kept in contact, for sufficiently long times, at temperatures near or above T_g of one of the glasses a reaction interface between them can be observed (91). This reaction is described in terms of a diffusion process of the different constituents of the glasses. Results of SiO_2 and Al_2O_3 diffusion in reactions between commercial plate glasses using an etching technique and R.I. measurements by optical interferometry (92), Ca interdiffusion profiles between $\text{Na}_2\text{O-CaO-SiO}_2$ glasses (93), and both K and Ca interdiffusion in $\text{K}_2\text{O-CaO-SiO}_2$ glasses have been reported (94). Reactions between SiO_2 glasses and $\text{K}_2\text{O-SiO}_2$ melts with SiO_2 contents between 64 and 85 wt.% have

been investigated (95).

EFFECT OF COOLING RATE:

The cooling rate necessary to avoid a given volume fraction crystallized can be estimated from:

$$V^{\beta}/V \approx \pi / 3 I_v u^3 t^4 \quad (4-1)$$

where, V is the volume of the sample, V^{β} is the volume of the transformed region, I_v is the nucleation rate, u is the growth rate/unit area of the interface and t is the time.

TTT curves can be drawn, that is, a particular fraction crystallization is selected and the time required for the volume fraction to form at a given temperature is calculated.

The nucleation rates are calculated from:

$$I_v \approx n_0 \tau \exp(-\Delta G_m / kT) \exp(-\Delta G^* / kT) \quad (4-2)$$

where τ is the molecular jump frequency, ΔG_m is the activation energy for transport across the nucleus-matrix interface, n_0 is the number of molecules/unit volume and ΔG^* is the free energy of formation of critical size nucleus.

The growth rates are measured experimentally or from formulae and calculated repeatedly for a series of temperature and possibly for various fraction crystallized. The nose of the TTT curve, corresponding to the least time for the given volume fraction crystallized, results from a competition between the driving force for crystallization, which increases with decreasing temperature and the atomic mobility, which

decreases with decreasing temperature. The cooling rate to avoid crystallization is roughly estimated from:

$$(dT/dt)_c \approx \Delta T_n / \tau_n \quad (4-3)$$

where, $T_n = T_0 - T_n$; T_n being the temp. at the nose of the TTT curve, τ_n is the time at the nose of the TTT curve.

Materials such as Al_2O_3 , H_2O and Na_2O-SiO_2 which are quite fluid over a range of temperatures below their melting points can only be obtained as glasses by achieving very rapid cooling.

The driving force for nucleation is given by the difference between the tangent line drawn to C_0 (figure 69) and the free energy curve of the phase being formed at the composition of interest.

EFFECT OF CATIONS:

Role of cations in glass formation depends on valence and coordination number and the related value of single-bond strength.

When a network modifying oxide like Na_2O is added to a network forming oxide like SiO_2 (96), the cation Na^+ goes into holes in the network which exist between the oxygen tetrahedra. These holes are statistically distributed since the framework is without periodicity and symmetry. For each Na_2O molecule added to SiO_2 two nonbridging oxygens are formed, causing a gradual breakdown of the silicon-oxygen network with

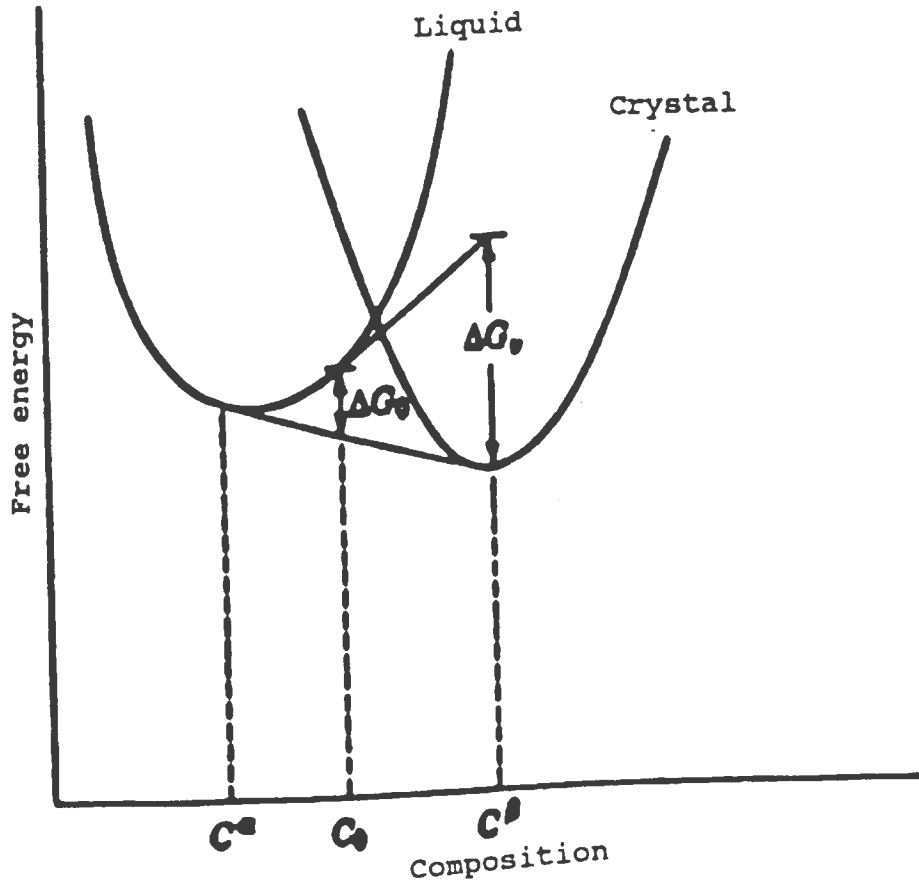


Fig. 69-FREE ENERGY VS COMPOSITION CURVE

the alkali ions randomly distributed in the network. However, this random distribution of cations offers no satisfactory explanation for several changes in physical properties as a function of composition. In binary and multicomponent oxide glasses, experimental evidence favors a preferred clustering of the modifying cations. Moreover the tendency for phase separation, both above and below the liquidus line, can be observed. The result of this immiscibility can be amorphous phase decomposition or glass-in-glass separation. The mechanism of the decomposition will be determined by the initial state of the material which in the case of a sub-liquidus separation maybe thermodynamically metastable or unstable. In the metastable region, decomposition occurs by classical nucleation and growth. Microstructures developed by this mechanism are typified by irregular diffuse phase boundaries and both phases are continuously interconnected.

The ion mobility, though, depends on the melt atmosphere. The surface behavior of alkali ions varies depending on the composition of the glasses. This surface behavior was studied in $\text{Li}_2\text{O}\cdot 0.3\text{SiO}_2$ and $\text{Na}_2\text{O}\cdot 0.3\text{SiO}_2$ glasses using simulation techniques. The simulations reproduce the observed excess of Na(K) at the outer surface of the appropriate glass and the lack of such excess of Li ions at the surface of $\text{Li}_2\text{O}\cdot 0.3\text{SiO}_2$ glass. Elevated temperatures enhance the surface excess of alkali in the Na(K) case, but does not appear to do so in the

Li case. In order to show the dependence on melt atmosphere sodium ion mobility was studied in high purity GeO_2 glasses, (97) for glasses melted under varying oxygen partial pressures. Increased oxygen partial pressure during melting increases the sodium ion mobility for glasses melted at the same temperature. This effect is attributed to the effect of oxygen partial pressure upon intrinsic defect concentrations within the glass which influence the structure of the energy states in which the Na^+ resides and through which it moves. Alkali ions get transported under the influence of electric fields through high purity silica and germania glasses. The effects of the partial pressures are manifested primarily through changes on the entropy of activation for Na^+ ion motion.

The illustration of the effect on the structure of silica on the addition of mono-valent or divalent oxide that act as a network breaker is shown in figure 65c (88). The metal oxide is indicated as cross-hatched spheres. These serve the purpose of increasing the ionic character of the melt and also in reducing the melting point.

EFFECT OF IMPURITIES:

Impurities, including atmospheric impurities and departures from stoichiometry, can appreciably increase the growth rate in many oxide materials and certainly in many of

the important glass-forming materials like H_2O and O_2 in SiO_2 . The use of H_2O and other mineralizing agents to increase the rate of crystallization in oxide systems has been known (88). It is expected that these effects should be most important for compositions having a network characteristic and for pure materials. A transition from interface controlled growth to diffusion controlled growth is anticipated as progressively large concentrations of impurities are added to materials such as SiO_2 . For solute species which increase the growth rate, their rejection and buildup at the interfaces may result in a greatly enhanced growth rate which increases with time. In such cases, specimens may be completely crystallized before anything like steady state growth conditions are maintained. Such autocatalytic effects should be more likely to initiate in the regions between 2 advancing interfaces where the buildup of solutes is most significant.

MISCIBILITY GAP IN SILICATE MELTS:

A study on the binary system Na_2O-SiO_2 showed that at 14.8 mole % Na_2O , 4 hours at $680^\circ C$ dispersed particles in a continuous matrix are seen. At 14.8 mole % Na_2O , 8 hours at $600^\circ C$ two interconnected phases, unstable region is seen (96). As a consequence, most binary or multicomponent glasses are non-homogeneous on a fine scale, since most of them had to pass through the critical temperature region, even without

special heat treatment which was necessary to form microstructures. For compositions outside the unstable region (figure 70), the chemical potential of a given component increases with the density of the component and a homogeneous solution is stable or metastable, depending on whether the given composition lies inside or outside the miscibility gap. Within the gap but outside the spinodal, a homogeneous solution is stable against infinitesimal fluctuations in compositions, but can separate into an equilibrium two phase system by a nucleation and growth process.

The addition of modifier oxides to SiO_2 often leads to liquid-liquid immiscibility. Miscibility gaps are found when MgO , FeO , ZnO , CaO , SrO , or BaO are added to SiO_2 , and only in the case of BaO additions is the miscibility gap metastable (88). Among the alkali silicates, metastable miscibility gaps are found in the $\text{Li}_2\text{O}-\text{SiO}_2$ and $\text{Na}_2\text{O}-\text{SiO}_2$ systems. Metastable miscibility gap in the $\text{K}_2\text{O}-\text{SiO}_2$ system at low temperatures in the region of the glass transition and below for all compositions exist. For alkaline earth borates there is a stable miscibility gap while alkali borates have metastable gaps. The $\text{TiO}_2-\text{SiO}_2$ systems have large miscibility gaps that are stable over a wide range of compositions. The extension of immiscibility into ternary systems is important for effective use of TiO_2 as a nucleating agent in many glass-ceramic systems.

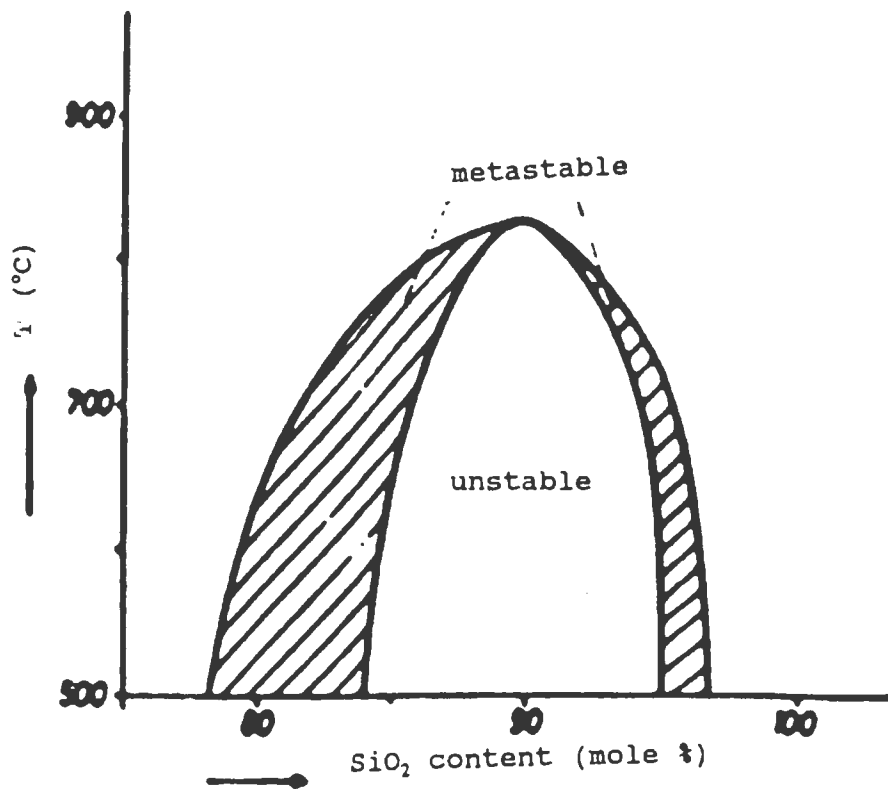


Fig.70-METASTABLE AND UNSTABLE REGIONS OF SILICATE GLASS.

Thus, liquid-liquid immiscibility is widespread in glass-forming systems and many glasses which appear optically homogeneous may be phase-separated on a scale of 30 to 50 Å upto a few 100 Å. Interconnected structures may form by spinodal decomposition or by the growth and coalescence of discrete particles and such structures coarsen with time, retaining a high degree of connectivity in some cases and necking off and spheroidizing in others. Such two phase structures may be developed to a sufficiently coarse scale so that they scatter light strongly, resulting in opacity. Even single phase glasses are characterized by fluctuations in density and compositions.

From these considerations, it was concluded that the addition of a glass former like silica and a glass modifier like CaO, in various compositions to the SPL would be an ideal point to begin the preliminary work on the glass formation characteristics of SPL.

4.3. EXPERIMENTAL WORK

MATERIALS USED:

Spent Potliner supplied by ALCOA was used for the analysis. The silica and calcium oxide that was added to this was of technical grade. X-ray analysis of the silica showed that it was relatively pure. The Calcium oxide contained traces of calcium hydroxide and calcium carbonate. A

Inductotherm Induction furnace, and a Lindberg box furnace capable of heating upto 1500°C were used for melting and fusing purposes. Jaw crushers were used to crush the SPL. Graphite crucible containers (1040 grade) were used for melting the samples.

PREPARATION OF SAMPLES:

After unfruitful attempts at melting the spent potliner in an induction furnace (temperature as high as 1800°C), it was decided that the SPL had to be calcined before making another attempt. One possible reason for its' not melting at these high temperatures could be the high amounts of carbon as graphite contained in it (as seen from Appendix 4). Calcining was carried out at 500°C for 8 hours. The calcined SPL was then fused in the induction furnace. The mass was then crushed to sizes of 2-3 mm. Additions were made to this fused SPL.

It was necessary to predetermine the amount of additives to be made to the SPL. Preliminary viscosity measurements conducted in the laboratory (98) indicated that the lower viscosities of the spent potliner could be obtained with additions of CaO and SiO_2 . At 1560K, the viscosity of pure SPL is 347.2 poise (extrapolated) which was decreased to 0.132 poise and 30.81 poise (extrapolated) with 20wt% additions of CaO and SiO_2 , respectively. Hence, various additions of silica (10, 14, 18 and 20 wt%) and same amounts of calcium oxide were

made. These samples were fused and the solidified samples were crushed to a 200 micron size. The chemical analysis were carried out on these samples along with those of the as received and the fused SPL. A block diagram of the sample preparation procedure is shown in figure 71.

4.4. RESULTS AND DISCUSSIONS

The samples were prepared as discussed in the preceding section. The powdered samples were analyzed using a X-ray diffraction and SEM techniques. The results of as received SPL, the fused SPL and the SPL with silica additions and calcium oxide additions are discussed below. A summary of the X-ray peak intensity variations in the various compounds present are given in table 10. The X-ray diffraction patterns and SEM micrographs are presented in figures 72 to figures 81.

AS RECEIVED SPL:

From X-ray studies, (figure 72) the major constituents of SPL were found to be sodium fluoride (villiaumite), and carbon as graphite. Substantial amounts of calcium fluoride (fluorite), alumina (corundum) and sodium aluminum fluoride (cryolite) were identified. Traces of a compound similar to sodium aluminum silicate were also observed. The SEM picture (figure 73) shows graphite and the other constituents uniformly distributed throughout. There are some extremely bright spots which are identified to be of elemental iron.

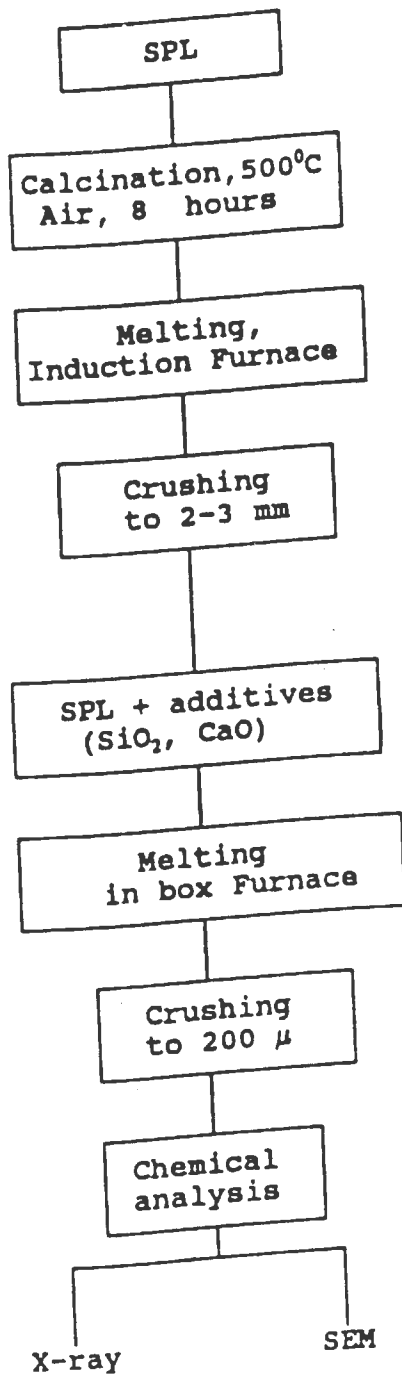


Fig.71-Sample preparation for chemical analysis

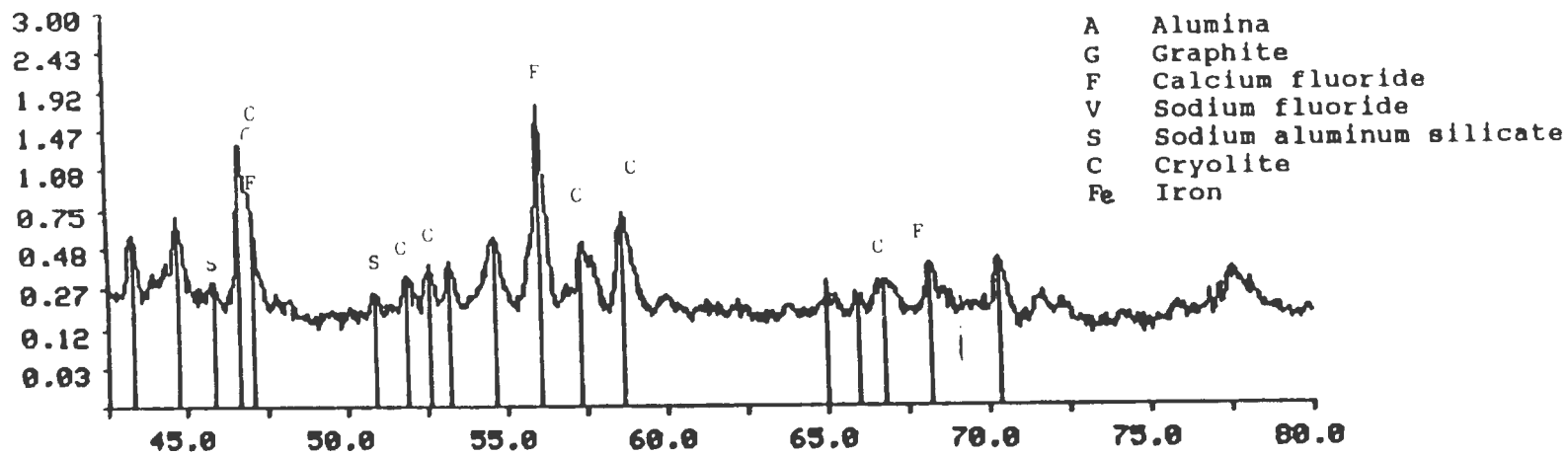
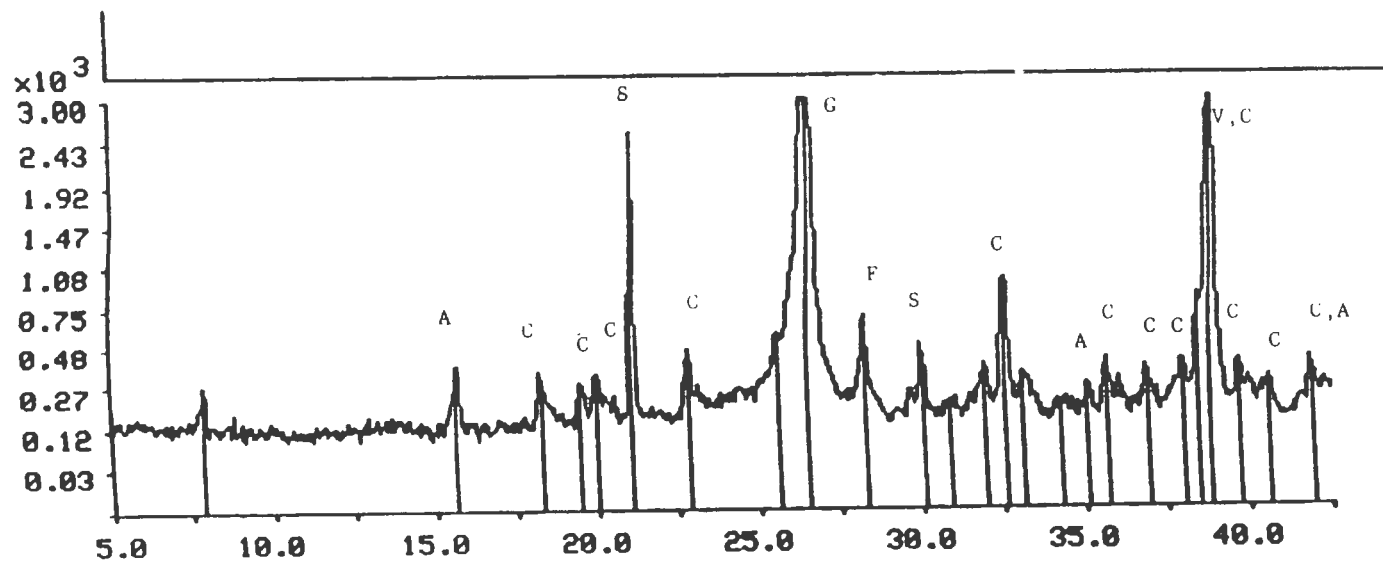


Fig.72-X-RAY DIFFRACTION PATTERN OF SPL (AS RECEIVED)

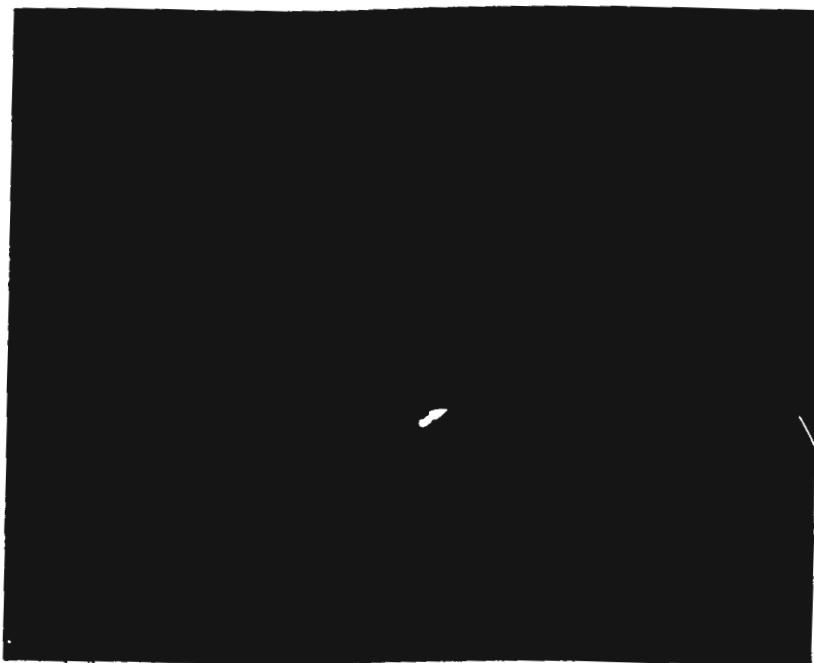


Fig.73-SEM MICROGRAPH OF SPL (AS RECEIVED)



Fig.74-SEM MICROGRAPH OF FUSED SPL

This was confirmed by the X-ray analysis. The iron probably was from the steel shell of the aluminum electrolytic cell.

FUSED SPL:

After calcination, for 8 hours at 500°C, most of the Carbon that was present in the SPL initially, was removed. The carbon reacted with oxygen in the air to give carbon dioxide gas. The calcined SPL was homogenized by fusing in an induction furnace and these were analyzed. As seen from the patterns on figure 72 and 75, the Carbon peak intensity decreased from 5402 counts to 193 counts. At the same time, the intensity of the calcium fluoride (CaF_2) peak, and cryolite (Na_3AlF_6) increases while that of the sodium fluoride (NaF) peak decreases. The amount of alumina is also reduced considerably. The intensity of the compound similar to sodium aluminum silicate is increased from 1490 counts in the as received SPL to 2510 counts. Thus there is probably, a reaction between the alumina, silica and sodium fluoride to form cryolite and sodium aluminum silicate.

Comparison of the SEM pictures of the as received SPL in figure 73 and the fused SPL in figure 74 confirms the above observations.

FUSED SPL WITH SILICA ADDITIONS:

Various mixtures of the fused SPL with 14, 18 and 20 wt

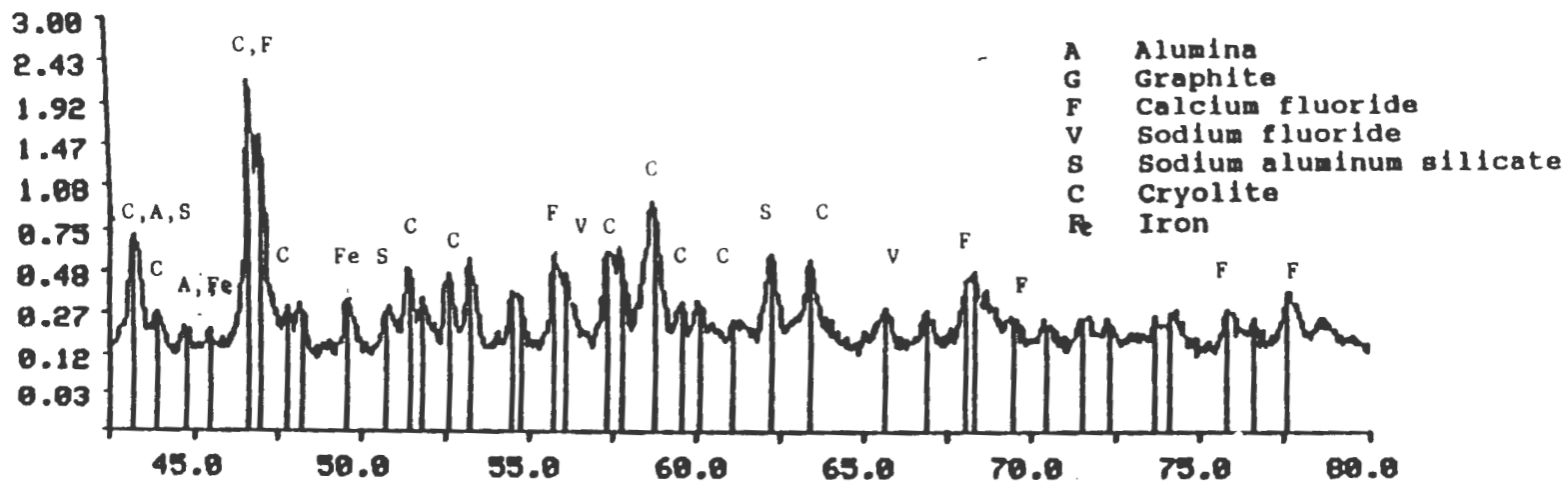
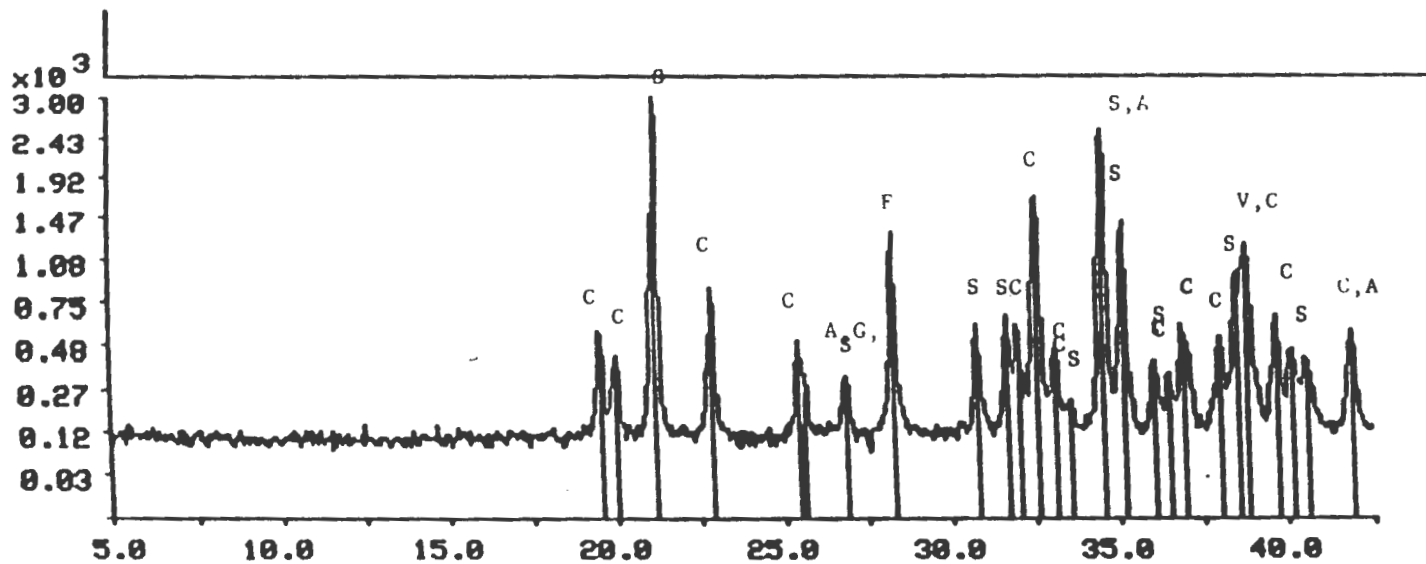


Fig.75-X-RAY DIFFRACTION PATTERN OF FUSED SPL

pct. of silica were melted. The X-ray diffraction patterns, of 14 and 20 wt pct. are shown in figures 76 and 77. A relatively lower number of peaks, indicates the formation of a more glassy material. The major phases observed were calcium fluoride and cryolite. The compound similar to sodium aluminum silicate was not observed. The compound has decomposed to give minor quantities of alumina, silica and NaF phases.

The SEM pictures of SPL with 20% silica additions are shown in figure 78. The various other minor components embedded in the matrix are observed in these. These include carbon (the very dark portions) and elemental iron (bright white spots). At a higher magnification it was observed that the Ca rich portions of calcium fluoride were affected by the SEM beam. It was probably as a result of the volatile nature of the fluoride which is vaporizing as it gets heated up by the beam current. At a higher magnification the calcium rich portions were observed to have some porous, hollow regions.

As the silica content was increased from 10 to 20 wt pct. the intensity of the calcium fluoride peak decreases. The decrease is evident upon the comparison of the plots of the SPL (figure 72), fused SPL (figure 75) and SPL with 14% and 20% additions of silica (figures 76,77). From this we can conclude that for the complete elimination of calcium fluoride and other crystalline phases, more than 20 wt % silica is required.

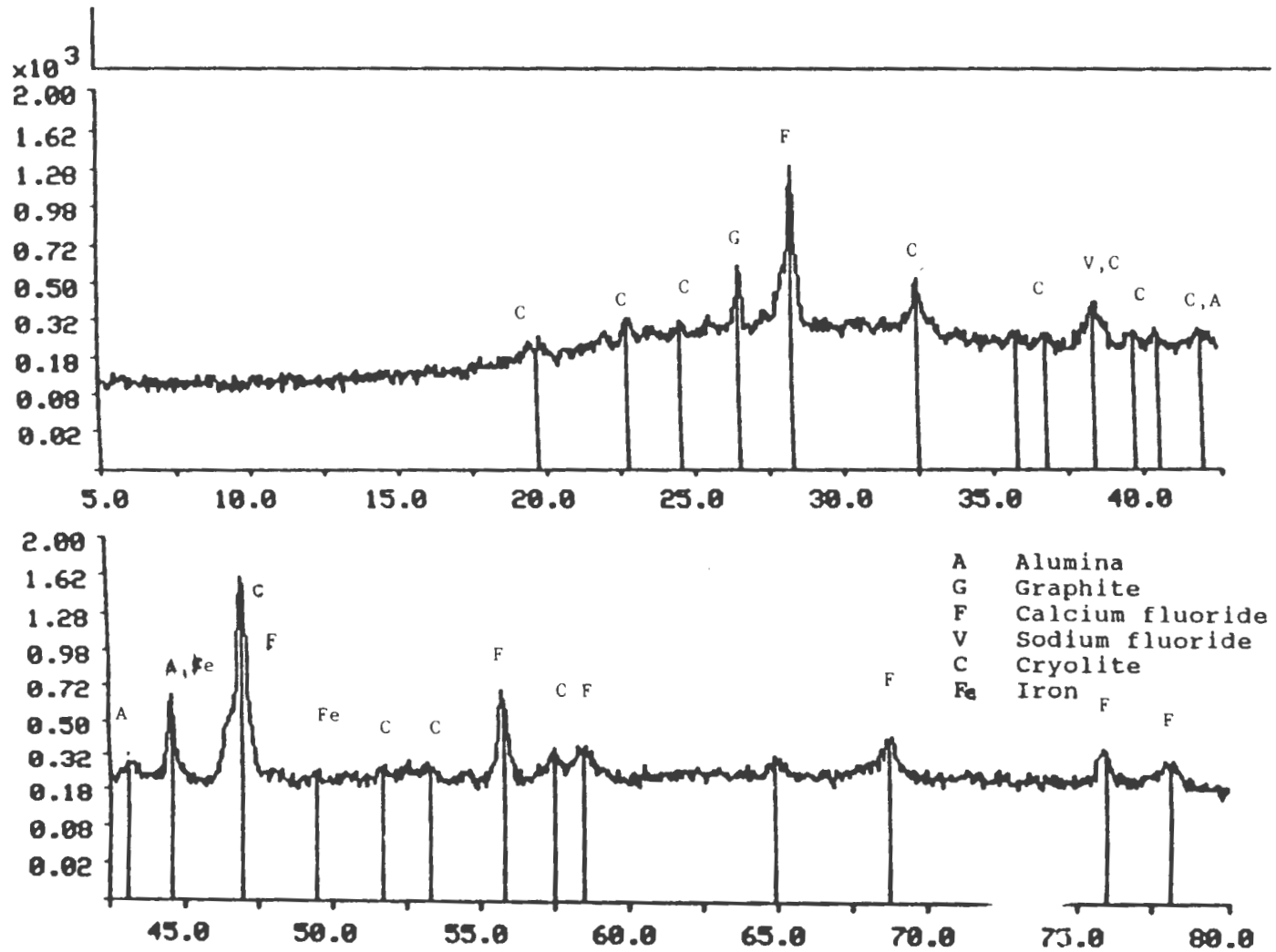


Fig.76-X-RAY DIFFRACTION PATTERN OF SPL + 14%SiO₂

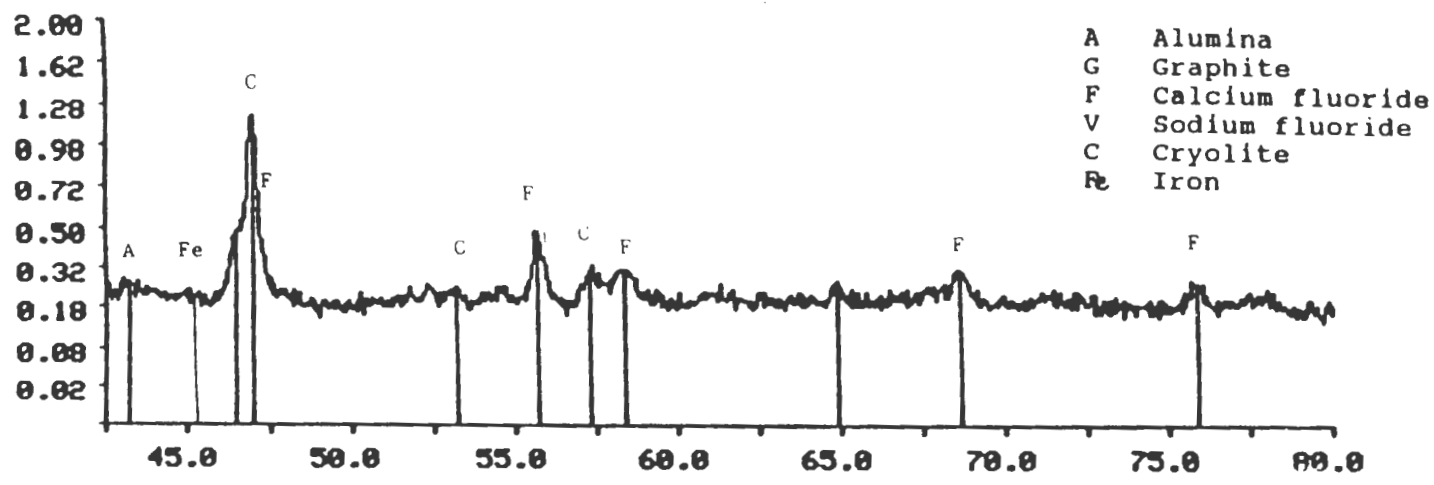
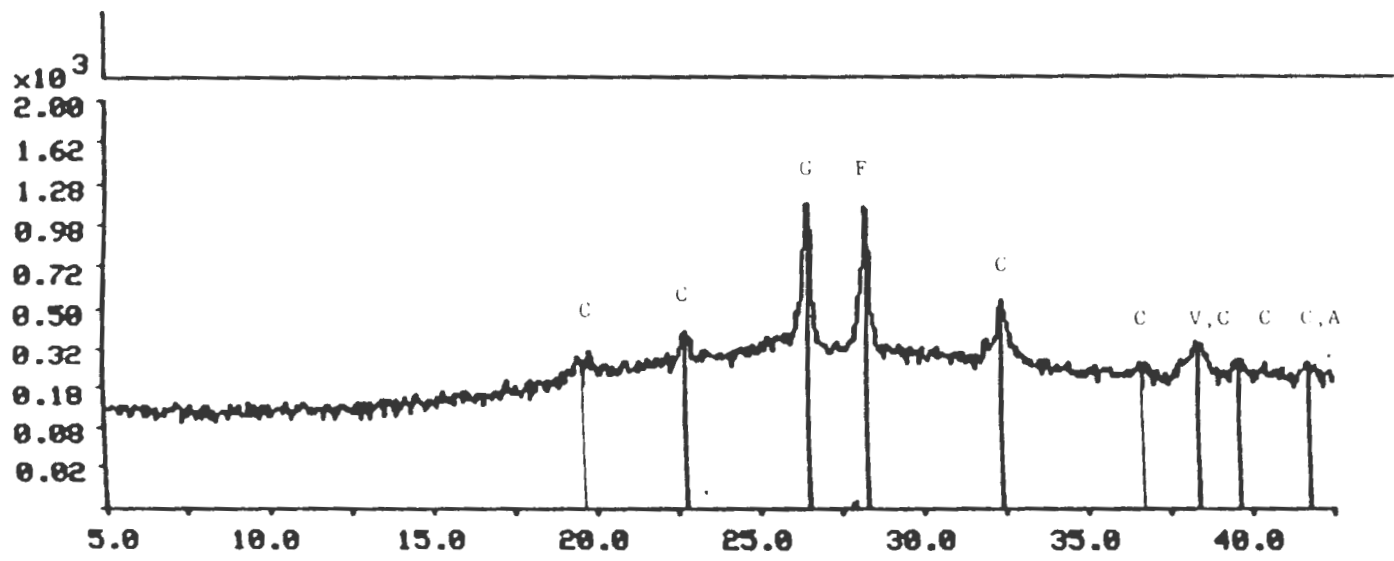


Fig.77-X-RAY DIFFRACTION PATTERN OF SPL + 20%SiO₂

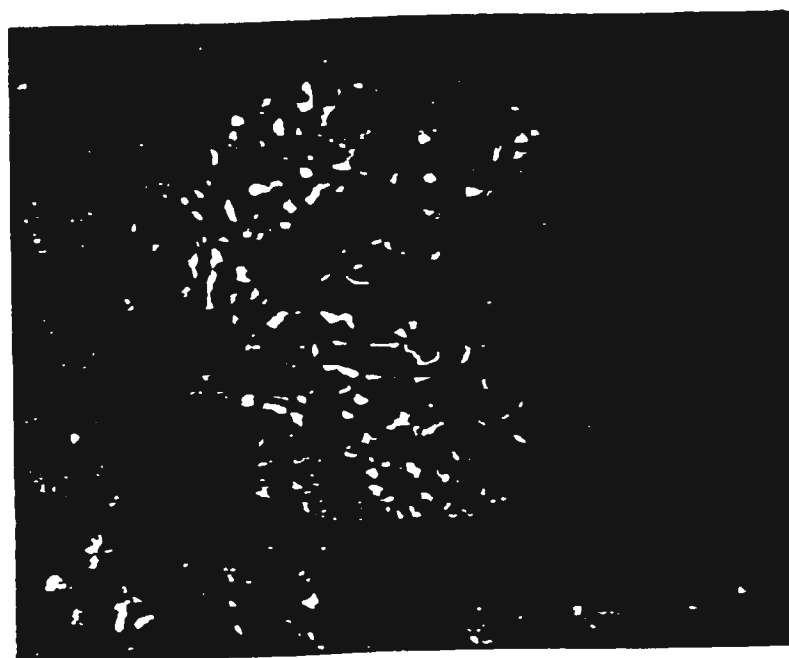
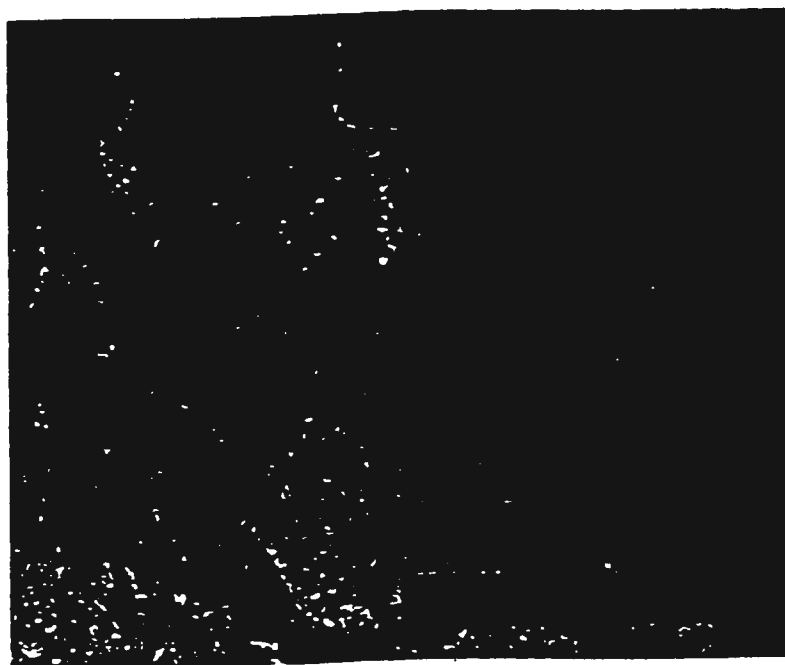


Fig.78-SEM MICROGRAPH OF SPL + 20%SiO₂

FUSED SPL WITH CALCIUM OXIDE ADDITIONS:

The X-ray patterns for 14 and 20 wt% additions of CaO are shown in figures 79 and 80. A comparison of the X-ray patterns of as received SPL, fused SPL and 14% and 20% CaO (figures 72,75,79,80) shows that the CaF_2 increased with increasing additions of CaO. This is due to the fixation of more fluoride as calcium fluoride. Minor amounts of C, Na_3AlF_6 , NaF and Al_2O_3 were also observed. As the CaO content is increased the amount of cryolite gets reduced to minor amounts while the amount of NaF increases. Simultaneously, the compound $\text{Na}_4\text{Ca}_3(\text{AlO}_2)_{10}$ appears and increases in intensity as the amount of CaO is increased. This confirms that the cryolite is reacting with the CaO to form the ternary complex and NaF. The intensity of the compound that was similar to sodium aluminum silicate also decreased as the CaO additions were increased. At 20% CaO additions the compound was reduced to 231 counts as against 2510 counts that was observed in the as received SPL. Also the total number of peaks decreased on the addition of CaO.

The SEM micrograph shown in figure 81 indicates the calcium fluoride matrix with the other constituents embedded in it. Finer crystalline phases are formed with the calcium oxide additions as compared to that of the silica additions to the fused SPL.

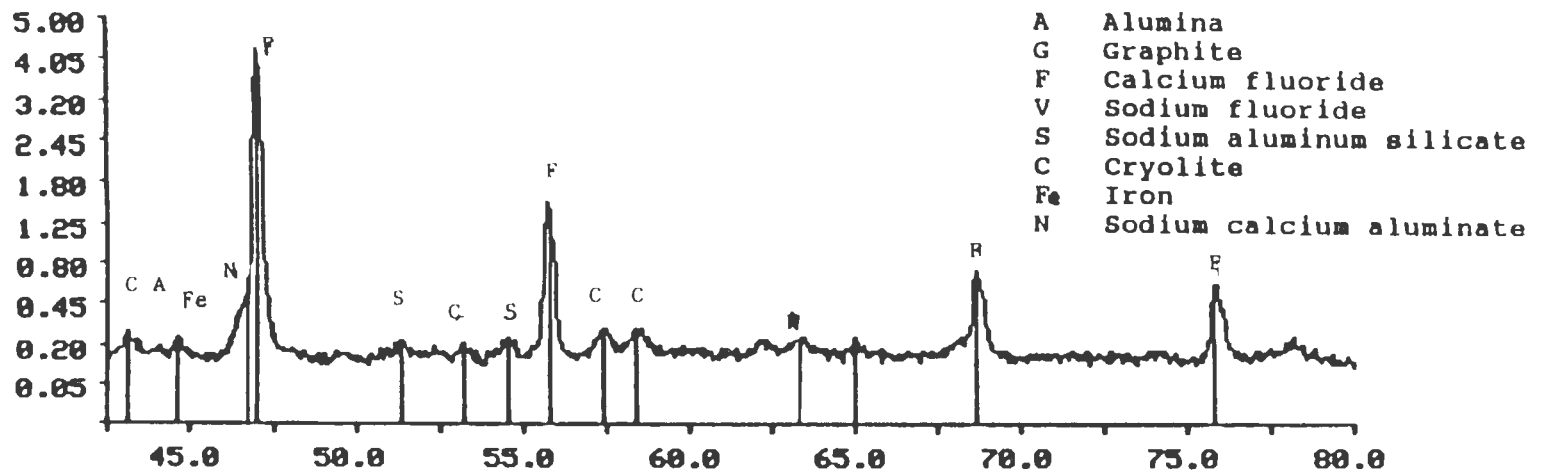
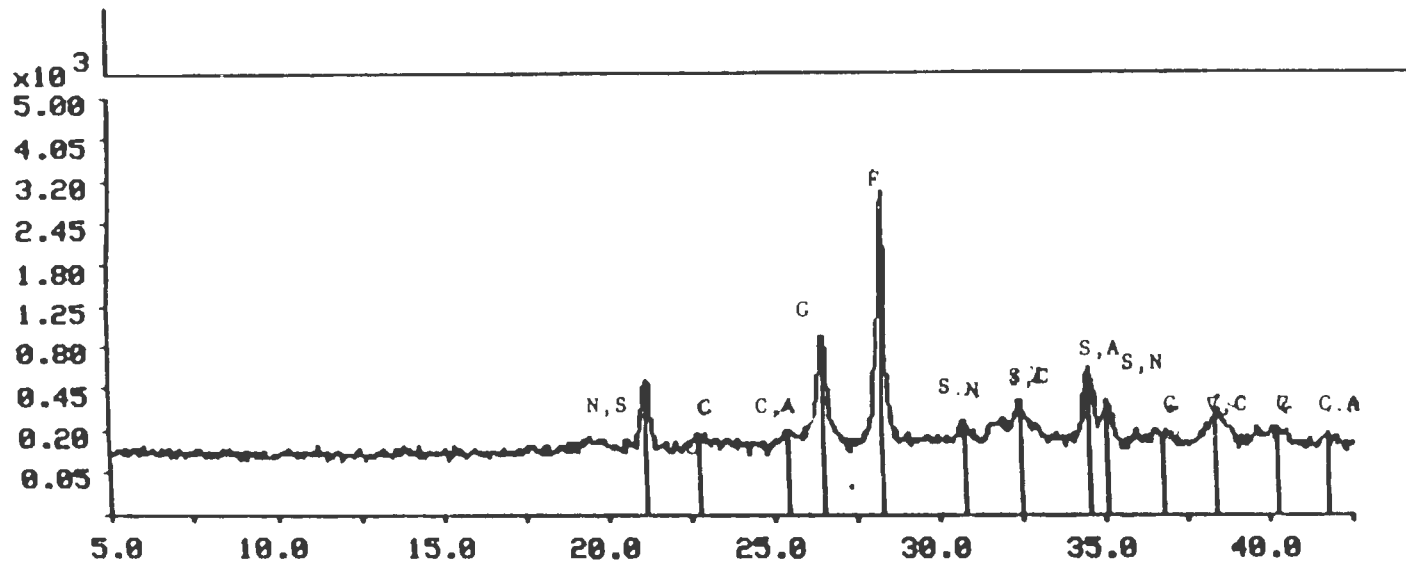


Fig.79-X-RAY DIFFRACTION PATTERN OF SPL + 14%CaO

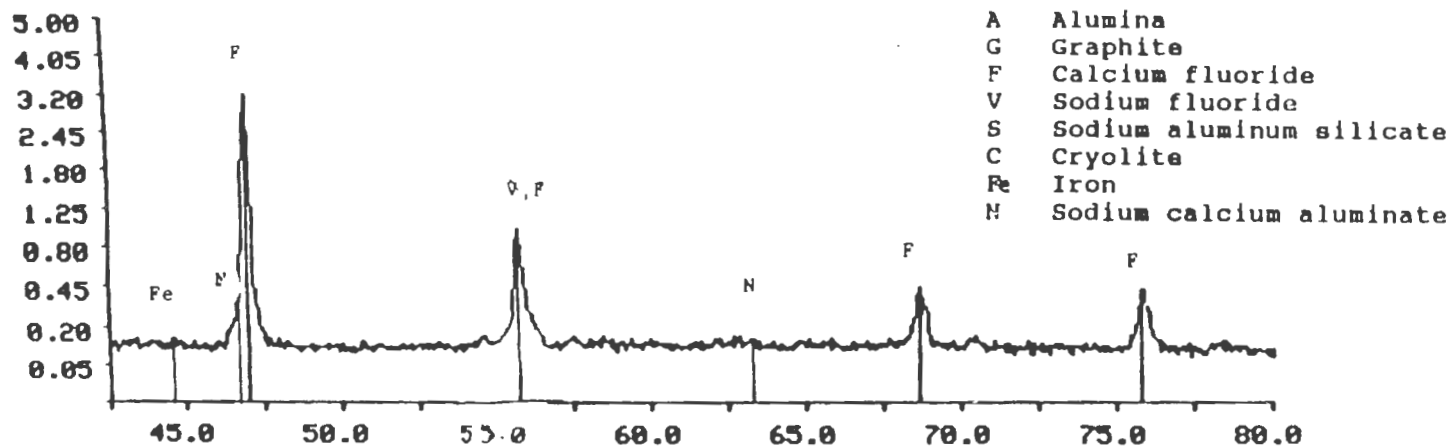
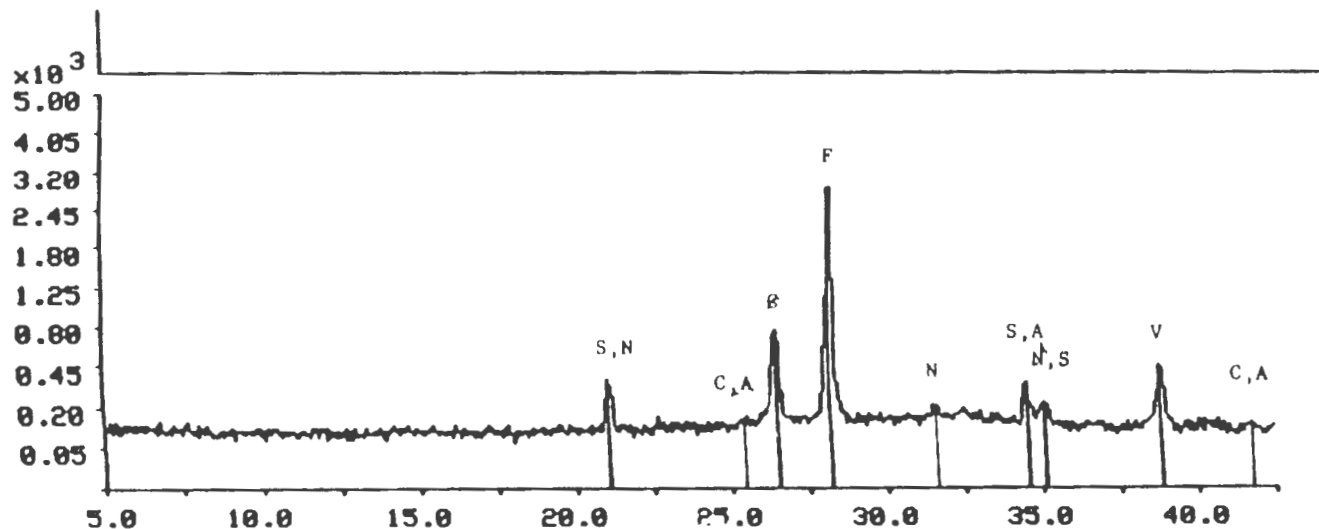


Fig.80-X-RAY DIFFRACTION PATTERN OF SPL + 20%CaO

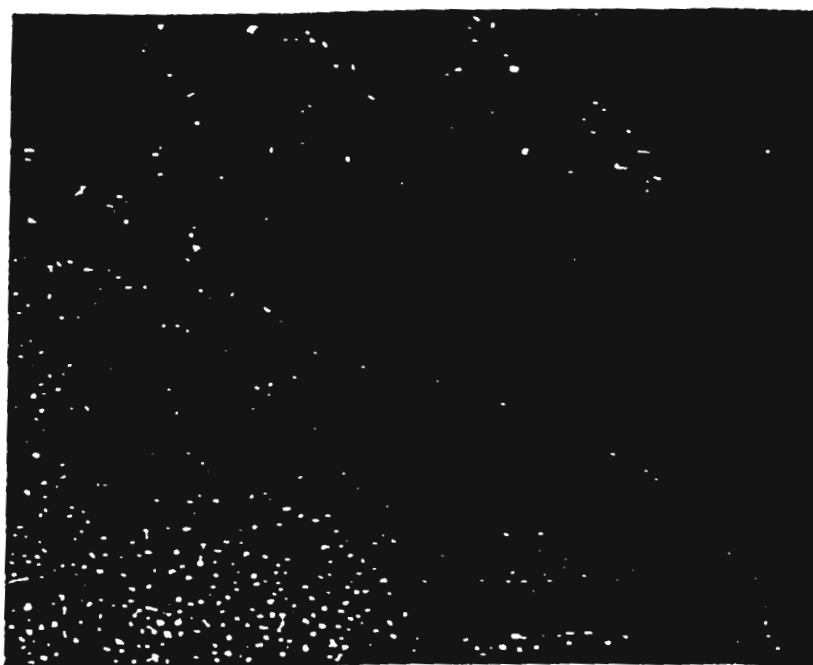
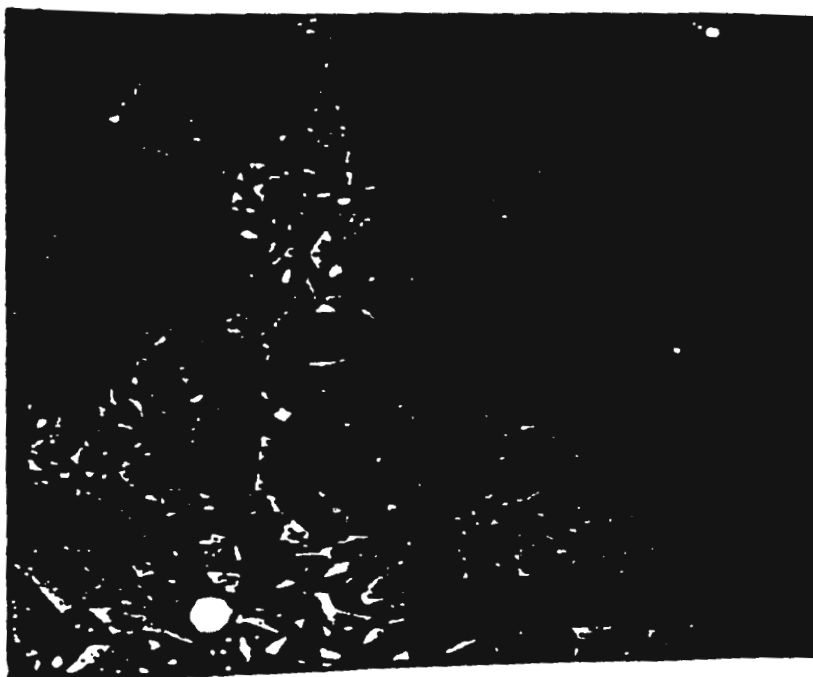


Fig.81-SEM MICROGRAPH OF SPL + 20%CaO

Concluding, it could be said that the addition of a mixture of silica and calcium oxide seems to be better for the formation of a complete glassy matrix. The small amounts of other minerals like silicates were not detected in the diffraction patterns. Additional research using other analysis techniques like SEM microprobe would be required to identify the minerals present in these relatively small quantities.

TABLE 9-COMPARISON OF RELATIVE INTENSITIES IN THE SPENT POTLINER STUDIES⁽⁷⁾

| ELEMENT | CaF ₂ | NaF | Na ₃ AlF ₆ | C |
|----------------------------|------------------|-------|----------------------------------|------|
| SPL | 1.3 | 10.0 | 6.5 | 10.0 |
| Calcined SPL | 3.5 | 2.2 | 10.0 | 0.7 |
| SPL + 14% SiO ₂ | 2.3 | trace | 1.3 | 0.5 |
| SPL + 20% SiO ₂ | 1.6 | trace | 1.1 | 0.9 |
| SPL + 14% CaO | 10.0 | 0.3 | trace | 2.0 |
| SPL + 20% CaO | 9.1 | 0.8 | trace | 1.8 |

* Only the major constituents have been listed.

Note: The highest peaks of CaF₂ and Na₃AlF₆ have d-spacings that are very close (1.93 and 1.94 respectively) and hence the determination of the intensities may not be very accurate.

CHAPTER 5. CONCLUSIONS

PART A

A structure based viscosity model which uses the hole theory and random network theory has been modified. Correlations of E , the energy required to break the silicate bond and move it to an adjacent hole, as a function of NO^o , which is the number of oxygens bonded to only one silicon atom and the temperature, T have been made. All the available experimental viscosity data have been used in obtaining these correlations. The deduced expressions were used in predicting viscosities of several binary and ternary silicate systems. The model can be applied in the entire composition range of 0.1 to 1 mole fraction silica.

The following conclusions can be made from the present study:

1. The viscosity of pure silica was predicted using E to be equal to 519000 joules. The predicted data was seen to be in excellent agreement with the available experimental data. Hence, the viscosity expression was used to predict viscosities of pure silica at all temperatures.
2. The viscosity of several $MO-SiO_2$ melts (where M is Ca, Mg, Mn, Ba, Sr and Fe) were predicted as a function of temperature and composition. The average percentage deviation varied from -3.1 to -9, which was, on an average less when compared to the models of Riboud et al and Urbain et al. The

proposed model is consistent in predicting the effect of solids on the pure melt viscosities. Predictions were made to verify this in the case of FeO-SiO₂ melts. It was also shown that for a given temperature, the viscosity of the melts increases with increase in the silicate mean chain length. Thus, the viscosities of CaO-SiO₂ melts are lower as compared to the MnO-SiO₂ melts at corresponding compositions.

3. In the case of M₂O-SiO₂ melts, the viscosities of Na₂O-SiO₂, K₂O-SiO₂ and Li₂O-SiO₂ melts were predicted and are in good agreement with the experimental data. The average percentage deviation varies from 1.6 to 25. The model predicts a sharp decrease in the viscosity values, in all three cases, at around 0.35 mole fraction of silica. But there were no available experimental data to ascertain if this was indeed true.

In general, it can be concluded from the various MO-SiO₂ and M₂O-SiO₂ systems that have been considered, that the viscosity increases with increasing XSiO₂ and decreases with increasing temperature at a fixed XSiO₂.

4. The binary model was extended to predict the viscosities of ternary silicate systems. Viscosities of several MO-NO-SiO₂ (where M and N are Ca, Mn, Mg and Fe) were predicted as a function of temperature and composition. The predicted viscosities are in fairly good agreement with the experimental data. However, the predicted isoviscosity contours differ

significantly in shape and magnitude in the case of calcium manganese silicate and iron manganese silicate melts. These may be improved by refining the free energy term by inclusion of higher order free energy terms, which are not available at present. Further work on these lines is suggested.

PART B

Preliminary studies on the safe disposal of SPL by fixing it in a glassy matrix have been completed. The effect of silica and calcium oxide additions to the calcined and fused SPL have been studied using X-ray diffraction and SEM techniques.

1. The major phases in SPL have been identified to be sodium fluoride and carbon along with substantial amounts of other complex fluorides and oxides. The presence of carbon made it impossible to melt the SPL and calcining was required for several hours before it could be fused. Almost all the carbon was removed on calcining.
2. The addition of 20 wt. % silica to the melt gives a more glassy matrix, with calcium fluoride and cryolite being the major phases. The complex oxides decompose to give simpler compounds.
3. The addition of calcium oxide was seen to give calcium fluoride as the major phase as a result of the fixing of the fluorides by calcium. Another complex oxide gets formed as a

result of a reaction between cryolite and calcium oxide.

Hence, the formation of a more glassy matrix with these additions is quite distinct. From the study, it can be suggested that future work can be directed toward making a completely glassy matrix by keeping the amount of calcium oxide constant at 20 wt % and studying the effect of silica on the glass formation characteristics of SPL. In general, it should be possible to obtain a complete glassy matrix by the addition of a mixture of calcium oxide and silica, thus making the SPL safe for disposal.

CHAPTER 6

REFERENCES

1. Ochotin M.W., Steklo Keram., Vol.11, pp.7, 1954.
2. Lyon K.C., J. Res. Natl. Bur. Stand., Vol.78, pp.497, 1974.
3. McCauley W.D., and Apelian D., Canad. Metall. Quart., Vol.20, 1981, pp.247.
4. Mairy B., Private Communication, Centre Recherches Metallurgique, Liege, Belgium.
5. Bottinga Y. and Weill D.F., Am. J. Sci., Vol.272, May 1972, pp.438.
6. Shaw H., Am. J. Sci., Vol.272, 1972, pp.870.
7. Watt J.D., and Fereday d., J. Instr. Fuel, Vol.338, 1969, pp.99.
8. Bokamp, Inst. of Gas Technol. Preparation of a coal conversion systems Technical data Book. Energy Res. and Dev. Admin. Report Fe-1730-21, 1976.
9. McCauley W.L., and Apelian D., Second Int. Symposium on Met. Slags and Fluxes: Edited by Fine H.A. and Gaskell D.R., TMS-AIME, 1984, pp.925.
10. Hofmaier G., Urbain G., and Stewart G.H., Sci. of Cer., London, British Cer. Soc., 1968, pp.25.
11. Euler R., and Winkler H.G.F., Glastech. Ber., Vol.30, 1957, pp.325.
12. Glasstone S, Laidler K.J., and Eyring H., The theory of rate processes, McGrae Hill, NY 1941.
13. Browstow W., and Maynadein P., High Temp. Sci. Vol.11, 1979, pp.7.
14. Riboud P.V., Roux Y., Lucas L.D. and Gaye H., Fachber. Huttenpraxis Metalveiterverarb., Vol.19, 1981, pp.859.
15. Urbain G., Cambier F., Deletter M. and Anseau M.R., Trans. J. Brit. Ceram. Soc., Vol.80, 1981, pp.139.

16. Urbain G., *Steel research* Vol.58(3), 1987, pp.111.
17. Hu H. and Reddy R.G., *Casting of Near Net Shape Products*, Edited by Sahai Y., Battles J.E., Carbonara R.S. and Mobley C.E., TMS, 1988. pp.705.
18. Elliott J.F., *Second Int. Symposium on Met. Slags and Fluxes*, Edited by Fine H.A. and Gaskell D.R., TMS-AIME, 1984, pp.45.
19. Report - Technical Division, Savannah River Lab., June 27, 1986.
20. Roscoe R., *Br. J. Appl. Phys.*, Vol.3, 1952, pp.267.
21. Bockris J.O'M., Reddy A.K.N., '*Modern Electrochemistry*', Plenum Press, NY, 1970, pp.574.
22. Hu H., and Reddy R.G., *High Temp. Sci.*, Vol.28, 1990, pp.155.
23. Masson C.R., Smith J.B. and Whiteway S.G., *Can. J. of Chem.*, Vol.48, 1970, pp.1456.
24. Gaskell D.R., *Met. Trans. B*, Vol.8B, Mar. 1977, pp.131.
25. Fincham C.J.B., and Richardson F.D., *Proc. Roy. Soc.*, Vol.223, 1954, pp.40.
26. Toop G.W., and Samis C.S., *Trans. TMS-AIME*, Vol.224, 1962, pp.878.
27. Frohberg G.M., Kapoor M.L., and Mehrotra G.M. *Arch. Eisenhuettenwes.*, Vol.45, 1974, pp.213.
28. Yokakawa T., and Niwa K., *Trans.JIM*, Vol.10, 1969, pp.2.
29. Lin P.L., and Pelton A.D., *Met. Trans. B.*, vol.10B, Dec.1979, pp.667.
30. Flood H., and Knapp J., *J. Am. Ceram. Soc.*, Vol.51(5), pp.64.
31. Gaskell D.R., *Can. Met. Quart.*, Vol.20(1), 1981, pp.3.
32. Kaneko Y., and Suginochara Y., *JIM*, Vol.41(1-6), 1977, pp.375.
33. Chase M.W., Davies C.A., Downey Jr J.R., Frurip D.J., McDonald R.A., and Syverud A.N., *JANAF Thermodynamic*

- Tables, 3 edn., NBS Vol.14, 1985, pp.1489.
34. Turkdogan E.T., Physical Chem. of high Temp. Tech., Academic Press Inc., NY, 1980, pp.8.
 35. Hetherington G., Phys. Chem. glasses, Vol.5, 1964, pp.130.
 36. Richardson F.D., 'Physical Chem, of melts in Met.', Vol.1, Academic Press, NY, 1974, pp.195.
 37. Bruckner R., Glastechn., Ber., Vol.37, 1964, pp.413.
 38. Rossin R., Bersan J. and Urbain G., Rev. Int. Hautes Temp. Refract., Vol.1, 1964, pp.159.
 39. Mills K.C. and Keene B.J., Int. Mat. Reviews, Vol.32(1&2), 1987, pp.18.
 40. Mizoguchi K., Yamane M. and Suginochara Y., J. Japan Inst. Metals Vol.50(1), 1986, pp.76.
 41. Bockris J.O'M. and Lowe D.C., Proc. R. Soc. Vol.226A, 1954, pp.423.
 42. Endell K. and Heidtkamp G., Hax L., Arch. Eisenhüttenwes., Vol.10, 1936, pp.85.
 43. Saito T. and Kawai Y., Sci. Rep. Res. Inst. Tohoku Univ. A, Vol.3, 1951, pp. 491.
 44. Schenk H. and Froberg M.G., Arch. Eisenhüttenwes., Vol.33, 1962, pp.421.
 45. Shiraishi Y. and Saito T., Nippon Kinzoku Gakkaishi (J. Jpn. Inst. Met.) Vol.29(6), 1965, pp.614.
 46. Kawai Y., Nippon Kinzoku Gakkai Kaiho (Bull. Jpn. Inst. Met.), Vol.18, 1979, pp.244.
 47. Kozakevitch P., Rev. Metallurgie, Vol.57, 1960, pp.149.
 48. Hofmaier G., Berg und Huttenm. Monatsh. Montan. Hochschule in Loeben, Vol.113, 1968, pp.270.
 49. Phase diagram for ceramists, Levin E.M., Robbins C.R., McMurdie H.F., Edited by Reser M.K., Amer. Ceram. Soc., 1979.
 50. Bockris J.O'M., Mackenzie J.D. and Kitchener J.A., Trans.

- Faraday Soc., Vol.51, 1955, pp.1734.
51. Hofmann E.E., Berg Hutt. Mann. Monatsh., Vol.106, 1959, pp.397.
 52. Towers H. and Gworek J., J. West Scot. Iron Steel Inst., 1943-44, pp.123.
 53. Bell H.B., Personal Communication, Strathclyde Univ., Glasgow, 1985.
 54. Mizoguchi K., Okamoto K., and Suginoara Y., J. Japan Inst. Metals, Vol.46(11), 1982, pp.1055.
 55. Kozakevitch P., Rev. Metall., Vol.46(8), 1949, pp.505.
 56. Rontgen P., Winterhager H. and Kammel L., Erzmetall., Vol.9, 1956, pp.207.
 57. Shiraishi Y., Ikeda K., Tamura A., and Saito T., Trans. Jpn. Inst. Met., Vol.19, 1978, pp.264.
 58. Williams P., Sunderland M., and Briggs G., Trans. Inst. Min.Metall. Eng., Vol.92C, pp.105.
 59. Kaiura G.H., Toguri J.M., and Marchant G., Can. Metall. Q., Vol.16, 1977, pp.156.
 60. Bodnar L., Tomasek K., Bobok L., and Schmiedl J., Hutn, Listy, Vol.33(7), 1978, pp.497.
 61. Urbain G., CR hebd. Seances Acad. Sci, II, Vol.232, 1951, pp.330.
 62. Myslevic T., Wozniak J., Cerny V., Sb. Ved. Pr. Vys. Sk. Banaske Ostrave, Vol.20, 1974, pp.57.
 63. Urbain G., Bottinga Y., and Richet P., Geochemica et Cosmochimica Acta, Vol. 46, 1982, pp.1061.
 64. Bowen . and Schairer ., Am. J. Sci., (5th series) Vol.24(141), 1932, pp.177.
 65. Schuhmann Jr. R., and Ensio P.J., J. Metals, Vol.3(5), 1951, pp.401.
 66. Reddy R.G., Hu H., and Blander M., (to be published).
 67. Shartsis L., Spinner S., and Capps W., Am. Ceram. Soc. Journal, Vol. 35, 1952, pp.155.

68. Heidtkamp G., Endell K., *Glastech. BER.* Vol.14, 1936, pp.89.
69. Suginochara Y., Yanagase .., and Ito H., *Trans. JIM*, Vol. 3, 1962, pp.227.
70. Hu H., Thesis, Master of Science, Univ. of Nevada, Reno.
71. Flood H., and Grjotherm K., *JISI*, Vol.171, 1952, pp.64.
72. Segers L., Fontana A., and Winard Y., *Trans. Inst. Min. Metall. Eng.*, Vol. 88(C), 1979, pp.53.
73. Kawahara M., Mizoguchi K., and Suginochara Y., *Bull. Kyushu Inst. Technol.*, Vol.43, 1981, pp.53.
74. Glasser F.P., *J.Am. Ceram. Soc.*, Vol.45, 1962, pp.245.
75. Gulytai I.I. *Izv. Akad. Nauk SSR. Otdel. techn. NAuk Metall. Toplivo*, Vol.5, 1962, pp.52.
76. Machin J.S. and Yee T.B., *J. Am. Ceram. Soc.*, Vol.37, 1954, pp.177.
77. Adolf Z., and Myslevic T., *Kovove Mater.*, Vol.16(3), 1978, pp.319.
78. Kozakevitch P., *Rev. Metall.*, Vol 46(9), 1949, pp.572.
79. Sokolov V.I., Popel S.I., Esin O.A., *Izv. VUZ Chernaya Metall.*, Vol. 13(4), 1970, pp.40.
80. Byers L., *Light Metals*, 1984, pp.1024.
81. Blayden L.C. and Epstein S.G., *J. of Metals*, July 1984, pp.22.
82. Proc. of the Workshop on Storage and recovery of SPL, The Aluminum Association, Washington D.C., 1981.
83. Byers R.L., *Light Metals 1982*, AIME 1982.
84. Spironello V.R., and Nafziger R.H., U.S. Bureau of Mines, RI 8530, 1981.
85. Spironello V.R., U.S. Bureau of Mines, RI 8775, 1983.
86. Zachariasen W.H., *J. Am. Chem. Soc.*, Vol.54, 1932, pp.3841.

87. Warren B.E., J. Appl. Phys. Vol.8, 1937, pp.645.
88. Kingery W.D., Bowen H.K., Uhlmann D.R., Introduction to Ceramics, Second Edn., John Wiley & Sons, NY, 1975.
89. Baumgart W., Dunham A.C., and Amstutz G.C., Process Minerology of Ceramic Materials, Elsevier Sci., NY 1984.
90. Nitta A., Miura T., Komatsu T., and Matusita K., J. Am. Ceramic Soc., Vol.72(1), 1989, pp.163.
91. Rawson H., Inorganic glass forming systems, Academic Press, NY 1967.
92. Becker H., Glastechn. Ber., Vol.35, 1966, pp.519.
93. Sucov E.W., and Gorman R.R., J. Am. Ceram. Soc., Vol.48, 1965, pp.426.
94. Engelke H., Dissertation, Universitat Erlangen, 1972.
95. May H.B., Lauder I., and Wollast R., J. Am. Ceram. Soc., Vol.57, 1974, pp.197.
96. Frischat G.H., Ionic Diffusion in oxide glasses, Trans Tech., Ohio, 1937.
97. Magruder III R.H., Kinser D.L., and Weeks R.A., Amer. Ceram. Soc., Communications, Vol.69, 1986, C10.
98. Hu H., and Reddy R.G., Light Metals, TMS, 1989, pp.801.

APPENDIX 1
Free Energy data for Binary Silicate systems

155

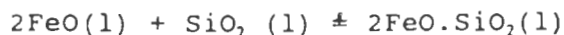
| Reaction | Free Energy (Joules/mol) |
|---|--------------------------|
| 1. $2\text{CaO}(l) + \text{SiO}_2(l) = 2\text{CaO} \cdot \text{SiO}_2(s)$ | -287811.1 + 42.96T |
| 2. $2\text{MgO}(l) + \text{SiO}_2(l) = 2\text{MgO} \cdot \text{SiO}_2(l)$ | -160686.6 - 26.4T |
| 3. $2\text{MnO}(l) + \text{SiO}_2(l) = 2\text{MnO} \cdot \text{SiO}_2(l)$ | -82417.35 + 27.04T |
| 4. $2\text{BaO}(l) + \text{SiO}_2(l) = 2\text{BaO} \cdot \text{SiO}_2(l)$ | -286926.1 + 50.199T |
| 5. $2\text{SrO}(l) + \text{SiO}_2(l) = 2\text{SrO} \cdot \text{SiO}_2(l)$ | -373909.1 + 61.95T |
| 6. $2\text{FeO}(l) + \text{SiO}_2(l) = 2\text{FeO} \cdot \text{SiO}_2(l)$ | -38387.1 - 5.92T |
| 7. $\text{Na}_2\text{O}(l) + \text{SiO}_2(l) = \text{Na}_2\text{O} \cdot \text{SiO}_2(l)$ | -243480.9 - 9.55T |
| 8. $\text{K}_2\text{O}(l) + \text{SiO}_2(l) = \text{K}_2\text{O} \cdot \text{SiO}_2(l)$ | -239626.1 - 35.91T |
| 9. $\text{Li}_2\text{O}(l) + \text{SiO}_2(l) = \text{Li}_2\text{O} \cdot \text{SiO}_2(l)$ | -184318.1 + 21.37T |

APPENDIX 2

CALCULATIONS FOR MC-SiO₂ AND M₂O-SiO₂ SYSTEMS

The calculations for these type of systems has been illustrated for the iron silicate systems for a mole fraction of the iron oxide of 0.748 and at a temperature of 1523K.

The free energy expression for the reaction



is given as: (appendix 1)

$$\Delta G^\circ = -19193.55 - 2.96T \text{ joules/mol}$$

$$R = 8.3144 \text{ joules/mol}$$

$$X_{\text{MO}} = X_{\text{FeO}} = 0.748 = X_{\text{SiO}_2} = 1 - X_{\text{FeO}} = 0.252$$

NO° was calculated using the following expression:

$$(1 - \exp(\Delta G^\circ/RT)) (\text{NO}^\circ)^2 + (2X_{\text{MO}} - 4) (\text{NO}^\circ) + 8X_{\text{MO}}(1 - X_{\text{MO}}) = 0$$

i.e.

$$(1 - \exp(-23701.63/(8.3144 \times 1523))) (\text{NO}^\circ)^2 + (2 \times 0.748 - 4) (\text{NO}^\circ) + (8 \times 0.748 \times 0.252) = 0$$

Solving this expression, we get NO° as 0.8415246. The NO° is calculated from this using the expression given below:

$$\text{NO}^\circ = 4 - 4X_{\text{MO}} - \text{NO}^\circ / (2(2 - X_{\text{MO}}))$$

i.e.

$$\text{NO}^\circ = 4 - 4 \times 0.748 - 0.8415246 / (2(2 - 0.748)) = 0.06648377$$

2. Now, $\eta = 4.9 \times 10^{-9} \text{NO}^\circ T^{1/2} \exp(E/RT)$ poise

Thus, $E = RT \ln(\eta / (4.9 \times 10^{-9} \text{ NO}^\circ T^{1/2}))$

The experimental viscosity at X_{SiO_2} of 0.252 is 0.31 (according to Shiraishi et al) (57)

Using this in the above expression the E can be calculated as:

$$E = 8.3144 \times 1523 \ln(0.31 / (4.9 \times 10^{-9} \times 0.06648377 \times (1523)^{1/2})) \\ = 215387.49 \text{ cal/mol}$$

3. Curvefitting was done of all the E values calculated in this manner as a function of NO° at 1523K.

A fourth order polynomial gave the best fit for $\text{NO}^\circ = 0.05$ to 1 with the constants being $\alpha=240344$; $\beta=-413313$; $\gamma=2044100$; $\delta=3392080$; $\epsilon=2028100$. (A sixth order polynomial in the case of $\text{M}_2\text{O}-\text{SiO}_2$ type of systems equation 2-17)

4. These constants and the ones at various other temperatures were fitted separately i.e fittings of α vs T, β vs T etc. where T ranged from 1523 to 2073K for $\text{MO}-\text{SiO}_2$ systems. Various expressions were obtained for each of the constants (refer equations 2-12 to 2-16 and 2-18 to 2-24).

Plugging in $T=1523\text{K}$ in the various expressions of the constants the constants could be recalculated as: $\alpha=2402226.23$; $\beta=-419024$; $\gamma=2036506$; $\delta=-3351700$; $\epsilon=2004757.82$.

5. These constants were substituted into the fourth order polynomial expression to get E. Thus,

$$E = (2402226.23 + (-419024 \times 0.06648377)) + (2036506 \times (0.06648377)^2)$$

$$\begin{aligned} & -3351700 \times (0.06648377)^3 + 2004757.82 \times (0.06648377)^4 \\ & = 220740.792 \end{aligned}$$

6. Now, the viscosity is predicted as:

$$\begin{aligned} \eta_{\text{cal}} &= 4.9 \times 10^{-9} \times 0.06648377 \times (1523)^{1/2} \exp(220740.792 / (8.3144 \times \\ & \hspace{15em} 1523)) \\ &= 0.46 \end{aligned}$$

7. The deviation was calculated as $\log(\eta_{\text{cal}}) - \log(\eta_{\text{exp}})$
i.e $\log(0.46) - \log(0.31) = 0.17$

APPENDIX 3

CALCULATIONS FOR TERNARY SYSTEMS

The calculation of viscosities in ternary systems is illustrated using the CaO-MnO-SiO₂ system at 1773K. The following mole fractions are used: silica = 0.5, CaO = 0.2, MnO = 0.3

The first step was the calculation of binary NO°'s for both the individual binary systems, CaO-SiO₂ and MnO-SiO₂. This was done using the procedure given in step 1 of Appendix 2.

The following values were calculated:

ΔG° (for the system CaO-SiO₂ at 1773K, designated as ΔG_1°) is equal to -105821.6 joules/mol

NO° is equal to 0.9992389, which in turn gives a NO° of 0.333587, using $X_{MO} = 0.5$.

$E_{CaO-SiO_2}$ is calculated using expression (2-11) as 257813.6

ΔG° (for the system MnO-SiO₂ at 1773K, designated as ΔG_2°) is equal to -17237.72 joules/mol

NO° is equal to 0.8219116, which in turn gives a NO° of 0.3926962 using $X_{MO} = 0.5$.

$E_{MnO-SiO_2}$ is calculated as 263313.6

2. The next step was the calculation of NO° for the ternary system.

This was done as follows:

$$\Delta G^\circ = X_M^{2+} \Delta G_1^\circ + X_N^{2+} \Delta G_2^\circ$$

i.e. $\Delta G^\circ =$

$$\frac{(2 \times 0.2)}{(2 \times 0.2 + 2 \times 0.3)} \times -105821.6 + \frac{(2 \times 0.3)}{(2 \times 0.3 + 2 \times 0.2)} \times -17237.7$$

NO^o was calculated using the following expression:

$$[1 - \exp(\Delta G^o/RT)] (NO^o)^2 + [2(X_{MO} + X_{NO}) - 4] NO^o + 8[(X_{MO} + X_{NO})(1 - X_{MO} - X_{NO})] = 0$$

Substituting the values of ΔG^o , and $X_{MO}=0.2$, $X_{NO}=0.3$, NO^o is calculated as =0.9740411

From this NO^o_{ternary} is calculated using:

$$NO^o = [4 - 4(X_{MO} + X_{NO}) - NO^o]/2[2 - (X_{MO} + X_{NO})]$$

Substituting the values calculated afore: NO^o_{ternary} was calculated as equal to 0.3419863

E_{ternary} is calculated using the following expression:

$$\ln E_{\text{ternary}} = X_M^{2+} \ln E_{MO-SrO_2} + X_N^{2+} \ln E_{NO-SrO_2}$$

Substituting the relevant values this becomes:

$$\ln E_{\text{ternary}} = \frac{(2 \times 0.2)}{(2 \times 0.2 + 2 \times 0.3)} \times 257813.6 + \frac{(2 \times 0.3)}{(2 \times 0.3 + 2 \times 0.2)} \times 213616.6$$

From this E_{ternary} is found to be = 261099.5

Substituting NO^o_{ternary} and E_{ternary} into the viscosity expression (1-4) η can be calculated as = 3.47 which is in good agreement with the experimental value of 3.

APPENDIX 4
APPROXIMATE COMPOSITION OF SPENT POTLINER

| ELEMENT | PERCENTAGE |
|-----------|----------------|
| Carbon | 25.0±1.78 |
| Fluorine | 16.8±0.65 |
| Sodium | 15.5±0.41 |
| Silicon | 4.53±0.12 |
| Aluminum | 11.0±0.40 |
| Iron | Not determined |
| Calcium | 2.54±0.06 |
| Magnesium | Not determined |
| Cyanide | 0.15±0.01 |